University of Nevada, Reno

**Sensitivity Analysis of Probabilistic Multi-model
Ensemble Forecasts of Wintertime Fronts over Northwestern Nevada**

A thesis submitted in partial fulfilment of
the requirements for the degree of Master of Science
in Atmospheric Sciences

by

Amanda K. Young

Dr. Darko R Koračin/Thesis Advisor

December, 2014

THE GRADUATE SCHOOL

We recommend that the thesis
prepared under our supervision by

AMANDA K. YOUNG

Entitled

Sensitivity Analysis Of Probabilistic Multi-Model Ensemble Forecasts Of Wintertime Fronts Over Northwestern Nevada

be accepted in partial fulfillment of the
requirements for the degree of

MASTER OF SCIENCE

Darko R. Koracin, Ph. D., Advisor

John M. Lewis, Ph. D., Committee Member

Anna K. Panorska, Ph. D., Graduate School Representative

David W. Zeh, Ph.D., Dean, Graduate School

December, 2014

University of Nevada Reno

ABSTRACT:

Sensitivity Analysis of Probabilistic Multi-model
Ensemble Forecasts of Wintertime Fronts over Northwestern Nevada

Amanda K. Young

Chair of the Supervisory Committee:
Professor Darko R. Koračin, Ph. D.
Atmospheric Sciences

Probabilistic ensemble forecasting has become an essential tool to numerical weather prediction. With the chaotic nature of the atmosphere, decisions made by operational meteorologists are made with imperfect weather models. These deterministic numerical weather forecasts can be complemented with the use of regional ensemble predictions incorporating enhanced probabilistic, statistical analysis tools. The challenge is providing better statistical information using ensemble probabilistic information forecasts of mesoscale frontal features to better characterize frontal precipitation fields, intensity, and direction of movement.

The purpose of this study was aimed at drawing attention to certain probabilistic distribution patterns for specific mesoscale circulations when physical parameterizations and/or initial conditions are varied for specific ensemble forecast members. A statistical sensitivity error-trend analysis of multi-model (MM5, COAMPS, and WRF) ensemble prediction system (EPS) was conducted to provide insight into how inherent changes to model parameterizations,

i.e. PBL, convection, radiation, and microphysics can manifest intrinsic variability to ensemble predictability. Most studies in ensemble prediction used a single model in an ensemble mode, using variations in model initial conditions as the basis to produce simulation ensemble members and in most cases the total ensemble members were limited to 6-10. A total of 153 ensemble members with a horizontal resolution of 36 km were evaluated for this study using three state of the art regional-mesoscale models. Its focus was directed towards the use of a multi-model EPS to measure the statistical sensitivity of a sequence of three winter-time fronts observed over western Nevada during the period of 12-27 December 2008. The corresponding analysis and evaluation underscored a process through which 500 hPa thermal field dataset temperature differences, as it applied to rank data calculated for the three cold frontal systems observed over the period of the 15 day simulation, can also be applied to ensemble model spread and error trend analysis. This study enabled the extension of the forecast simulation period to two weeks, which is the assumed predictability limit for atmospheric simulations. Therefore, it became apparent that the use of statistical rank data error trends and ensemble model spread can improve predictability of certain aspects of frontal activity based on COAMPS smaller (high a priori forecast accuracy) ensemble simulation spread as compared to MM5 and WRF larger (low a priori forecast accuracy) ensemble spread.

Acknowledgements:

I would first like to express my gratitude to my Committee members, Professors Mark C. Green, John M. Lewis, and Anna K. Panorska. To my advisor, Professor Darko R. Koracin, who facilitated my entry into the field of chaos and its application to ensemble research. His suggestions, wisdom, and patience concerning the direction of my research were invaluable, and his philosophy of providing students with the maximum opportunity to perform independent, intuitive investigations proved helpful for my research. I also want to recognize my fellow DRI team members who contributed greatly to this study and my understanding of the ensemble process, Dr. Ramesh Vellore, Dr. Jinhua Jiang, Ming Xiao, Travis McCord, Robert Rabin, and Kristian Horvath. To the insightful discussions with Professor Mike Kaplan whose suggestions improved my understanding of mesoscale dynamical systems and related topics. I am most thankful to Professor Melanie Wetzel who heartened and aided my entry into graduate school atmospheric sciences program. I am also indebted to many students and staff at DRI for their help and support. I also owe a debt of gratitude to the men and woman of Fleet Weather Center San Diego Strike Detachment Fallon for their unwavering support. I owe special thanks to Sydney Minich who helped me prepare the draft forms of my thesis and encouraged me to finish. To my kids whose love gave me strength. Finally, to my most loved Cynthia. This thesis would not be complete if not for her encouragement and infinite patience.

Table of Contents

List of Tables:

Table 1	(a) The following formulas were used to calculate the temperature decrease between observed and modeled data for 500 hPa over KREV during passage of associated 500hPa upper trough. (b) This formula was used to calculate the duration of forecast Temp500hPa decrease during period of passage of 500 hPa upper trough over KREV. (c) The final formula was used to calculate the phase shift of the 500 hPa trough axis when compared to observed radiosonde data over KREV.
Table 2	The top-ten Front rank data for each ensemble member and associated front is included below to include the representative simulation run used to select BIAS,RMSE and BIAS+RMSE rank values for error-trend analysis.
Table 3	The top-ten Total-Model rank data for each ensemble member and associated front is included above to include the representative simulation run used to select BIAS,RMSE and BIAS+RMSE rank values for error-trend analysis.
Table 1A	Ensemble simulation set of physical parameterizations for MM5.
Table 2A	Ensemble simulation set of physical parameterizations for WRF.
Table 3A	Ensemble simulation set of physical parameterizations for COAMPS.
Table 1B	Front 1: Ensemble ranking with respect to physical parameterizations for COAMPS.
Table 2B	Front 1: Ensemble ranking with respect to physical parameterizations for MM5..
Table 3B	Front 1: Ensemble ranking with respect to physical parameterizations for WRF.
Table 4B	Front 2: Ensemble ranking with respect to physical parameterizations for COAMPS.
Table 5B	Front 2: Ensemble ranking with respect to physical parameterizations for MM5.
Table 6B	Front 2: Ensemble ranking with respect to physical parameterizations for WRF.
Table 7B	Front 3: Ensemble ranking with respect to physical parameterizations for COAMPS.
Table 8 B	Front 3: Ensemble ranking with respect to physical parameterizations for MM5.
Table 9 B	Front 3: Ensemble ranking with respect to physical parameterizations for WRF.

List of Figures:

List of Equations:

Equation 1	Equation for the calculation of the Bias.
Equation 2	Equation for the calculation of the Root Mean Square Error (RMSE).

Introduction:

Deterministic chaos or just "chaos" theory has been well known for decades and is well researched and documented. Ensemble prediction is relatively new, however, and is based on the scientific concept of non-linear dynamic systems. Taking into consideration the primary assumption when referring to chaos, unstable system have finite predictability – chaos – and stable systems are infinitely predictable. Also, chaos in not random, but is generated by physical instabilities. In Kalnay (2003), it was emphasized the ensemble forecasting approach should replicate in the initial perturbations the statistical uncertainty in the initial conditions. Ideally the leading eigenvectors of the analysis error covariance should be the initial perturbations. The ensemble forecasting approach should reflect model imperfections and our uncertainty about these model deficiencies. Keep in mind, predictability is closely related to the Lyapunov-exponent spectrum. Lyapunov exponents are the average rates of exponential divergence or convergence of nearby orbits. The spectrum of Lyapunov exponents provides a quantitative measure of the sensitivity of a nonlinear system to initial conditions. It is the most useful dynamical diagnostic for chaotic systems. An example is the divergence of neighboring chaotic trajectories exponentially in time. The estimation of Lynapunov exponents and predictability is usually related to the growth of small initial errors. Figure 1 can illustrate how each physical process when started with different initial conditions, like that done for ensemble forecasts, can actually favor certain patterns, regions, or regimes. This is what determines the difference between a "Good" ensemble and a "Bad" ensemble forecast.

One of the earliest pioneers of chaos theory, Edward Lorenz, showed that numerical
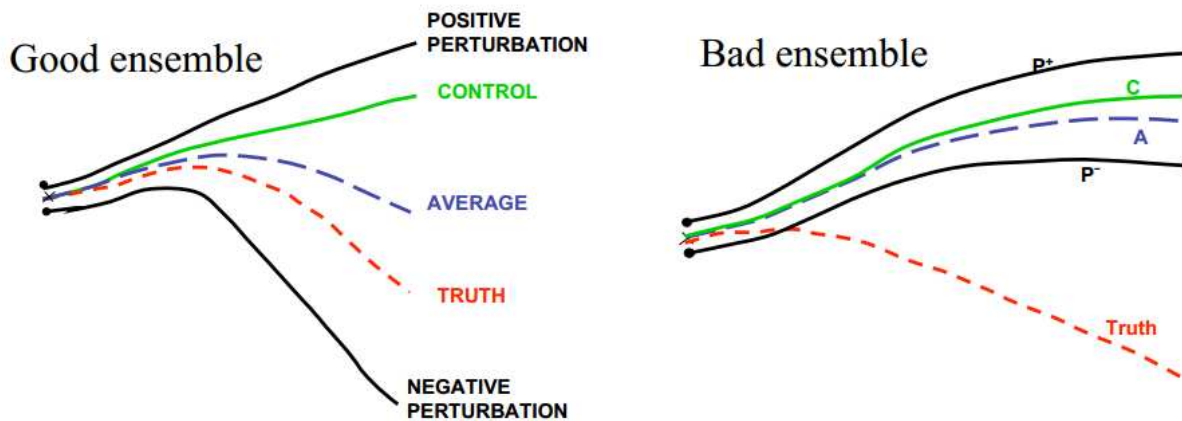
Figure 1: This figure illustrates the components of ensemble forecasts. Three points are emphasized: 1. An ensemble starts from initial perturbations to the analysis. 2. In a good ensemble ”truth” looks like a member of the ensemble. 3. The initial perturbations should reflect the analysis "errors of the day." This is what determines the difference between a "Good" ensemble and a "Bad" ensemble forecast. © E. Kalnay, Lectrure 3, Alghero, May 2008, "Bred vectors: theory and application in operational forecasting."

simulations of the atmosphere were subject to what he referred to as "sensitive dependence on initial conditions." From his initial discovery, Lorenz showed that the atmosphere can exhibit what appears to be chaotic behavior, including a high degree of sensitivity to the initial conditions from which a forecast starts. His discovery that the degree of numerical precision in the initial conditions applied to a numerical weather prediction (NWP) model affected the resulting forecast significantly after only a few days of forecast time (Lorenz 1963). The varying results obtained when NWP models run with identical initial conditions, but selecting differing model dynamics and parameterizations, demonstrated categorical evidence of the degree to which mathematical chaos heavily influenced nonlinear dynamical systems like Earth's atmosphere.

Lorenz (1987) posed a question: "Among the many question which have inspired considerable debate among meteorologists, or in particular for one that attracted some prominent

mathematicians – should the weather be treated as a deterministic or a stochastic process for the purpose of making the best attainable weather forecasts?" From this question, two different objective methods evolved into what is known as modern state-of-the-art numerical weather prediction. The latter one attempts to establish formulas which minimize the expected mean-square error in probabilistic prediction using parameterized physical processes, past weather observations applied in the data assimilation step, and perturbed initial conditions. The former method, however, attempts to predict future atmospheric states by the integration of a deterministic system of differential equations representing the governing physical laws of atmospheric circulation using observed atmospheric variables as initial conditions. Lorenz's fortuitous research and its unexpected outcomes showed that even the smallest of errors in this particular Earth system (and others like it) mattered a great deal.

Ensemble prediction was the next logical step to develop a process by which to consolidate a stochastic approach to probabilistic prediction. By producing future states of the atmosphere through the use of a stochastic distribution of all possible outcomes and relying upon the "best" guess. This concept is based on the standard deviation of predicted states developed from a spread of forecast outcomes over a range of varying physical parameterizations modelled at both the regional and global numerical regimes. It took increased computational power, developed in the last decade of the 20th century, to allow investigation into possible applications of chaos theory to operational forecasting. The work of Tracton and Kalnay 1993, Toth and Kalnay 1993, and others resulted in the development of an advanced suite of ensemble forecasting techniques. These techniques utilize the chaotic nature of the atmosphere and the large, massively parallel computing environments now available during recent times to produce NWP model forecasts that estimate the relative predictability of specific weather outcomes, both

in the short (60 hours or less) and medium (3-15 day) ranges.

Stochastic processes, or as occasionally referred to as random processes, are used to represent over time the evolution of some random value or system. This concept is sometimes referred to as the probabilistic counterpart to a deterministic system. In practical problems, however, the physical laws governing the motions and progression of the atmosphere must use initial data that are not entirely known with absolute certainty. Conversely, conventional deterministic forecasts use the governing equations to describe the predicted growth of a single initial state that is regarded as the "true initial state". The concept underling stochastic dynamic estimations is to permit the deterministic governing equations to operate on the probabilistic statistics describing the uncertainty about the initial state of the atmosphere. The probabilistic approach produces, as regional or global forecasts, probability distributions representing uncertainty about the future state of the atmosphere. Since current operational NWP models are imperfect and their incompleteness add to forecast uncertainty.

To think globally when referring to ensemble predictive systems, one could easily be distracted from the essential qualities of any stochastic process in calculating and assessing the probability that certain physical processes will be accurately predicted. Although the approach used in this study differs from the approach demonstrated by Froude (2010) to analyze, assess, and calculate trajectories of mid-latitude cyclones, it is the intent of this research to utilize basic stochastic principals to analyze statistically the predictability of frontal features observed during the period of the EPS simulation used during the period of 12-27 December 2008.

Up to the present time, regional ensemble forecasts were applied to severe weather events. This study extended the forecast experiment to a sequence of three winter frontal systems. In addition, in previous studies the number of ensemble members was limited to 6-10,

but for this study the number was extended to a total of 153 ensemble members. This study Also, three state-of-the-art regional/mesoscale models were used to complete the ensemble simulation while various studies in the literature generally include only a single model in an ensemble mode. The forecast period was extended to 2 weeks which is assumed as a predictability limit for atmospheric simulations when normally, other ensemble forecasts covered only periods of 3-7 days. There was emphasis placed on model initial conditions with consideration organized toward the use of variations in physics parameterization options (PBL, microphysics, radiation, and convection) as methodology for generating ensemble members for three models.

The first section outlines information regarding the multi-model prediction system as a NWP predictability tool as well as a discussion of the various forecast centers using ensemble predictive systems operationally. Section 2 covers a discussion of the ensemble multi-model system employed and methods used in this study, to include abbreviated model microphysics code located in this study's appendix. The third section discusses analysis of the synoptic situation covering the forecast period. Section four will discuss initial perturbation analysis of the COAMPS, MM5, and WRF model outputs used to create the 51 run ensemble probabilistic forecast set for each model. Lastly, a summary and conclusion will finalize this study.

1. The Multi-model Prediction System

1.1   Ensemble Prediction Systems: Using NWP Models as a Predictability Tool

Numerical model sensitivity is a function of model design, those physical processes most influenced by the air-land-sea interface, and the initial conditions applied to simulated atmospheric conditions within the Earth system. For regional and mesoscale models, boundary conditions need to be known for the entire simulation period. Forecast uncertainty is heavily influenced by the non-linear dynamical behavior or aperiodicity in model mnemonic processes. Modifying ensemble forecast physical parameterizations slightly alters how the model simulates actual meteorological phenomenon at the synoptic and mesoscale domains. Different approximations, therefore, of the actual state of the atmosphere are calculated which further adds to forecast uncertainty and ambiguity.

A perfect or "near" perfect NWP model is well beyond the reach of the current level of science and available technology. In the future, when ensemble model predictions can run in a perfect or "near" perfect computational environment, they will likely continue to be subjected to numerical breakdown due to errors in initial conditions applied at the beginning stages of the model run. The current state of terrestrial observation and assimilation systems will widen the NWP forecast gap further until better technologies are available to enhance observations includinf rapidly developing remote sensing capabilities.

An ensemble prediction system (EPS) calculates a trio of statistical outcomes based on a varying suite of initial conditions and/or multi-model ensemble parameterization system. These outcomes include the following three results:

- Ascertaining a range of possible forecast outcomes.

- Estimating the probability for any individual forecast outcome

- Calculating the most likely forecast outcomes within an acceptable margin of error.

Using an uncertainty and bias intrinsic within the initial conditions, these measures can be used as a basis for calculations of forecast outcomes of each member within the EPS.

Today's operational forecast centers use some form of EPS to generate a range of possible forecast probability outcomes as a means to improve medium and long range forecast accuracy and reduce error within the operational forecast array. Whether it is the use of the model imperfections in the structure and dynamics of the forecast model system or the uncertainty inherent in the initial conditions of a multi-model system, these ensemble prediction processes are used as a gauge to measure the chaotic behavior and determine the predictability of ensemble forecast outcomes.

The atmosphere is considered an aperiodic process within the Earth system. In terms of a fluid system undergoing steady forcings, it is much less predictable for moderately unstable systems. The predictability of mesoscale motions in the troposphere is, therefore, confined by the rapid multi-scale transfer of energy from the large scale synoptic systems into mesoscale as well as microscale regimes. In contrast, inevitable errors or uncertainties in initial conditions in the small scale of motion will propagate toward larger scales and will reach the mesoscale sooner than the large scale, thereby rendering the mesoscale less predictable. Thus, predictability of mesoscale events are also sensitive to initial condition inputs to the various operational mesoscale numerical prediction models. The predictability of mesoscale phenomena that does not exist at the start of a numerical simulation is less influenced by the accuracy of the initial conditions used in the mesoscale numerical prediction system. Under these circumstances, the mesoscale circulations are normally forced by surface inhomogeneities (thermal and orographic) and internal adjustments. Note that there are processes developed on small scales (local circulations, convection) that are upscaled to larger scales.

It is noteworthy to mention that larger-scale flow patterns, mesoscale instabilities, and multiple spatial and (or) temporal scale energy transfers are from either the larger scale to the microscale or the interaction of cloud physical or dynamical processes. If a mesoscale feature, already exists at the beginning of the numerical predictive process, then it is necessary to include the observed and analyzed motions as well as thermodynamic variables in the initial conditions to construct the most accurate numerical model prediction. Previous investigations suggest that the accuracy of the numerical prediction processes must rely more on observational data during the data assimilation-initialization step and less on the model dynamical system representation. This is an important consideration since it takes time for the model in the "spin-up" process to gain the necessary initial knowledge to accurately represent mesoscale motions during the period of the first 120 hours of the forecast run.

Due to the need to resolve complex atmospheric processes on smaller scales than the global models, regional and mesoscale models generally have larger numbers of physical parameterization options (Stensrud 2007). This means that a large number of various option combinations have to be considered to cover a wide spectrum of model trajectories that would provide a sufficient probability density functions (PDFs) of atmospheric parameters. Since high-resolution mesoscale and regional scale simulations are computationally expensive, it is valuable to consider cost-effective methods that can be used for operational forecasting. Additionally, there are a large number of community accepted regional and mesoscale models that have similarities and differences in the model structure, numerical methods, and physical parameterizations. Consequently, it is important to examine the use of various models in constructing more reliable PDF, that is, the use of multi-model ensembles.

During the period 12 through 17 December 2008, output products from the following numerical models were analyzed to provide insight into how the relative precision ensemble forecast products can resemble actual mesoscale meteorological features when physical parameterizations are varied for each ensemble forecast run. For this analysis, ensemble output products derived from the Weather and Research Forecasting (WRF) model (Skamarock et al., 2008), Fifth-Generation Penn State/NCAR Mesoscale Model (MM5; Grell et al. 1994), and the U.S, Navy's Coupled Ocean/Atmosphere Mesoscale Prediction System (COAMPS; Hodur 1997; Hodur et al. 2002; were compared with the associated 500 hPa level analysis for the same time period. This implementation was adopted to assess which physical parameterization utilized for each ensemble run most closely compared physically to the actual mesocale-synoptic atmospheric conditions.

1.2 Discussion of the multi-model Ensemble Prediction System (EPS)

The improvement in skill of numerical weather prediction over the last 40 years is due to four factors:

- The increased power of supercomputers, allowing much finer numerical resolution and fewer approximations in the operational atmospheric models.

- The improved model structure, numerical schemes, and representation of small-scale physical processes (high-resolution topography and vegetation, clouds, precipitation, turbulent transfers of heat, moisture, momentum, and radiation) within the models.

- The use of more accurate methods of data assimilation, which result in improved initial conditions for the models.

- The increased availability of data, especially satellite and aircraft data over the oceans and the Southern Hemisphere.

In the United States, research on numerical ensemble weather prediction takes place in the national laboratories such as the National Centers for Environmental Prediction, the National Oceanic and Atmospheric Administration (NOAA), the National Aeronautics and Space Administration (NASA), the National Center for Atmospheric Research (NCAR), and in universities and centers such as the Desert Research Institute, Oklahoma State University, Penn State University, and University of Washington. The NCEP ensemble, the Global Ensemble Forecasting System, uses a technique known as vector breeding. Toth and Kalnay (1997) explained that the initial perturbations to the control analysis should adequately sample the space of possible analysis errors for efficient ensemble forecasting. It was shown that the analysis cycle is like a breeding cycle and acts as a nonlinear perturbation model upon the evolution of the real atmosphere. Surface and upper observations are used to "scale down" at regular intervals the perturbations carried forward in the first-guess forecasts. The result is growing model errors associated with the evolving state of the atmosphere which developed within the analysis cycle and then dominated subsequent forecast error growth. The bred vectors provide estimates of fastest sustainable growth and thus represent probable growing analysis errors. It is a simple and powerful method to find the growth and shape of the model instabilities which dominate these forecast errors (Kalnay 2008).

In Europe, the primary numerical modeling center is located in the United Kingdom, at the European Centre for Medium-Range Weather Forecasts (ECMWF). The EPS maintained by ECMWF utilizes singular vectors to simulate the initial probability density functions used to

calculate probabilistic forecast. The singular vector method (Buizza and Palmer 1995) are the perturbations that, under dynamics linearized about a basic flow state, grow most rapidly over a given time interval and in a given measure of amplitude, or vector norm. As applied to forecast error growth and ensemble forecasting, these nonlinear optimal perturbations show the greatest linear growth in total energy over the extra-tropical northern and southern hemisphere over a 48 hour period following the analysis time. The principal objectives of the Centre include but are not limited to:

- Operation of global models and data-assimilation systems for the dynamics, thermodynamics and composition of the atmosphere and interacting parts of the Earth-system, development

- Quality control of forecast models through scientific research and operations.

- Model output collection, processing, and storage

Other numerical centers, such as the Chinese Meteorological Administration (CMA), assist in the centralization of ensemble model forecast data archives which are used to enable extensive data sharing and research with other international partners. The THORPEX Interactive Grand Global Ensemble (TIGGE) is research program, with a key component of THORPEX being that it is a program chartered to accelerate advancements in the accuracy of 1-day to 2 week ensemble weather predictions. Under this program, CMA is designated as a TIGGE archive center. After agreement amongst research partners was reached in 2005 with regards to research data requirements and archive planning, active archive collection commenced in October 2006.

The Meteorological Service of Canada (MSC) is a division of Environment Canada conductd research on a System Simulation Approach to ensemble prediction. From Houtekamer

et al. (1996), this approach produced error statistics from a representative ensemble of forecast. The ensemble is generated by simulating the the process of error growth where for different ensemble members the uncertain elements of the forecasts are perturbed in different ways. In order to perturb the ensemble and initiate the necessary error growth, different model options for the parameterizations of horizontal diffusion, deep convection, radiation, gravity wave drag, and terrain were used. This ensemble scheme, which mathematically described a Monte Carlo method, attempted to produce a set of representative error fields at the initial time of a forecast. At the time, the MSC was the first agency to propose using this numerical scheme to simultaneously perform medium-range ensemble forecast and a number of model validations.

2   Methods

2.1   COAMPS Overview

In the late 1980s, NRL director and expert modeler John Hovermal provided a code for a non-hydrostatic model and Richard Hodur began modifying and using athis code as the starting point for predicting air-sea interaction in the Arctic. The model came to be called Coupled Ocean/Atmosphere Mesoscale Prediction System (COAMPS). Initially, the COAMPS development and testing was limited to studies of idealized simulations of arctic leads, tropical cyclones, and lake-effect snowstorms. By 1993, COAMPS incorporated a real-data capability into the atmospheric model part. This modeling system eventually transitioned to operations at Fleet Numerical Meteorology and Oceanography Center (FNMOC) and replaced NORAPS. Although COAMPS was originally developed for Navy use, interested domestic and international institutions are now able to register and obtain the model code. Details on the

COAMPS structure are found in Hodur (1997) and Hodur et al. (2002).

During the early 1990s, a next generation mesoscale modeling capability beyond the U.S. Navy's Operational Regional Atmospheric Prediction System (NORAPS, circa 1982) led to development of a non-hydrostatic atmospheric model coupled to an ocean model – COAMPS. The atmospheric component of COAMPS can be used or real-data or for idealized applications. For the real-data applications, the COAMPS analysis can use either global fields from the Navy Global Environmental Model (NAVGEM) or the most recent COAMPS forecast - the now decommissioned Navy Operational Global Atmospheric Prediction System (NOGAPS) as the first-guess. Observations from aircraft, radiosondes, ships, and satellites are blended with the first-guess fields to generate the current analysis. For idealized experiments, the initial fields are specified using an analytic function and/or empirical data (such as a single sounding) to study the atmosphere in a more controlled and simplified setting. The atmospheric model uses nested grids to achieve high resolution for a given area and it contains these parameterizations for: Sub-grid scale turbulence mixing, convective parameterization, radiation, and microphysics.
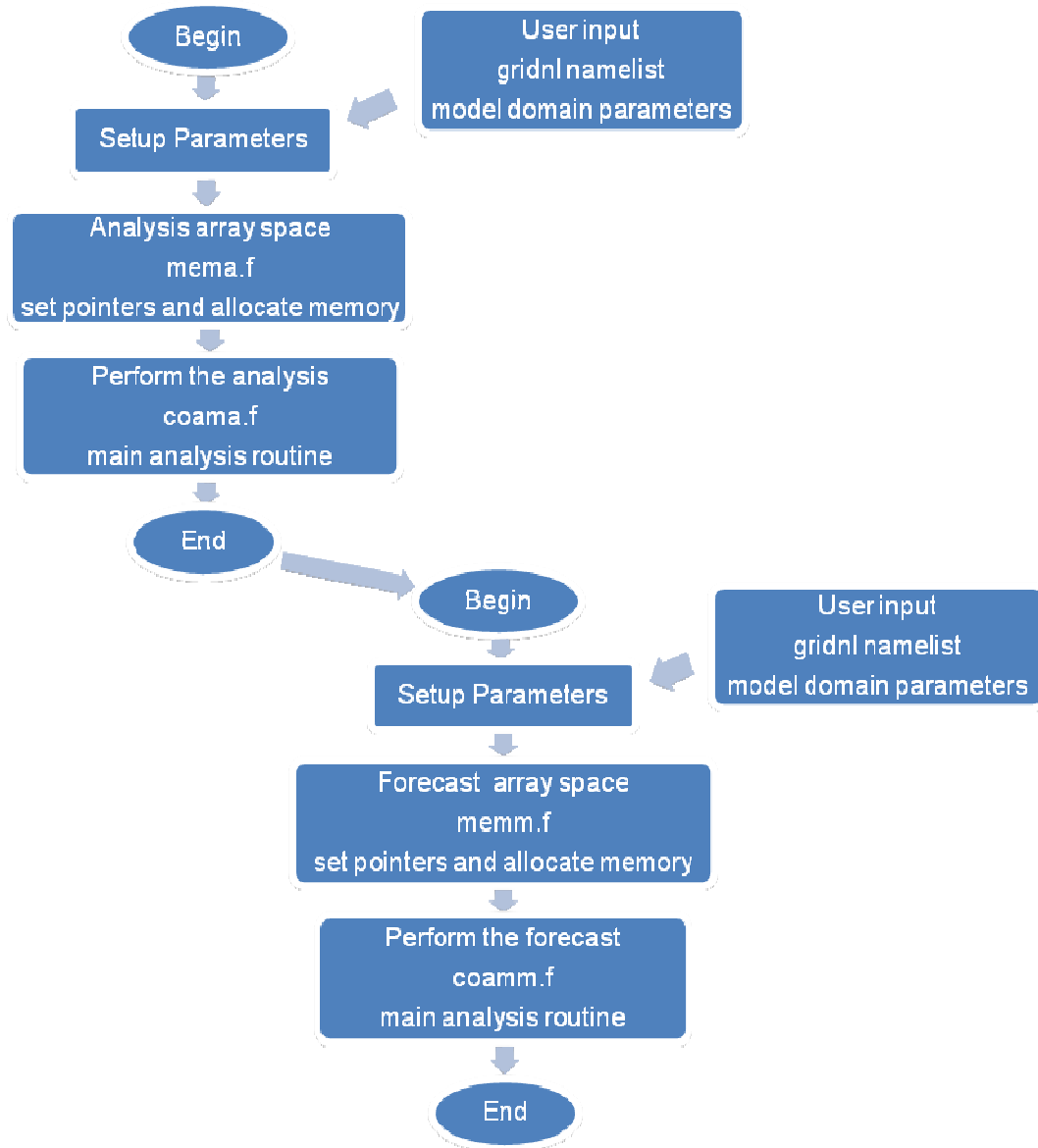
Figure 2: Flow chart of the COAMPS driver programs coamps_analysis.f and oamps_forecast.f. The model domain specifications are read in through the gridnl namelist and the pointers and array space are setup in subroutines mema.f and memm.f before calling the main analysis and forecast subroutines coama.f and coamm.f.

The COAMPS atmospheric system consists of two major components: analysis and forecast. Figure 2 illustrates the general flow of the COAMPS driver programs coamps_analysis.f and oamps_forecast.f. The COAMPS analysis executable is run first to prepare the initial and boundary files used in the forecast model. The COAMPS forecast

executable performs time integration of the model numerics and physics. It then outputs prognostic and diagnostic fields in pressure, sigma, or height coordinates. Options for running the analysis and forecast are specified through several Fortran namelists. Examples of mesoscale phenomena to which COAMPS has been applied include mountain waves, land-sea breezes, terrain-induced circulations, tropical cyclones, mesoscale convective systems, coastal rain-bands, and frontal systems. The COAMPS model domain typically covers a limited area over the Earth. The model horizontal grid resolution may range from a few hundred kilometers (synoptic scale) to approximately 100 meters. The actual dimensions applied depend on the scale of phenomena that the user is interested in simulating. The model dimensions can be set to produce any rectilinear pattern. In addition, it can be rotated to align with any surface feature, such as the terrain or a coastline. COAMPS can be run with any number of nested grids, with the requirement that the horizontal grid resolution in any mesh be one-third that of the next coarser mesh.

Following is a summary of the physical processes in COAMPS that are modeled at each time step in the forecast cycle. The model domain specifications are read in through the gridnl namelist and the pointers and array space are setup in subroutines mema.f and memm.f before calling the time step at individual grid points:

a) The total diabatic heating per time step

    1. From (resolvable) scales

    2. From (sub-grid) scales

b) The total moisture/day per time step

    1. From (resolvable) scales

2. From (sub-grid) scales

c) The total acceleration/deceleration per time step

1. From (resolvable) scales

2. From (sub-grid) scales
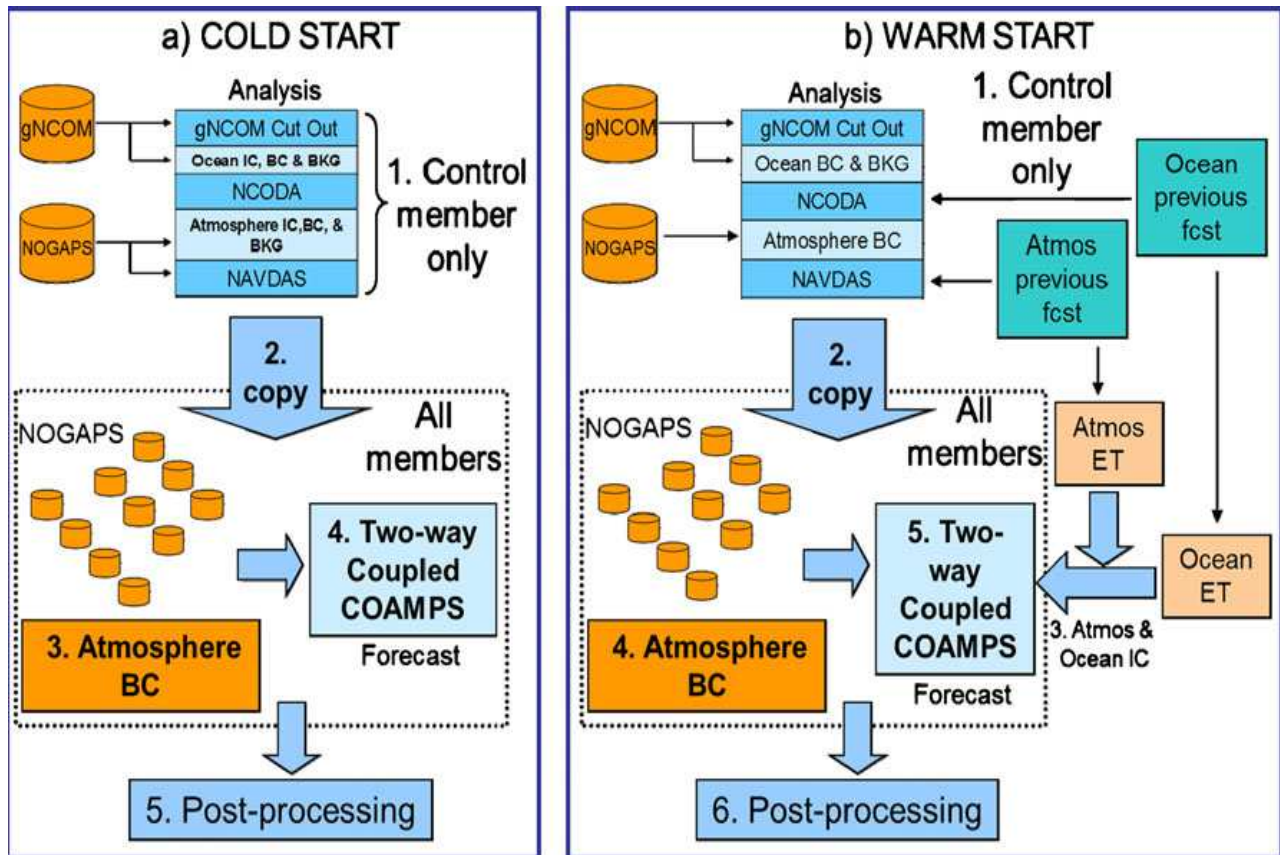
Figure 3: Schematic showing the implementation of the air–ocean coupled ensemble system for a cold start and a warm start model initiation. © Naval Research Laboratory (NRL)

The above steps are executed slightly differently and according to whether the system undergoes a warm or cold startup. The execution of atmospheric and ocean forecasts are used in model initialization for a warm system start whereas this step is not required for cold system starts as illustrated in figure 3.

2.1.1 COAMPS Model Physics Options

Numerical schemes developed by Rutlege and Hobs (1983) are the currently used method to predict single-moment bulk mixing-ratios. The COAMPS scheme is based on research compiled by Lin et al. (1983) for the bulk configured microphysical model, which incorporated single-moment predictions of mixing ratio for five microphysical variables: water vapor, pristine ice, snow, rain, and cloud water. Size distribution calculations (Marshall and Palmer et al 1948), autoconversion (Kessler et al 1967), and nucleation of pristine ice (Fletcher et al 1962) are used as primary assumptions with within the numerical scheme matrices. Rain and snow terminal velocity fields are computed numerically while all other domain parameters are treated as scalar tracers.

After model dynamical variables are calculated and scalar value prediction variables for advection, diffusion, and moisture mixing process have been refreshed through the data assimilation process, the bulk scheme is initialized. Various microphysical driver subroutines compiled through Fortran algorithms perform the necessary updates. DXMESO parameter, for instance is written in as a namelist variable where below a given resolution in kilometers the cumulus parameterization scheme is turned off and above the predicted value the advection of
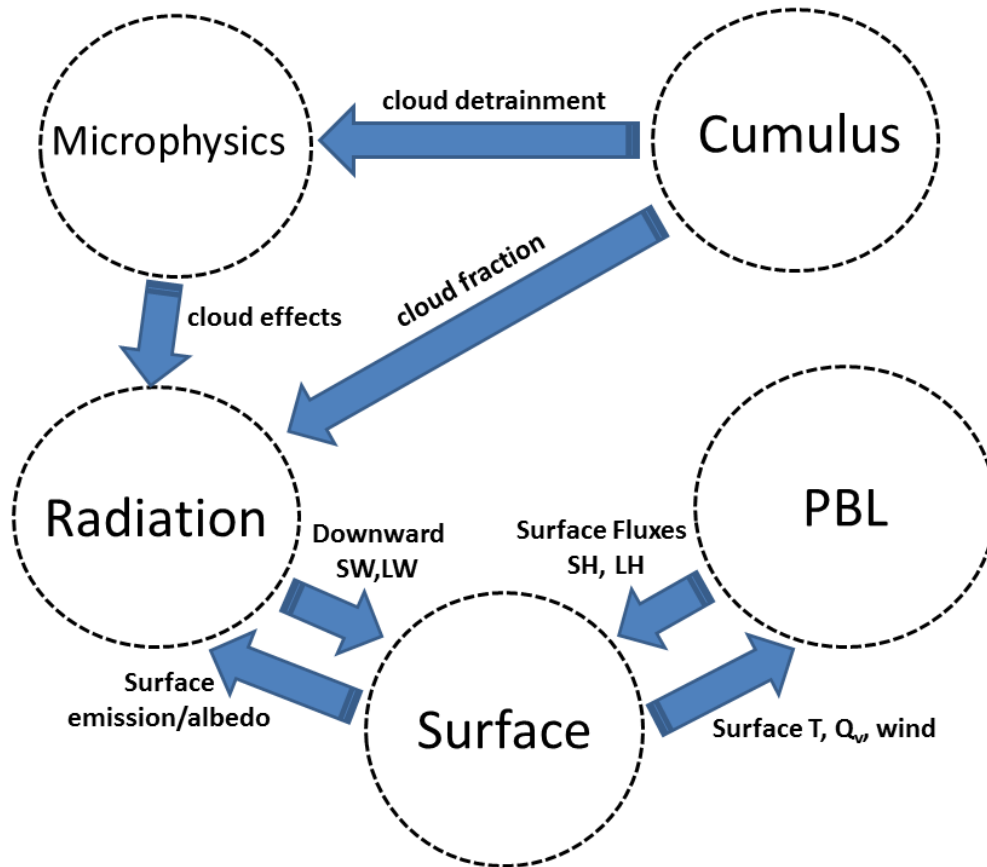
Figure 4: Direct Interactions of physical parameterizations processed within the MM5 model

rain-snow calculation is turned off as well.

2.2   MM5 (Weather Research & Forecasting Model) overview

From the late 1960s into the 1970s, Richard Anthes developed a 3-layer hurricane model as a basis for a general mesoscale model. This then evolved from Mesoscale Model 0 (MM0) into Mesoscale Model 3 (MM3).   The formulation for model development stemmed mainly from Anthes and Warner (1978). By the 1980s, PSU and NCAR developed an updated version Mesoscale Model 4 (MM4). The PSU/NCAR mesoscale model was developed as a limited-area, nonhydrostatic or hydrostatic (Version 2 only), terrain-following sigma-coordinate domain

structure designed to simulate or predict mesoscale and regional-scale atmospheric circulation. The support initially came from the Regional Acid Deposition Modeling Project (Anthes et al. 1987). A community model with annual workshops and tutorials evolved into a fourth version, MM4. A non-hydrostatic Mesoscale Model 5 (MM5) was released in the early 90s with many advanced characteristics including multiple nesting, four-dimensional data assimilation, and improved numeric, and physics parameterizations. It was supported by several auxiliary programs and continued to be developed as a community mesoscale model. Today, it is continuously being improved by contributions from users at several universities and government laboratories. More information can be obtained at the web site (http://www.mmm.ucar.edu/mm5/mm5v3.html). MM5 was being developed and supported until 2004 with the last version being 3.7. Subsequently, other than at the research level, there has been limited operational development. Details on the MM5 structure are shown by Grell et al. (1995)

The Fifth-Generation NCAR/PSU Mesoscale Model (MM5) was the latest in a series that developed from a mesoscale model used by Anthes at Penn State in the early 70s that was later documented by Anthes and Warner (1978). Since that time, it has undergone many changes designed to broaden its usage, including:

- multiple-nest capability
- nonhydrostatic dynamics, which allows the model to be used at a few-kilometer scale,
- multitasking capability on shared- and distributed-memory machines
- four-dimensional data-assimilation capability
- enhanced suite of physical parameterizations.

The MM5 Modeling System Flow Chart
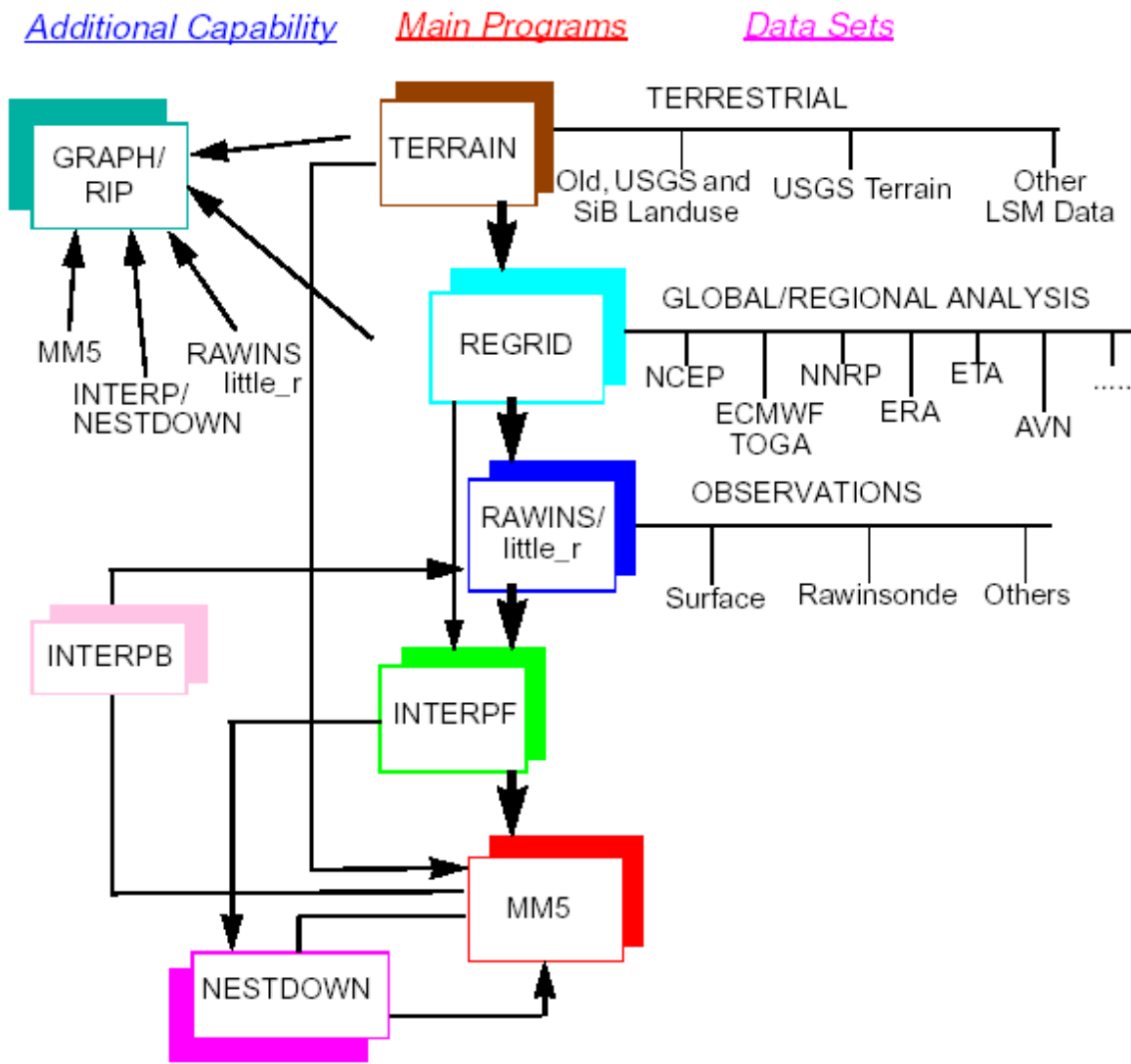
Figure 5: MM5 Modeling System operational Flow Chart. © University Corporation for Atmospheric Research (UCAR)

Terrestrial and isobaric meteorological data are horizontally interpolated (programs TERRAIN and REGRID) from a latitude-longitude mesh to a variable high-resolution domain on

Mercator, Lambert conformal, or polar stereographic projection. Since the interpolation does not provide mesoscale detail, the interpolated data may be enhanced (program RAWINS or little_r) with observations from the standard network of surface and rawinsonde stations using either a successive-scan Cressman technique or multiquadric scheme. Program INTERPF performs the vertical interpolation from pressure levels to the sigma coordinate system of MM5. Sigma surfaces near the ground closely follow the terrain and the higher-level sigma surfaces tend to approximate isobaric surfaces. Due to the variability of the vertical and horizontal resolution and domain size, the modeling package programs employ parameterized dimensions requiring a variable amount of core memory. Some peripheral storage devices are also used. Since MM5 is a regional/mesoscale model, it requires both an initial condition and a lateral boundary condition to run. To produce lateral boundary condition for a model run, gridded data is needed to cover the entire time period that the model is integrated.

2.3   WRF (Weather Research and Forecasting) model overview

In 1996, NCAR and NCEP initiated the development of the next generation weather research and forecasting model. Together with contributors from various universities and military scientific institutions, a beta release of the Weather and Research Forecasting (WRF) model was released in 2000. It has been undergoing continued rapid development so that today it is one of the most commonly used regional and mesoscale models worldwide (http://www.wrf-model.org <http://www.wrf-model.org/>). With respect to weather and climate forecasting, a primary motivation for WRF model development was a need to increase communication and links between the research, application, and education communities. There are two versions of the WRF Model with the same architecture but different core codes: ARW (Advanced Research

WRF) at NCAR and NMM (Non-Hydrostatic Mesoscale Model) at NCEP which is based on the Eta Model's code (Mesinger, 2005; Janjić; 1994; Black, 1994). The WRF model is a next-generation mesoscale numerical weather prediction system designed to serve both operational forecasting and atmospheric research purposes. It features multiple dynamical cores, 3-dimensional variational (3D-Var) and 4-dimensional variational (4D-Var) data assimilation systems, as well as software architecture allowing for computational parallelism and system managed extensibility programming. WRF has been used in a broad spectrum of applications across scales ranging from meters to thousands of kilometers and is suitable for execution on multi-processor computers. Such applications include research and operational numerical weather prediction (NWP), data assimilation, and model parameterizations research, downscaling climate simulations, driving air quality models, atmosphere-ocean coupling, and idealized simulations (e.g., boundary-layer eddies, convection, baroclinic waves). Details on the WRF structure are shown by Skamarock et al. (2005; 2008). The ARW version was used in the development of the 153-member series used in this study.

The Weather Research and Forecasting model–based variational data assimilation system (WRFVar) has been extended from three- to four-dimensional variational data assimilation (WRF 4D-Var) to meet the increasing demand for improving initial model states in multi-scale numerical simulations and forecasts. The initial goals of this development included improved operational applications and expanded support to the research community. It was shown to implicitly evolve the background error covariance and to produce a flow-dependent nature to the analysis increments. Preliminary results from real-data 4D-Var experiments in a quasi-operational setting were presented and the potential of WRF 4D-Var in research and operational applications was demonstrated. To impose a dynamic balance on the assimilation of real data to

the model interface, WRF 4D-Var uses the WRF model as a functional constraint. Development of model verification highlighted its capacity to implicitly evolve the background error covariance and to produce simulations which enhance the flow-dependent nature of the analysis process increments. It is believed that a wider distribution of the system to the research community will further develop model physics and enhance numerical boundary processes. Testing under different weather conditions and model configurations will encourage even greater capabilities of newer versions (Xiang-Yu Huang et al. 2009). In order to better support the research community, improved operational applications and expanded technical support have been at the forefront of this research initiative.

The effort to develop WRF has been a collaborative partnership, principally among the National Center for Atmospheric Research, the National Oceanic and Atmospheric Administration (the National Centers for Environmental Prediction (NCEP) and the Forecast Systems Laboratory (FSL), the Air Force Weather Agency (AFWA), the Naval Research Laboratory, Oklahoma University, and the Federal Aviation Administration (FAA). WRF allows researchers the ability to conduct simulations reflecting either real data or idealized configurations. WRF provides operational forecasting a model that is flexible and efficient computationally while offering the advances in physics, numerics, and data assimilation contributed by the research community. WRF is currently in operational use at NCEP and the U.S. Air Force Weather Service (AFWA-JAAWIN). The WRF Model Users Page (http://www2.mmm.ucar.edu/wrf/users/) provides information on the WRF effort and its organization, references to projects and forecasting involving WRF, and links to the WRF users' page, real-time applications, and WRF-related events.

The continuity equation for air, the species continuity equation, the thermodynamic energy equation, the three momentum equations, and the equation of state are referred to as the equations of atmospheric dynamics. Removing the species continuity equation for the above list and replacing the full vertical momentum equations yields the primitive equations. These equations represent the basic form of the Eulerian equations of fluid motion. A variety of atmospheric motions can be understood by looking at simplified forms of the primitive equations. Geostrophic wind, surface wind, the gradient wind, the surface wind around high-pressure and low-pressure centers, and atmospheric waves are modeled and studied.

The development of the Weather Research and Forecasting (WRF) modeling system is a multiagency effort intended to provide a next-generation mesoscale forecast model and data assimilation system that will advance both the understanding and prediction of mesoscale weather and accelerate the transfer of research advances into operations. The model is being developed as a collaborative effort among the NCAR Mesoscale and Microscale Meteorology Department of Defense's Air Force Weather Agency (AFWA), the Naval Research Laboratory (NRL), the Center for Analysis and Prediction of Storms (CAPS) at the University of Oklahoma, and the Federal Aviation Administration (FAA), along with the participation of a number of university scientists.

The WRF model is designed to be a flexible, state-of-the-art, portable code that is efficient in a massively parallel computing environment. A modular single-source code is maintained that can be configured for both research and operations. It offers numerous physics options, thus tapping into the experience of the broad modeling community. Advanced data

WRF Modeling System Flow Chart

External
Data Source

WRF
Pre-Processing
System

WRF Model

Post-
Processing &
Visualization

Alternative
Obs Data

Conventional
Obs Data

WRF
Terrestrial
Data

Gridded Data:
NAM, GFS,
RUC, NNRP,
NCEP2, NARR,
ECMWF, etc.

OBSGRID

WRFDA

WPS

REAL

Ideal Data
2D: Hill, Grav,
Squall Line & Seabreeze
3D: Supercell ; LES ;
Baroclinic Waves ;
Surface Fire and
Tropical Storm
Global: heldsuarez

ARW MODEL
(includes Chem
& Fire modules)

IDV

VAPOR

NCL

ARWpost
(GrADS)

RIP4

UPP
(GrADS /
GEMPAK)

MET

Figure 6: WRF-ARW Modeling System operational Flow Chart. © University Corporation for Atmospheric Research (UCAR).

assimilation systems are being developed and tested in tandem with the model. WRF is maintained and supported as a community model to facilitate wider use, particularly for research and teaching, in the university community. It is suitable for use in a broad spectrum of applications across scales ranging from meters to thousands of kilometers. Such applications

include research and operational numerical weather prediction (NWP), data assimilation and parameterized-physics research, downscaling climate simulations, driving air quality models, atmosphere-ocean coupling, and idealized simulations (e.g. boundary-layer eddies, convection, baroclinic waves). Closer ties will be promoted between these communitieswith WRF as a common numerical tool in many research Unisersities and operational forecast centers, In addition, research advances will have a direct path to operationsal forecast centers.

Figure 7: The above image displays the horizontal area of the 36 km resolution inner domain.
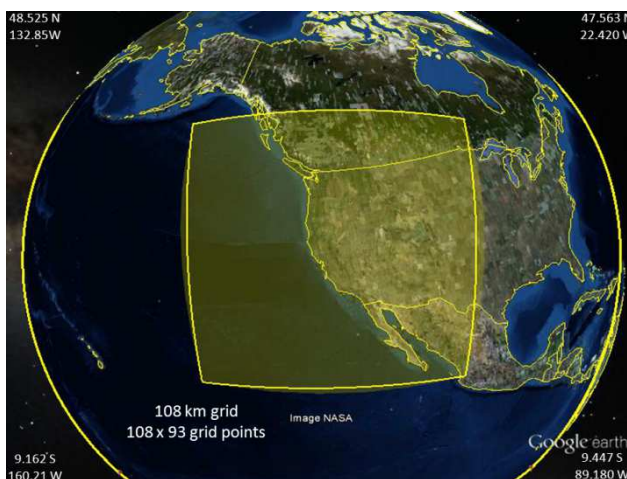
Figure 8: The above image displays the surface extent of the 108 km resolution course domain.

The principal components of the WRF system are depicted in Figure 6. The WRF Software Framework (WSF) provides the infrastructure that accommodates multiple dynamics solvers, physics packages that plug into the solvers through a standard physics interface, programs for initialization, and the WRF variational data assimilation (WRF-Var) system. The WRF Software Framework (WSF) provides the infrastructure that accommodates multiple dynamics solvers, physics packages that plug into the solvers through a standard physics interface, programs for initialization, and the WRF variational data assimilation (WRF-Var) system. At present, there are two dynamics solvers in the WSF: the Advanced

Research WRF (ARW) solver (originally referred to as the Eulerian mass or "em" solver) developed primarily at NCAR and the NMM (Nonhydrostatic Mesoscale Model) solver developed at NCEP. While there are multiple solvers, and while not all physics are available to both solvers, the WSF is common to all components.

2.4   Model parameterization options

Due to the need to resolve complex atmospheric processes on smaller scales than the global models, regional and mesoscale models generally have a larger number of physical parameterization options (Stensrud 2007). This means that a substantial number of various option combinations have to be considered to cover a wide spectrum of model trajectories that would provide a sufficient probability density functions (PDFs) of atmospheric parameters. Since high-resolution mesoscale and regional scale simulations are computationally expensive, it is valuable to consider cost-effective methods that can be used for operational forecasting. Additionally, there are many community accepted regional and mesoscale models that have similarities and differences in the model structure, numerical methods, and physical parameterizations. Consequently, it is important to examine the use of various models in constructing more reliable PDF. This will entail the use of multi-model ensembles.

The following analysis utilizes output data from a 153 ensemble member multi-model (MM5, COAMPS, WRF) medium-range regional ensemble forecasting experiment that was conducted for a period of fifteen days. The study focused on the relative efficiency of varying physical parameterizations (PBL scheme, microphysics, radiation algorithms, and cumulus
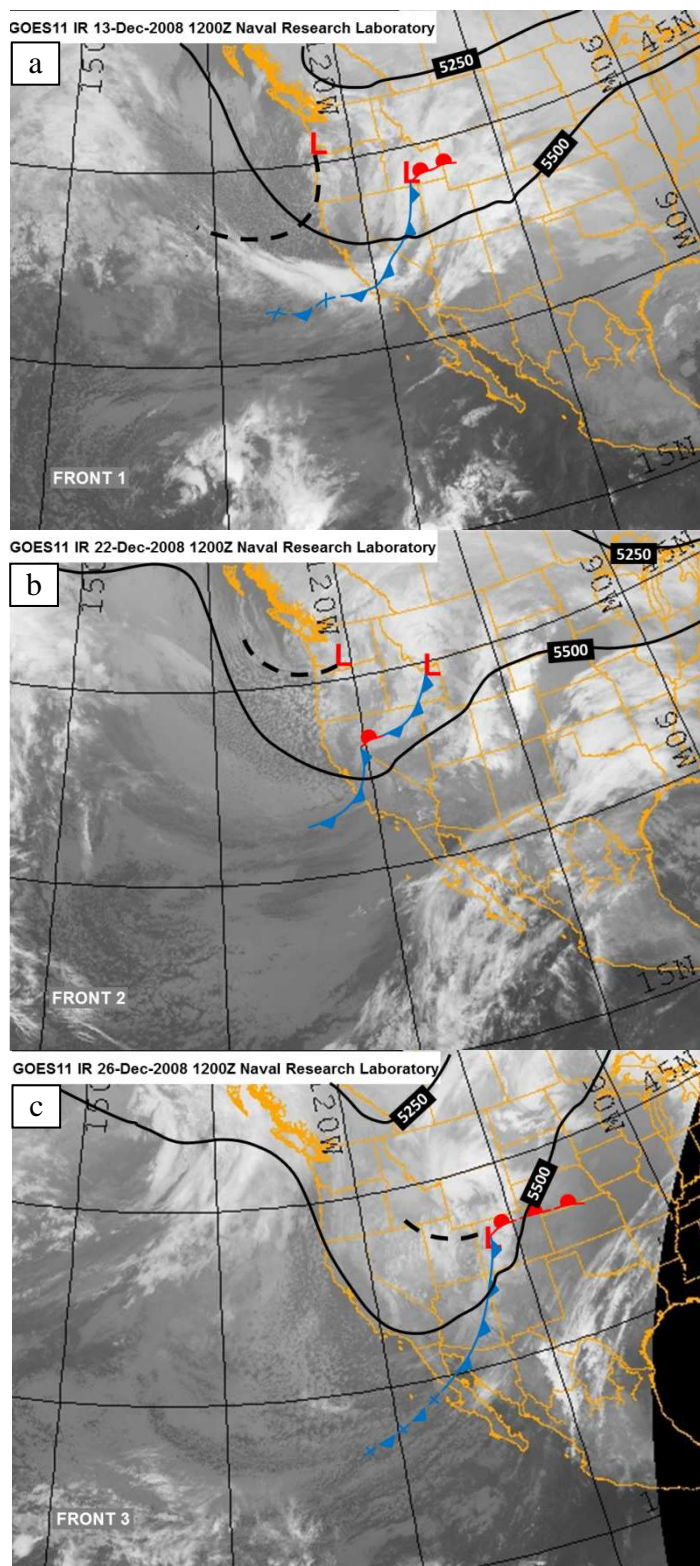
Figure 9a,b,c: The infrared satellite image depicts relative low pressure centers and associated fronts/troughs over the western United Sates for figure 9a) 1200Z, 13 December 2008, figure 9b) 1200Z, 22 December 2008, and figure 9c) 1200Z, 26 December 2008

parameterizations) and model setup parameters. Figure 7 and Figure 8 show the inner nested domain at 36 km resolution used for the ensemble members and coarse domain coverage at the 108 km grid resolution, respectively.

3.0 Synoptic Situation for the period of 12-27 December 2008

The period selected for the forecasting experiment was from 0000 UTC on 12 December 2008 to 0000 UTC on 27 December 2008. Initially, a thorough review of the North American synoptic situation during December 2008 indicated the existence of a relatively stable five-wave pattern around the northern hemisphere decreasing to a four-wave late in the ensemble series. Insofar as the weather over the western USA and Canada is concerned, it is noteworthy that the region over the North Pacific Ocean was characterized by an exceptionally

long baroclinic wave with troughs over the Kamchatka Peninsula in the Russian Far East, western U.S./Canada, and an elongated low-amplitude ridge over the intervening Pacific oceanic region.

During the forecasting period, three weather systems impacted the western U.S. These systems bore similar structures where short wave disturbances formed over Alaska (just east of the ridge line) and amplified as they moved southeast. These disturbances exhibited significant baroclinicity where 500 hPa temperature gradients of 20°C/5 degrees latitude were in evidence as the disturbances moved through California. The associated cold fronts passed Oakland, California (OAK) and Reno, Nevada (REV) on 13-14 December, 22-23 December, and 25-26 December 2008. Figures 9a, 9b, and 9c highlight the GOES West Composite Infrared imager overlaid with GFS geopotential heights 5250m and 5500m at 500 hPa during the three frontal passages analyzed for this study. Between the passages of these fronts, the western United States was typified by a persistent cut-off low pressure center that weakened prior to the passage of the second synoptic system.

National Weather Service forecasts prior to actual frontal passage outlined all the ingredients indicative of a damaging high wind event across much of western Nevada to include the eastern slopes of the Sierra Nevada Mountains. Those ingredients, as outlined by the NWS discussion, included evidence of a strong vertical shear profile following frontal passage, presence of a tropopause fold in the mid-high levels, and an increasing 700mb/250mb wind flow over their forecast area. These conditions, associated with the second cold front appearing during the ensemble forecast period, contributed to a measured peak wind in excess of 62.6 m/s over Virginia peak during the period of 18-19 Dec 2008. This location is also the location of the

NWS Reno WRS-88D Doppler weather radar. During the passage of the third cold front, complete radar dome failure occurred when wind speeds were in excess of 42.5 m/s over the same area during the period of 24-25 December. Both cold frontal events produced significant snowfall totals and high winds across widespread areas of western Nevada.

4. Discussion and analysis

4.1 Ensemble Model Parameterization Analysis

In Koracin 2014, a large number of ensemble members is ranked by a specific statistical parameter of success. This fundamental approach highlights the advantage of using a ranking methodology to measure the success with respect to different parameters that can then cede to summed (averaged) overall ranking and ultimately be used as a combined effect of success. The root mean square error (RMSE) was considered one of the important statistical parameters for the entire period with the lowest RMSE having the highest rank 1 (most successful) and subsequently the lower the RMSE the higher is the rank number for the variable being evaluated. The first parameter used as an example to illustrate this method was the predicted and observed temperature at 500 hPa using Reno, Nevada (KREV) rawinsonde data during the period of 12 to 27 December 2008. This data was used as the representative observation for the regional area of Western Nevada. In addition, the degree of success or failure in the prediction of the frontal passages is quantitatively determined through a ranking system that finds the difference between the observed characteristics and structure of the front with the forecasted structure. The features of the front that are quantitatively measured with respect to radiosonde data include the following: 1) magnitude of the temperature drop, 2) duration of the temperature drop, and 3) the

onset of the temperature drop. The quantitative measure was in terms of the absolute value of the differences.   It has been revealed (Buizza et al. (2005) that, due to the use of parameterized physical processes within the ensemble model structure, the addition of a stochastic perturbation to the tendency would complement the representation of the unavoidable random errors associated with the parameterizations of sub-grid scale physical processes.   The amplitude of random errors becomes proportional to the parameterized tendency of errors occurring in the EPS framework. Several diagnostics were described and applied both to single deterministic and ensemble integrations with model results from a set of output products generated from deterministic integrations suggesting a number of probable representative parameterizations. Analysis of ensemble products supported the conclusion that stochastic physics increased the ensemble spread and improved ensemble predictive performance.

When the ensemble mean error is compared with the ensemble spread, and the spread is calculated as the difference of the individual ensemble members and the ensemble mean, the ensemble mean error is expected to be at least equal to the ensemble spread in order for an EPS to remain statistically reliable.

Analysis of the top ten frontal rank data along with RMSE and Bias, showed some similarities but also marked differences in model physical parameterizations.   Although the simulations are notable for their similarities, the differences must be noted which outline other intrinsic processes forcing variability with regards to model accuracy and precision. If we look strictly at the physical parameterizations having the highest ranking number without placing emphasis on the actual model run number, it is hoped that more insight can be applied to model processes. For the Planetary Boundary Layer (PBL), COAMPS and WRF with reference to RMSE and frontal ranking calculations highlighted a nearly concurrent use of physical

parameterizations at the top ten ranking for those two ensemble members. MM5 PBL parameterizations, however, showed marked differences in the use of certain parameterizations occurring within the top-ten ranking when taking into consideration both RMSE and Frontal ranking counts.

4.1.1 COAMPS parameterization performance

Only two PBL parameterizations were used to characterize this specific physical process in the COAMPS model: the "standard" Mellor-Yamada (Mellor and Yamada 1982) and the modified MY versions. Some of the conclusions are as follows.

- The modified MY version does stand out at the top of the list for both RMSE and Frontal ranks.
- The cumulus (dxmeso) and the ice nucleation parameterizations show a similar trend when compared between the two ranks.
- The autoconversion factor does favor 0.004 inputs for the RMSE rank whereas there is an even distribution of process input values highlighted from computed rank values for the frontal rank analysis.

4.1.2 MM5 parameterization performance

Of the three ensemble members, MM5 displays the widest variety of physical parameterizations amongst the four physics option groups.

- For the PBL parameterization, Eta M-Y was the dominate option ranked in the top-five of the RMSE rank while Burk-Thompson option appeared twice among the options noted for the frontal rank method.

- When ranked using the RMSE statistical method, the Reisner 2 micro-physical parameterization appeared as the dominate process, appearing four times in the top-five for that particular model group. This same ensemble model parameterization was identified by the frontal rank analysis as one of the preferred numerical process for liquid-water.

- The Kain-Fritsch cumulus parameterization appeared in the top two spots when considering its relative error characterizations within the top-five physical parameterizations.

- The radiation parameterizations showed the widest variety of options identified as important ensemble mechanisms in the model parameterization performance.

- As a result of both the RMSE and frontal rank analysis, only the Simple cloud parameterization was identified as the dominate physics option for accuracy and precision.

4.1.3   WRF parameterization performance

The WRF was more consistent with regards to physics options appearing when applying RMSE and frontal rank analysis.

- Mellor-Yamada-Janjić PBL and YSU (new MRF) PBL option appear equally within the rank data.

- The WRF microphysics Lin et al. (1983) (MM5:GSFC) was the predominate parameterization, occurring at the top two spots within that model field for the RMSE ranking top-5 for the frontal ranking.

- The Eta microphysics and the Thompson method equally dominated the top five rankswithin that field category.

- The cumulus parameterization used to calculate cumulus properties in WRF favored the Kain-Fritsch method and the Betts-Miller methods as the featured method as determined by both RMSE and frontal ranking analysis. The Kain-Fritsch method, as calculated from the frontal rank analysis process, and the Betts-Miller method appear as the dominate cumulus parameterization as indicated from the RMSE error ranking.

- Within the WRF radiation parameterizations, the WRF radiation showed the largest divergence from a mean value and this condition was most pronounced using the RMSE rank calculation. The Dudhia/RRTM option was predominate with regard to radiation parameterization as identified through frontal rank calculations.
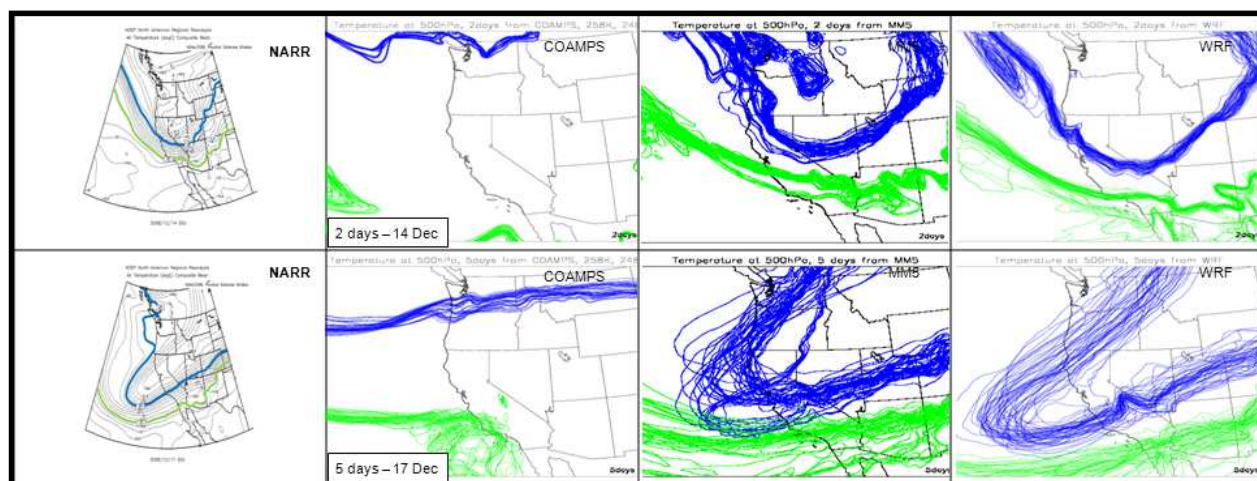
Figure 10: NARR isothem re-analysis at 500 hPa for times 2 and 5 days into the ensemble forecast. Included in this figure are the ensemble member isotherm "Spaghetti" plots for COAMPS, MM5 and WRF. For comparative analysis, the isotherm contour heights at 248^0K

(blue contour) and 258^0K (green contour) for the 500 hPa level are included for the forecast lead times of 2 and 5 days.
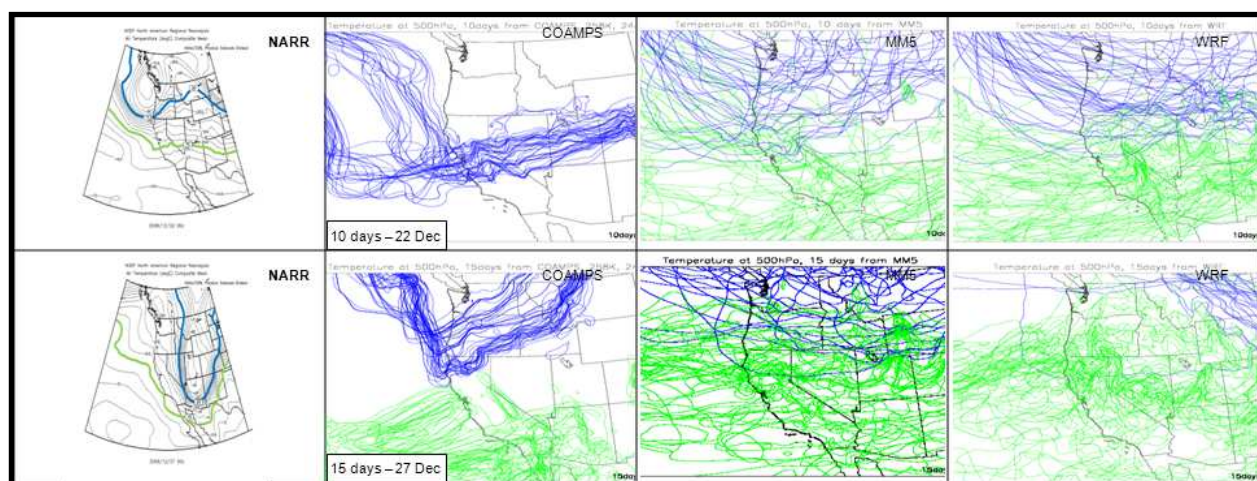
Figure 11: NARR isothem re-analysis at 500 hPa for times 10 and 15 days into the ensemble forecast. Included in this figure are the ensemble member isotherm "Spaghetti" plots for COAMPS, MM5 and WRF. For comparative analysis, the isotherm contour heights at 248^0K (blue contour) and 258^0K (green contour) for the 500 hPa level are included for the forecast lead times of 10 and 15 days.

4.2   Analysis Discussion

Remembering the following empirical rules consistent to popular investigation, number 8 "Never take anything for granted" and rule number 39   "There is no such thing as coincidence," © NCIS – CBS, an analysis and subjective model comparison was conducted of the 153

In order to evaluate frontal ranking for this study, three parameters specific to this frontal ranking analysis were considered and separately ranked.   These included temperature decrease across the boundary (delta-T), the duration of the temperature drop, and the time-phase difference of the cold frontal passage calculated for each of the forecast model outputs of the ensemble members used in this research.   Ensemble forecast model output for each model run was then compared with representative radiosonde observation data for each of the three parameters used in this analysis. For all members in the ensemble forecast group, each front was evaluated separately for rank based on each of these three characteristics. A front rank total was then created by ranking the summation of all analyzed fronts for each ensemble forecast member. Table column arguments corresponding to formula terms included in the rank value formulas are included above formulas for clarity. Figures 12 through 14 illustrate this method as they apply to each step in the frontal rank summing process. The best rank value is assigned to the lowest calculated value for the model predicted $\Delta T_{500\ hPa}$ value and error. A front rank was calculated according to the below formula with N equal to the number of frontal systems being evaluated.

ensemble forecast plots with the associated North American Regional Re-analysis (NARR) for the period when a third frontal system was predicted to pass through the western contiguous United States Steps in the analysis are as follows.

1. Subjective comparison (stochastic analysis) was employed to evaluate RMSE and BIAS computations based on 500 hPa temperature data calculated from the multi-model 153 member ensemble predictions. This also included temperature rise/falls, time interval of temperature decrease/increase,
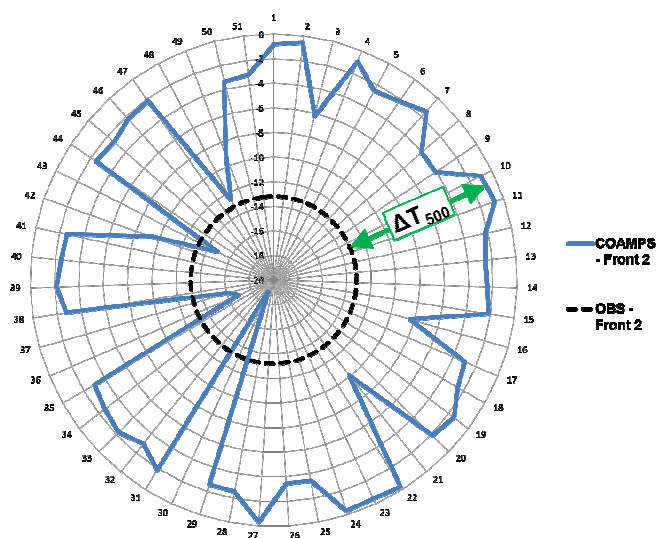
Figure 12: Temperature radial diagram showing ΔT for the 51 COAMPS ensemble simulations for 500hPa temperature data and KREV observational data.

and phase change computation over successive temperature changes from forecasted frontal passages forecasted over the range of ensemble simulations.

2. Focus was directed towards evaluation of total front rank data for the all analyzed cold fronts with the ensemble model stochastic rank calculations (RMSE, BIAS, RMSE+BIAS) rank data was made for each model: COAMPS, MM5, and WRF. Calculated ensemble rank data was first evaluated for the top-five rank data, but was expanded to the top-ten cold-front #3 rank data to better clarify the relative distribution of the top-ten simulation "hits" amongst statistical information calculated from the 3 ensemble members.

3. A more in-depth analysis was performed focusing on the top-ten ensemble member simulations with respect to their corresponding physical parameterizations.

Could computational resources cause variations in ensemble prediction output products? A comparative analysis using NARR and ensemble forecast outputs for the ensemble members COAMPS, MM5, and WRF was used to evaluate the relative accuracy of these three ensemble

members to upper air analysis at the 500 hPa level. Comparing each WRF output yielded at least one forecast output plot which closely represented the NARR analysis towards the end of the forecast model run. But this particular occurrence is consistent for an outlier in the probability density function (PDF). This particular function is used for density of a continuous random variable that describes the relative likelihood for a random variable to take on a given value or outcome

Research has been conducted by Koračin et al. (2014) to assess the value of the different modes of model verification included but was not limited to ranking forecast predictability based on observed and forecast temperature data at the 500 hPa geopotential level. The method defines three main parameters for the evaluation of the frontal passages. The parameters are: temperature drop in degrees Celcius over the period of the frontal passage, time duration in hours of the temperature decrease, and time-phase differences between observed and forecast 500 hPa temperature data were computed and ranked for the 153 ensemble simulations completed during the 15-day forecast period for the multi-model ensemble run.

The preceding frontal rank data, including the root mean square error (RMSE) and BIAS, was used to evaluate the multi- model predictability for the EPS as a whole with statistical rank calculations used to evaluate the frontal contributions to ensemble predictibility.

Statistical BIAS and RMSE are important statistical tools at the disposal of ensemble numerical modelers to make determinations of skill and precision of ensemble numerical products. These verification tools enable researchers to study how certain physical parameterizations affect probabilistic forecasts over a range of mass and thermal gradients and fluxes.
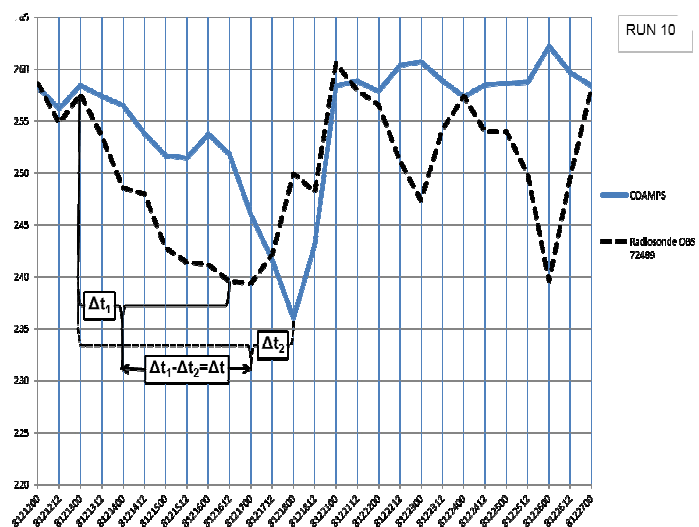
Figure 13: Time-series diagram showing Δt for duration of 500hPa temperature decrease and KREV observational data.
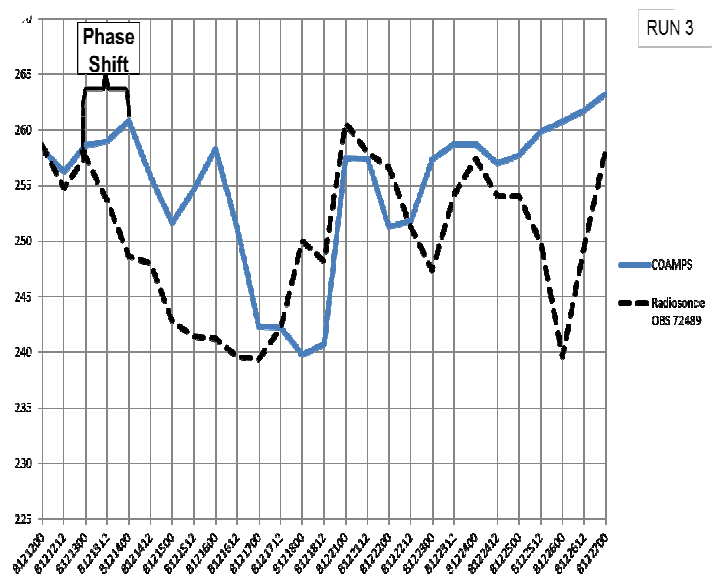
Figure 14: Time-series diagram showing phase-shift calculation for 500hPa trough axis shift and observed shift from KREV observation data over the period of the ensemble simulation.

The Frontal and Total-Model ranking calculations as displayed in table 2 and table 3, utilize three components; delta-T, delta-t, and time phase shift, analyzed to describe the frontal

characteristics over the range of ensemble model runs and displayed in figures 12 through 14. Another input value is Root Mean Square Error (RMSE) and statistical BIAS data rank data. This statistical based rank data is derived from the absolute value of the difference between 500 hPa temperature radiosonde observations and model data. The 500 hPa temperature advection calculations describe the magnitude of the delta-T values for the period of the ensemble forecast.

The RMSE is a commonly occurring mean for field forecasts. It operate on the gridded forecast and observed fields by specially averaging the individual squared difference between the two values temporally over the domain of model runs initialized for each member of the ensemble forecast.

Equations 1 and 2 were used to calculate the RMSE and BIAS for this study, respectively.

$$bias \ = \ \frac{1}{N} \sum_{n=1}^{N} \left(x_n^f \ - \ x_n^o \right) \qquad (1)$$

$$rmse = \left[\frac{1}{N} \sum_{n=1}^{N} \left(x_n^f - x_n^o \right)^2 \right]^{1/2} \qquad (2)$$

Where N is the total number of forecast (x_n^f) /observation (x_n^o) pairs over a given space-time interval, and the superscripts f and o represent the forecast and observed 500 hPa temperature values respectively. RMSE also has the advantage of preserving the units of the format variables used in the models provided and is easily interpretable as a typical error

magnitude for any analysis completed.   In order to evaluate frontal ranking for this study, three parameters specific to this frontal ranking analysis were considered and separately ranked. These included temperature decrease across the boundary (delta-T), the duration of the temperature drop, and the time-phase difference of the cold frontal passage calculated for each of the forecast model outputs of the ensemble members used in this research. Ensemble forecast model output for each model run was then compared with representative radiosonde observation data for each of the three parameters used in this analysis. For all members in the ensemble forecast group, each front was evaluated separately for rank based on each of these three characteristics. A front rank total was then created by ranking the summation of all analyzed fronts for each ensemble forecast member. Table 1 contains formulas used to calculate the temperature change between observed and modeled data for 500hPa over KREV during passage of associated 500 hPa upper trough. The temperature values were then used as the basis input values for the rank value formulas. The best rank value is assigned to the lowest calculated value for the model predicted ΔT_{500} values and error. A front rank was calculated according to the below formula with N equal to the number of frontal systems being evaluated.

     Frontal ranking for all frontal systems evaluated during the period of the ensemble model runs   was calculated in order to assess the relative predictability of certain ensemble simulations. This assessment was applied to the frontal analysis within the period with which the ensemble forecast plots were evaluated at their maximum ensemble spread. It was the intent of this analytical approach to observe whether individual model simulations among the ensemble members actually predicted the regional mesoscale phenomenon as displayed with the associated North American Regional Reanalysis (NARR) plot.   Over the spectrum of the ranking data,

Table 1(a) The following formulas were used to calculate the temperature decrease between observed and modeled data for 500 hPa over KREV during passage of associated 500hPa upper trough. (b) This formula was used to calculate the duration of forecast Temp500hPa decrease during period of passage of 500 hPa upper trough over KREV. (c) The final formula was used to calculate the phase shift of the 500 hPa trough axis when compared to observed radiosonde data over KREV.

(a) Dtemp	Dtemp(RAOB – model data)	ABS(Dtemp)
OBS500 – FCST500 = ΔTEMP500 = [ΔTEMP500]abs		
(b) Dtime	Dtime(RAOB − model data)	ABS(Dtime))
$DTime_{obs}$ - $DTime_{fcst}$ = [Δ Time]$_{abs}$		
(c) Shift	dShift (RAOB − model data)	ABS(dShift)
$Shift_{obs}$ − $Shift_{500}$ = [Δ Shift500]abs		

calculations for the three forecast fronts simulated by the EPS models, the top ten front rankingvalues were compared with calculated RMSE, BIAS, and RMSE+BIAS to create a comparison scale for all EPS simulations. The selected EPS simulation having the most representative ensemble forecast plots could then be compared to an associated NARR output plots.

Introduced earlier within this section was a discussion of the ensemble model spread at the 10-day and 15-days stage of the multi-model simulations. This property of multi-model ensembles at this stage of the model simulations was previously highlighted by Figure 10 and 11, illustrating the considerable model simulation spread that developed as a result of non-linear

Ensemble Frontal Temperature Flux (ΔT) for Cold Front 1

COAMPS - Front 1
MM5 - Front 1
WRF - Front 1
OBS - Front 1

Ensemble Frontal Temperature Flux (ΔT) for Cold Front 2

COAMPS - Front 2
MM5 - Front 2
WRF - Front 2
OBS - Front 2

Ensemble Frontal Temperature Flux (ΔT) for Cold Front 3

COAMPS - Front 3
MM5 - Front 3
WRF - Front 3
OBS - Front 3
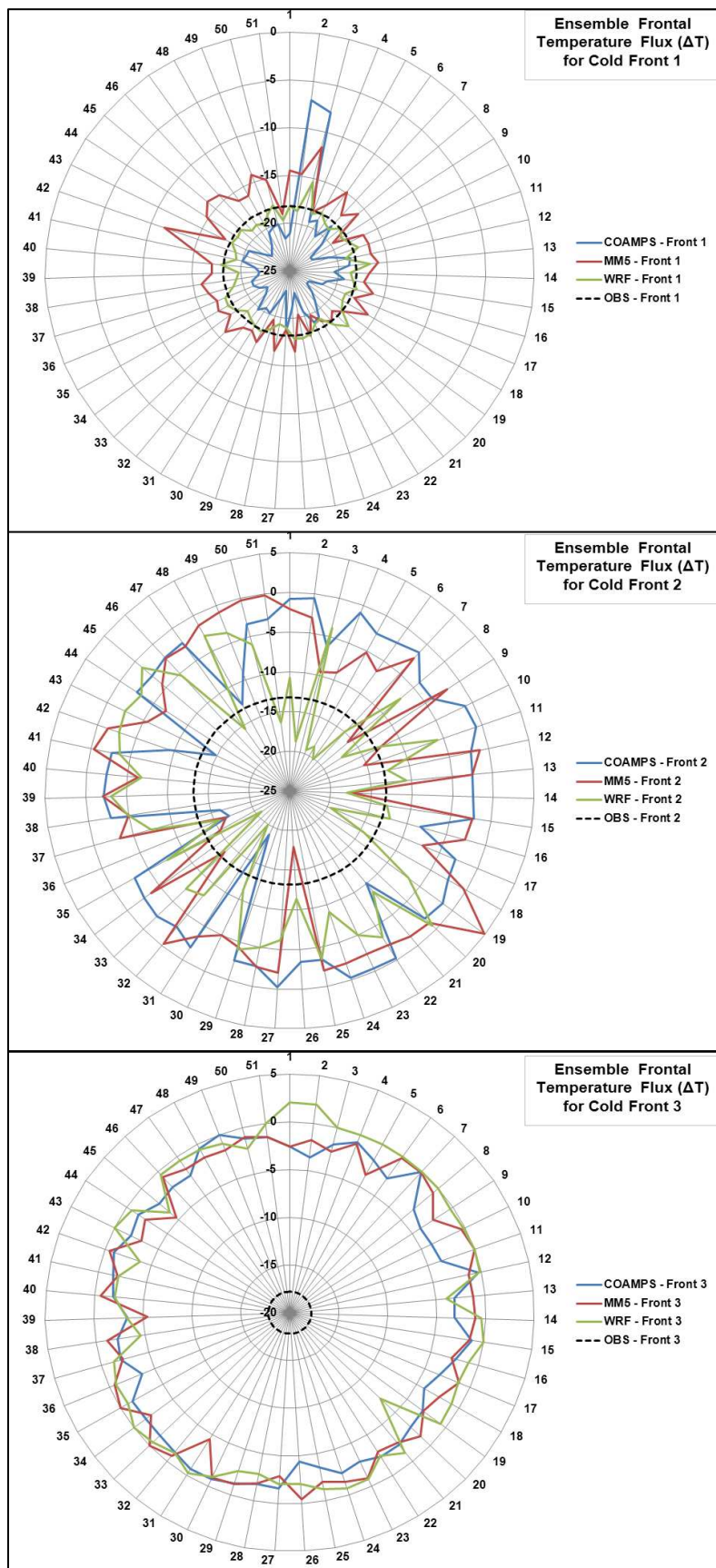
dynamical processes embedded in the model simulation cycle. In Figure 15, each temperature profile plotted and included in the radial diagrams for the 51 ensemble model simulations plotted a continual increase in temperature variability as the model simulation process progressed forward into the later phases of the ensemble run. Here, the three panel temperature radial diagrams profiled how non-linear processes reduced the symmetry of the temperature contours featured for each of the three frontal passages. Towards the last 72

Figure 15: The three panel radial plots for the ensemble forecast temperature difference for each of the three cold fronts identified during the period of the ensemble simulation. This panel shows notable variations in 500 hPa temperature as nonlinear processes begin to affect model output towards the finish of the ensemble simulation.

hours of the ensemble model run, during the approximate period of the passage of the third cold

front, ΔT values no longer approach or cross over the observed ΔT values showing a large temperature differences towards the end of the ensemble simulation.

Analysis of a comparison of frontal rank data to statistical RMSE, BIAS, and RMSE+BIAS calculated from observed and predicted 500 hPa temperature variations for all three models featured in the multi-model EPS are presented in this research.

Referring to the three panel display, Figure 16, the radial temperature profile for the first cold front illustrates the thermal gradient

Figure 16: The three panel radial plots for COAMPS forecast temperature flux for each of the three cold fronts identified during the period of the ensemble simulation. By passage of the third cold front, little or no temperature change is apparent towards the finals stages of the model simulations.
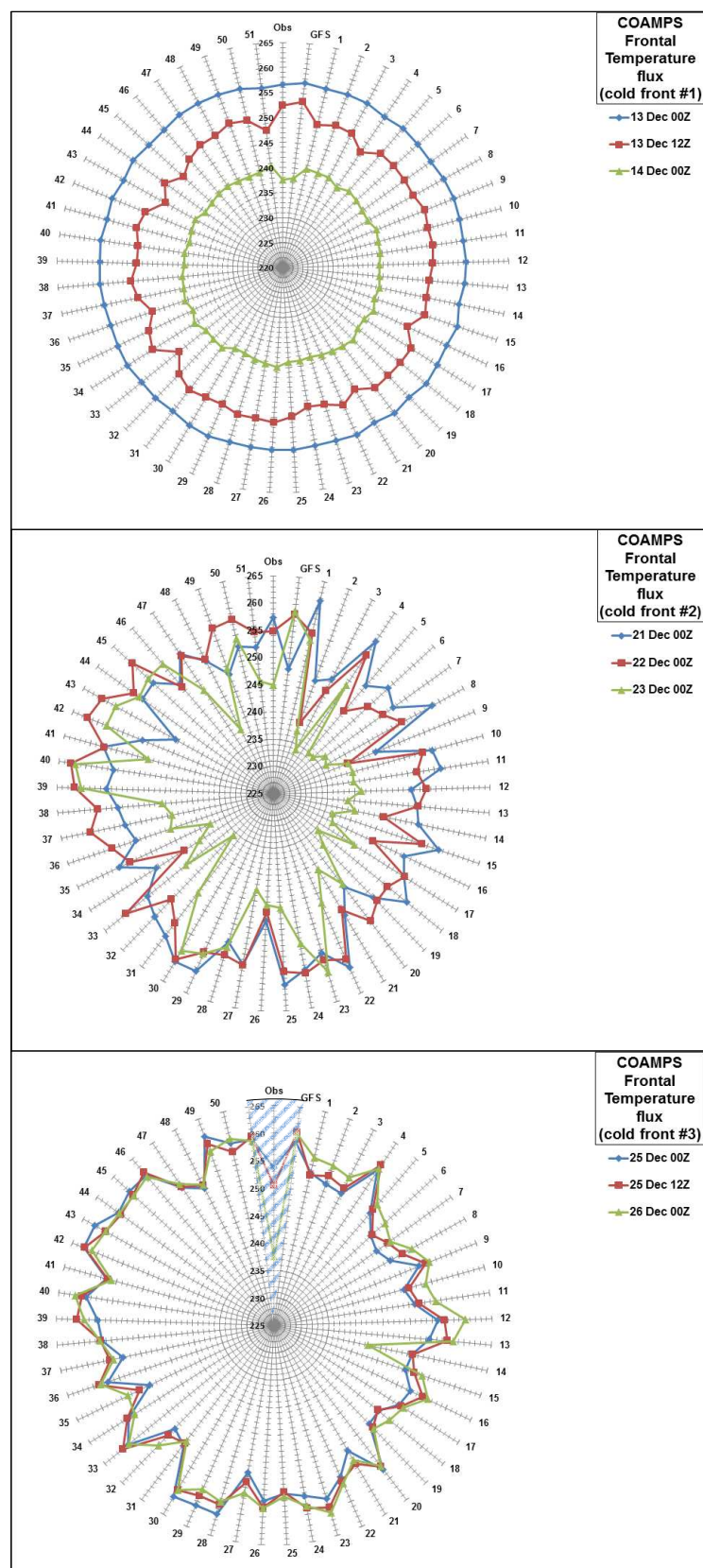
and cold air advection which is characteristic of a cold frontal passage. The 500 hPa temperature predictions for the 51 model simulations originating from the COAMPS ensemble member shows a relatively usual temperature decrease consistent with the initial period of the forecast simulation. Progressing from cold front 1 to cold front 2, frontal temperature gradient profile values at 500 hPa begin to vary greatly with 51% of the ensemble simulations continuing to show a horizontal thermal gradient to colder temperature values for that particular model simulation. By the time the third cold front moves through western Nevada, the COAMPS modeled forecast temperatures for the 500 hPa level showed a considerably weakened thermal gradient inconsistent with what was forecasted for the first cold front. Instead the model predictions show weak or no cold air advection as compared to the first cold front influencing the model output. Figure 16 also illustrates how the COAMPS model almost completely missed the third cold front. The triangular area marked in blue highlights the observed 500 hPa temperature decreases associated with both the cold front and upper trough passages. A modeled thermal gradient for the third observed cold front is practically nonexistent over the range of the simulation runs. Does this show a possible discrepancy within the model parameterizations used in the COAMPS model itself or can this be used as evidence for . the use of multi-model ensemble prediction systems to accurately ascertain the probabilistic outcomes within the mesoscale regime?

Numerical models often focus on a limited special domain in order to achieve high resolution for a reasonable calculation time, or a feasible physical size. Such limitations in the size of the model domain imply that the mechanical and thermal evolution of the area located outside the model domain need to be taken into account through boundary conditions. This

(a)							
Rank Count	run	COAMPS Front1 rank	run	MM5 Front1 rank	run	WRF Front1 rank
1	run7	10	run19	5	run24	4
2	run12	11	run24	5	run5	6
3	run13	12	run21	7	run16	6
4	run5	13	run22	15	run26	6
5	run23	14	run27	15	run40	6
6	run22	15	run17	16	run1	11
7	run15	16	run4	18	run8	11
8	run4	17	run31	18	run31	11
9	run32	18	run20	19	run34	11
10	run50	19	run39	19	run10	17
(b)						
Rank Count	run	COAMPS Front2 rank	run	MM5 Front2 rank	run	WRF Front2 rank
1	run30	14	run26	5	run14	13
2	run36	15	run36	7	run5	14
3	run37	16	run8	8	run9	15
4	run43	17	run35	10	run17	18
5	run21	19	run10	12	run31	20
6	run16	22	run30	19	run51	21
7	run3	23	run5	20	run1	23
8	run48	28	run11	26	run47	23
9	run42	31	run31	26	run13	24
10	run49	32	run3	27	run34	24
(c)						
Rank Count	run	COAMPS Front3 rank	run	MM5 Front3 rank	run	WRF Front3 rank
1	run36	7	run18	15	run42	22
2	run26	11	run37	22	run37	26
3	run20	22	run19	25	run38	28
4	run23	25	run22	25	run27	29
5	run14	26	run27	25	run39	32
6	run9	27	run16	28	run28	33
7	run10	28	run21	31	run29	34
8	run47	30	run9	32	run16	39
9	run2	31	run12	36	run50	41
10	run25	32	run25	37	run32	43

implies that a modification of the boundary conditions changes the assumptions that are made

Table 2: The top-ten front rank data for each ensemble member and associated (a): Front 1, (b): Front , and (c): Front 3 is included below to include the representative simulation run used to select BIAS,RMSE and BIAS+RMSE rank values for error-trend analysis.

concerning the thermal and mechanical state of the region outside the model domain. In other words, without control of lateral boundary conditions at the end of a data assimilation window, observations close to the lateral boundaries that influence the initial conditions or information related to phenomena observed well inside an inner domain during this latter part of the data assimilation period may be lost and worsen the subsequent forecast inside the domain. This may be the case with regards to the Navy's Operational Global Atmospheric Prediction System (NOGAPS) coarse model data at the data assimilation period consequently affecting Coupled Ocean/Atmosphere Mesoscale Prediction System (COAMPS) forecast outputs during the period **of the simulation run**

4.3 Probabilistic analysis of frontal rank data with statistical measures

Frontal rank data for all three cold fronts calculated earlier was applied to BIAS, RMSE, and RMSE+BIAS derived from 500 hPa ΔT values generated from the 153 simulation multi-model ensemble forecast run. The results from this analysis showed error trends which concurred with the ensemble spreading displayed from the 500 hPa geopotential and temperature spaghetti plot results, Figures 10 and 11, for the 2, 5, 10, and 15 day lead times for the ensemble simulation runs conducted for the period of 12-27 December 2008. (Koracin et al. 2014). Tables 2 and 3 are included in this section to clarify the selection of the top-ten frontal rank data from calculated tabular data for the BIAS, RMSE, and RMSE+BIAS and then plotted in yellow to highlight statistical data error trends.

Table 3: The top-ten Total-Model rank data for each ensemble member and associated front is included above to include the representative simulation run used to select BIAS,RMSE and BIAS+RMSE rank values for error-trend analysis.

Rank Count	total front1	RUN	COAMPS Front1 rank	total front1	RUN	MM5 Front1 rank	total front1	RUN	WRF Front1 rank	Total-Model Front1
1	4	run5	13	11	run5	24	2	run5	6	17
2	16	run24	27	1	run24	5	1	run24	4	18
3	14	run31	25	7	run31	18	6	run31	11	27
4	8	run4	17	7	run4	18	14	run4	24	29
5	6	run22	15	4	run22	15	27	run22	40	37
6	1	run7	10	11	run7	24	27	run7	40	39
7	20	run26	36	17	run26	37	2	run26	6	39
8	24	run40	40	13	run40	28	2	run40	6	39
9	9	run32	18	21	run32	42	14	run32	24	44
10	22	run17	38	6	run17	16	21	run17	32	49

Rank Count	total front2	RUN	COAMPS Front2 rank	total front2	RUN	MM5 Front2 rank	total front2	RUN	WRF Front2 rank	Total-Model Front2
1	2	run36	15	2	run36	7	17	run36	34	21
2	1	run30	14	6	run30	19	17	run30	34	24
3	15	run17	42	10	run17	27	4	run17	18	29
4	12	run8	39	3	run8	8	15	run8	31	30
5	23	run5	61	7	run5	20	2	run5	14	32
6	13	run26	40	1	run26	5	20	run26	43	34
7	27	run31	64	8	run31	26	5	run31	20	40
8	11	run9	35	32	run9	84	3	run9	15	46
9	20	run1	58	20	run1	52	7	run1	23	47
10	7	run3	23	10	run3	27	34	run3	78	51

Rank Count	total front3	RUN	COAMPS Front3 rank	total front3	RUN	MM5 Front3 rank	total front3	RUN	WRF Front3 rank	Total-Model Front3
1	13	run19	36	3	run19	25	16	run19	51	32
2	14	run22	37	3	run22	25	15	run22	48	32
3	25	run27	57	3	run27	25	4	run27	29	32
4	33	run37	75	2	run37	22	2	run37	26	37
5	3	run20	22	24	run20	61	11	run20	44	38
6	23	run39	56	10	run39	37	5	run39	32	38
7	30	run16	70	6	run16	28	8	run16	39	44
8	4	run23	25	18	run23	58	23	run23	65	45
9	10	run25	32	10	run25	37	26	run25	70	46
10	23	run28	56	17	run28	56	6	run28	33	46

Figures 17 through 34 are arranged according to the representative cold front and ensemble member. The blue block arrows overlaid onto the representative BIAS, RMSE, and BIAS+RMSE data displays indicate the error trends analyzed subjectively according to the general density of the frontal and Total-Model Top-Ten rank inputs from Table 2 and Table 3, The top-ten tabular data is highlighted in yellow for each plotted statistical rank data annotated for each error-trend   The density of yellow highlighted bars concentrated in either a left or right side of the statistical rank display indicates the direction of the decreasing or increasing error

values. Left directed arrows indicate trends toward approximate decreasing error; right directed arrows are set in the direction of approximate increasing error, and block arrows pointing in both directions indicate an approximate neutral condition that exists over the range of simulations vs. BIAS, RMSE, and RMSE+BIAS statistical error values. Neutral results in this study refer to the observed error-trend results equally distributed across the range of BIAS, RMSE, and BIAS + RMSE error rank diagrams for each of the ensemble members. Therefore, an error-trend result arrow pointing towards the left sides of the diagram indicate a lower error-trend while arrows directed to the right indicate an increasing error-trend for that representative classification diagram.

From the data presented in Figures 17 through 21, simulations selected from the top ten frontal rank data generally lead to lower error values for BIAS, RMSE, and RMSE+BIAS. This trend is consistent with minimal ensemble spread as exhibited from the day-2 and day-5 spaghetti plots in figure 10. Individual model analysis for both Front and Total-Model plots for Front 1 showed a neutral trend condition for the COAMPS model while the MM5 and WRF models trended towards values indicating lower error for BIAS, RMSE, and BIAS+RMSE. Therefore, from the above analysis, MM5 and WRF error trend comparisons for front 1 illustrate an ability to verify probabilistically with general confidence that the multi-model ensemble is performing generally good with regards to characterizing 500 hPa temperature forecasts. This is in contrast to the COAMPS model which showed ambiguous but neutral results for Front 1 with error trends not directed either in less or greater eroor when compared to its associated partner ensemble members. Still, MM5 displayed the best performance with error trends direct towards less error for Front and Total-Model Front 1 analysis plots.

Error trends derived from Figures 23 through 28 and frontal rank data selected from the top ten frontal rank data for the front 2 generally trended toward lower error values for BIAS, RMSE, and RMSE+BIAS for all three ensemble members. It is interesting that this trend occurs during the period of the day-10 ensemble spaghetti plot, Figure 11, where model ensemble spread increases initially. By this time, the passage of the cold front 2 is also taking place during this initial period of the day-10 500hPa temperature spaghetti plot. Upon further examination, the MM5 model exclusively trends toward lower error trend values for both Front and Total-Model for this second front. This is in contrast to its performance for cold front 1 for the Front 1 error trend for BIAS, RMSE, and BIAS+RMSE. The WRF and COAMPS models mostly continued a trend toward decreasing error for Front 2, but the COAMPS remained generally neutral for Front 2 Total-Model with the error trend distributed evenly over the rank values for BIAS, RMSE, and BIAS+RMSE.

Values for BIAS, RMSE, and BIAS+RMSE, a neutral condition is apparent upon direct evaluation of RMSE error for both models. MM5 performance is counter intuitive to comparisons for the cold front 2 tendencies. This further amplifies a sense of confidence with regard to the ensemble performance characteristics when using the associated day 10 spaghetti plots illustrated in Figure 11.

Now looking closer at figures 23 through 28, the MM5 and WRF model Total-Model analysis for front 2 showed the best performance for error trends toward lesser error similar to the MM5 Total-Model model analyzed for front 1. This trend towards reduced error was evident for all three statistical arguments; BIAS, RMSE, and BIAS+RMSE. The COAMPS model

Total-Model analysis for front 2 continued to display an error trend similar to the front 1 analysis displaying no definite trend in either direction as related to less or greater rank values. The top-ten front 2 rank inputs included model run error "hits" evenly distributed over the range of statistical error ranks. It is remarkable that a direct comparison of the MM5 and WRF ensemble spaghetti plots for 500 hPa temperature and height, the trend analysis for this dataset showed little correlation. Synoptic features displayed on the day 10, 22 December spaghetti plots for the COAMPS model, however, showed increased trough structure. Something that was not readily apparent from direct observations of MM5 and WFR outputs

Figure 17: Ensemble Front 1 Top Ten rank data highlighted in yellow used for selections of associated BIAS rank data. COAMPS and MM5 displayed evenly distributed error-trend. Bias trends for the WRF model indicated a probability of decreased ensemble error when considering front 1 characteristics.

Figure 18: Ensemble Total-Model Top Ten rank data for Front 1 highlighted in yellow used for selections of associated BIAS rank data. COAMPS and WRF displayed evenly distributed error-trend. Bias trends for the MM5 model indicated a probability of decreased ensemble error relative to front 1.
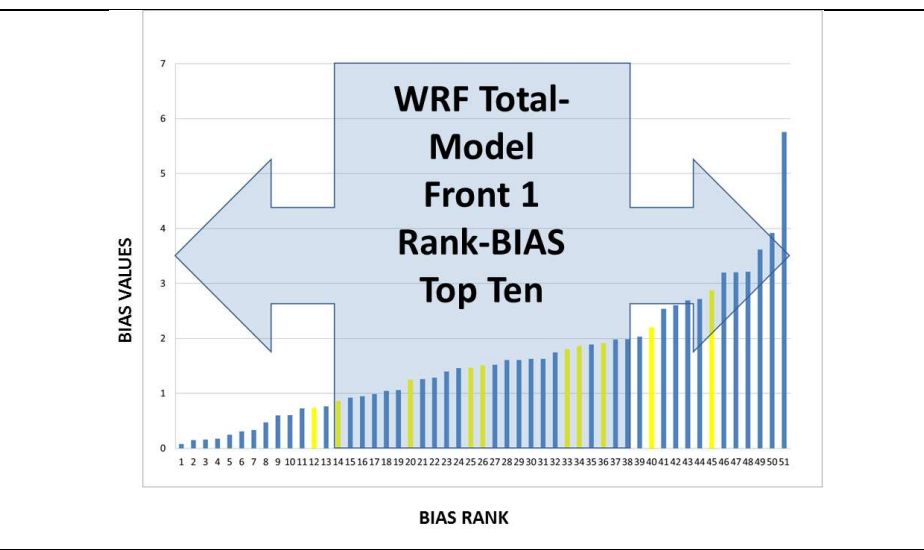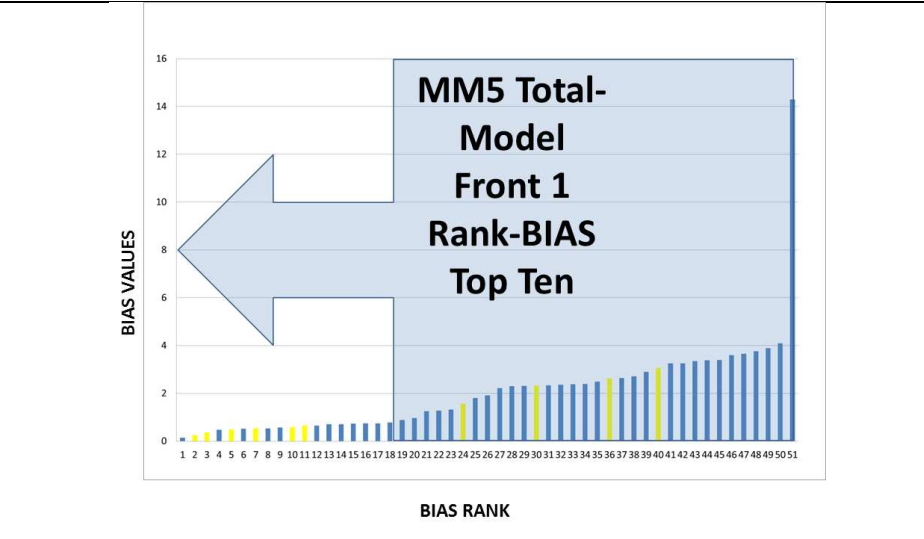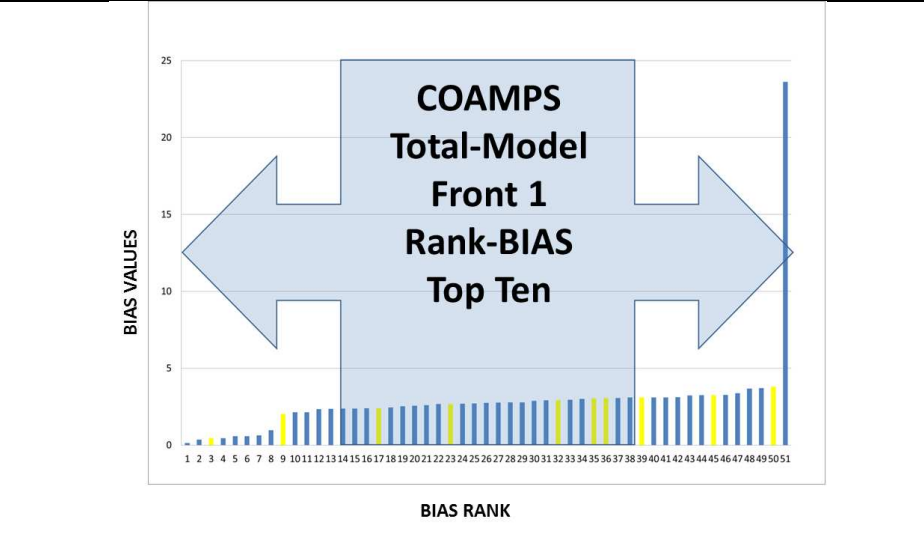
Figure 19: Ensemble Front 1 Top Ten rank data highlighted in yellow used for selections of associated RMSE rank data. COAMPS, MM5, and WRF RMSE error-trend indicated a pro-bability of decreased ensemble error asso-ciated with front 1.
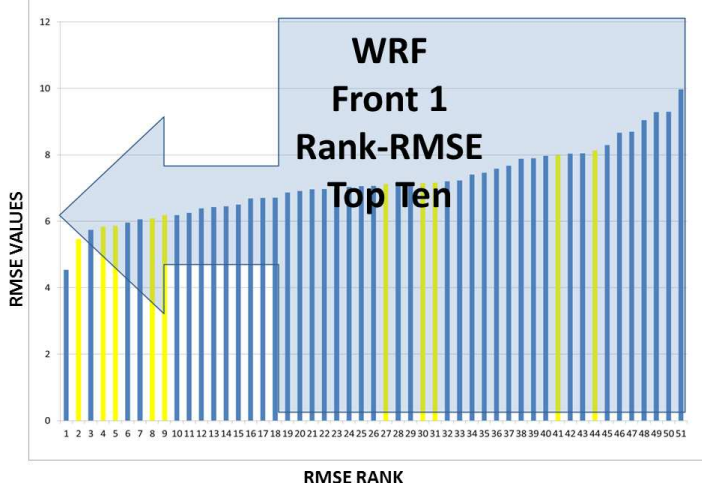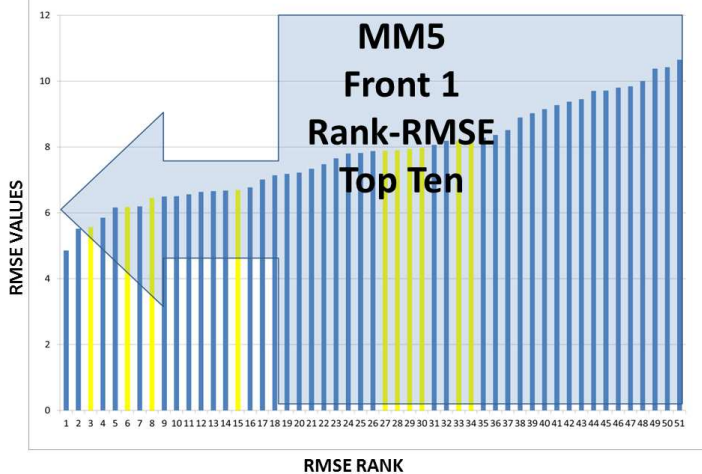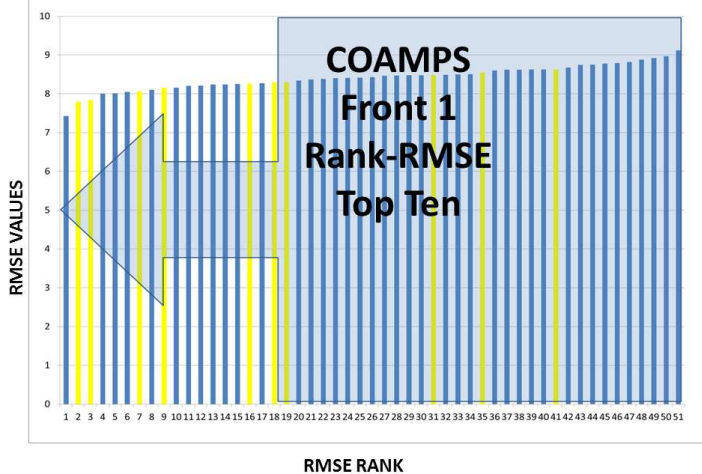
Figure 20: Ensemble Total-Model Top Ten rank data for Front 1 highlighted in yellow used for selections of associated RMSE rank data. COAMPS and WRF displayed an evenly distributed error- trend. RMSE trends for the MM5 model indicated a probability of de-creased ensemble error associated with front 1.
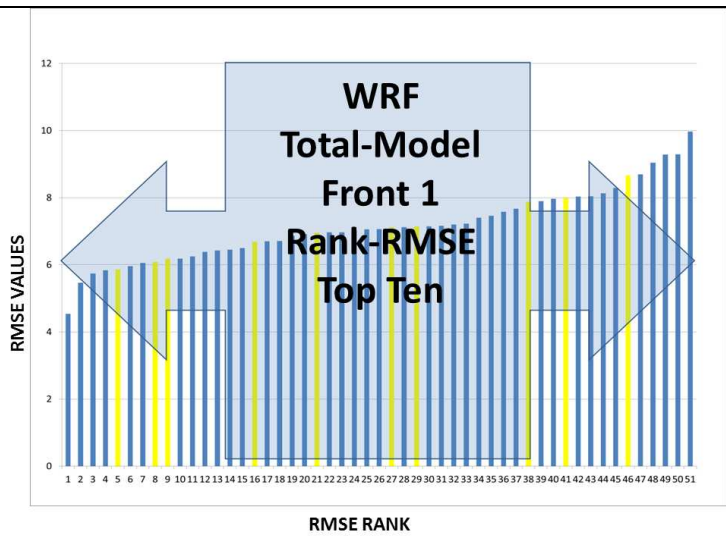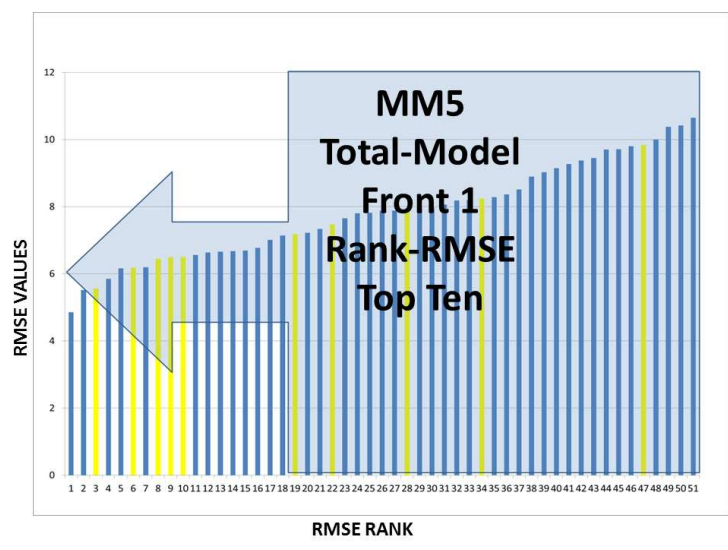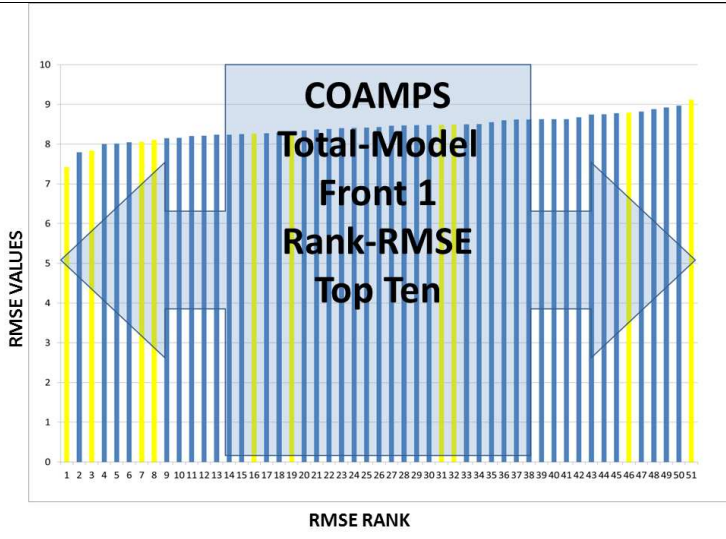
Figure 21: Ensemble Front 1 Top Ten rank data highlighted in yellow used for selections of associated BIAS+RMSE rank data. COAMPS and MM5 displayed an evenly distributed error-trend. Bias+ RMSE trends for the WRF model indicated a probability of de-creased ensemble error associated with front 1.
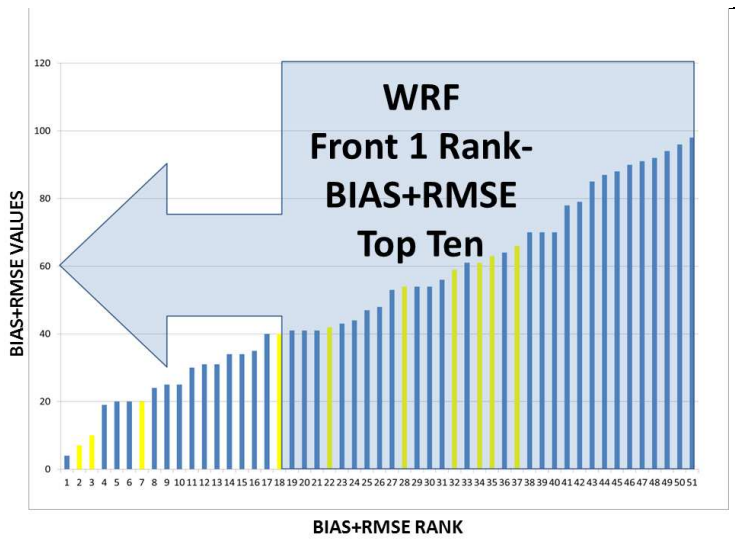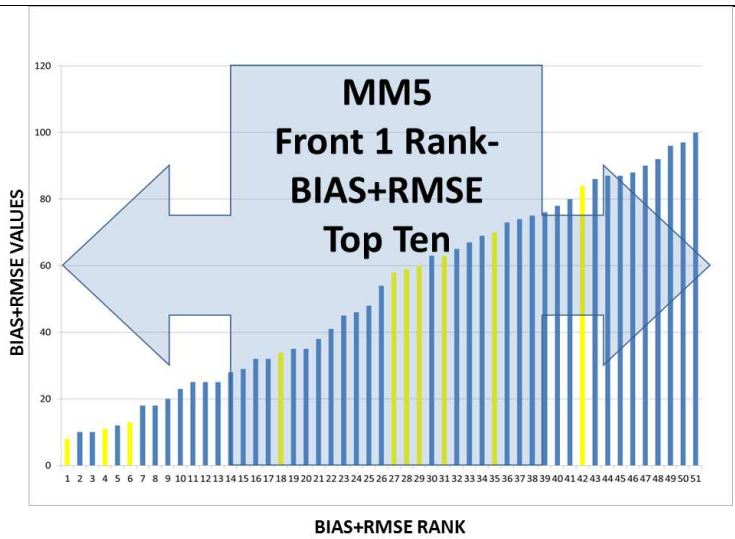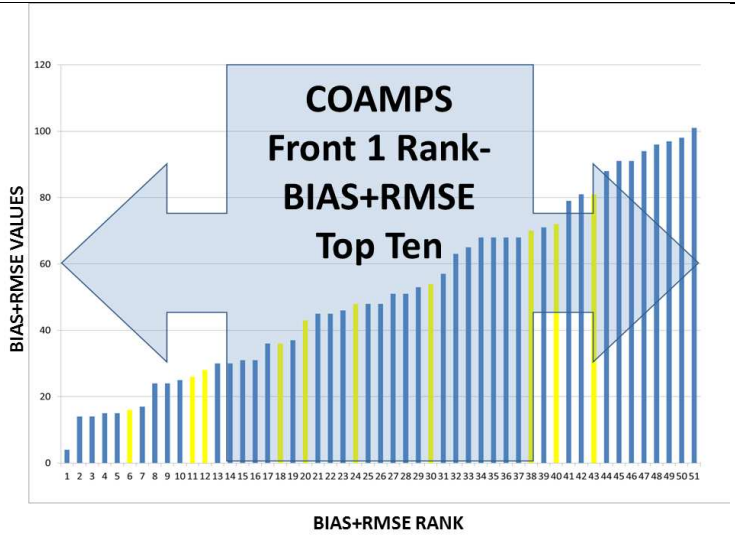
Figure 22: Ensemble Total-Model Top Ten rank data for Front 1 highlighted in yellow used for selections of associated BIAS+ RMSE rank data. COAMPS and WRF displayed an evenly distributed error- trend. BIAS+RMSE error-trends for the MM5 model indicated a probability of decreased ensemble error associated with front 1.
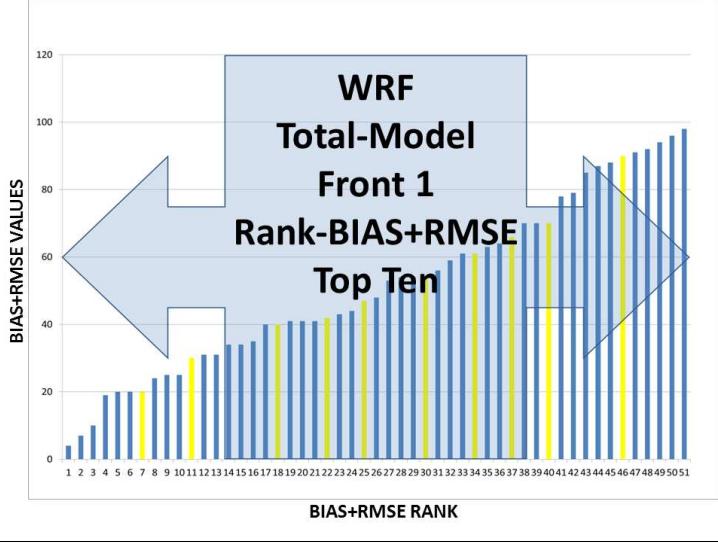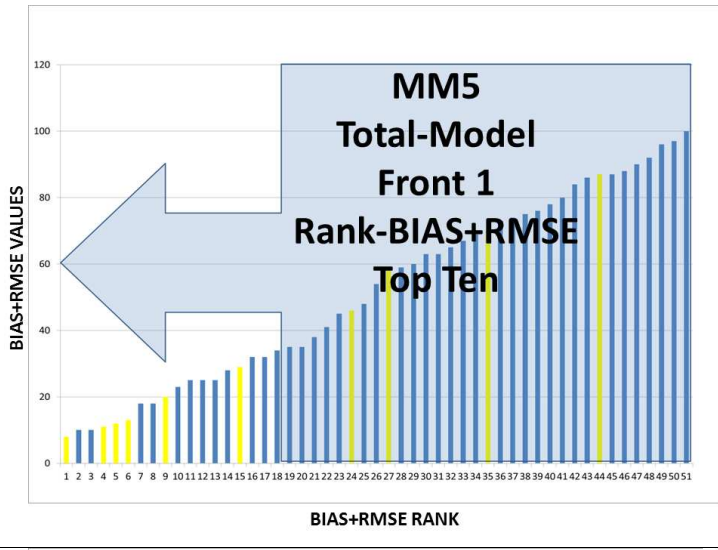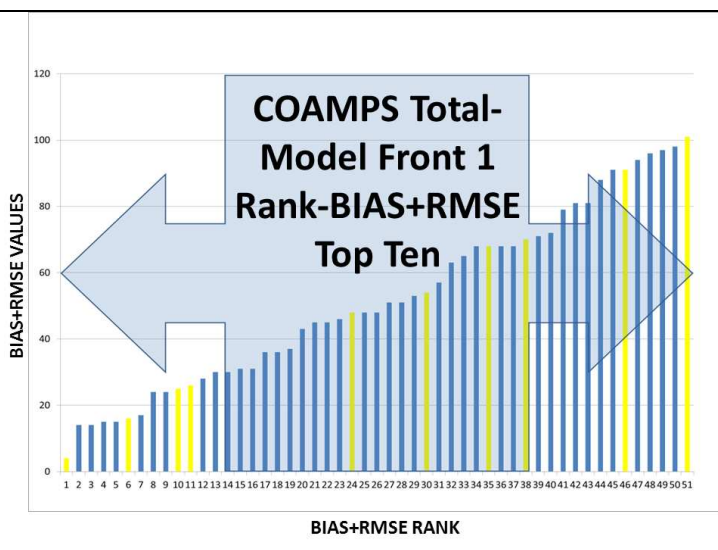
Figure 23: Ensemble Front 2 Top Ten rank data highlighted in yellow used for selections of associated BIAS rank data. All ensemble members displayed BIAS error trend results indicating a probability of de-creased ensemble error relative to front 2.
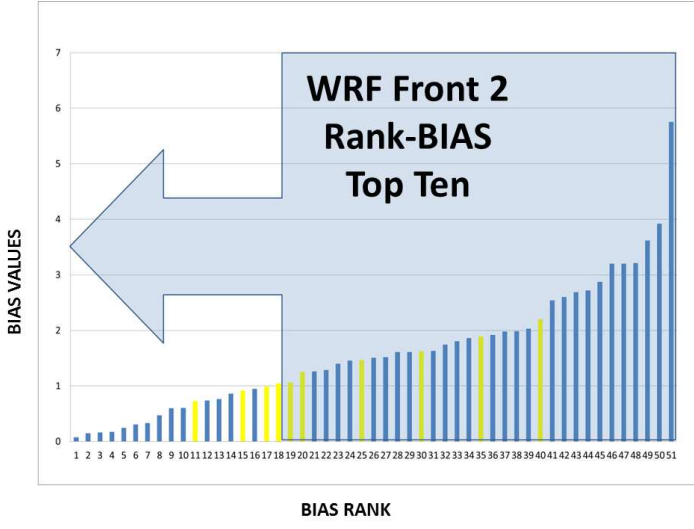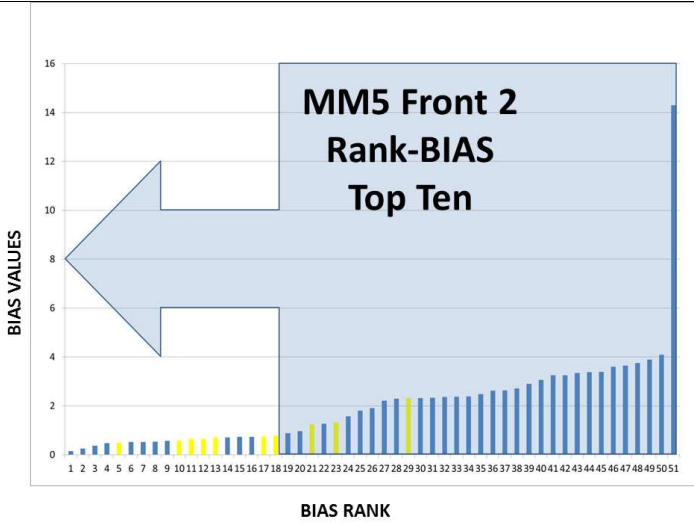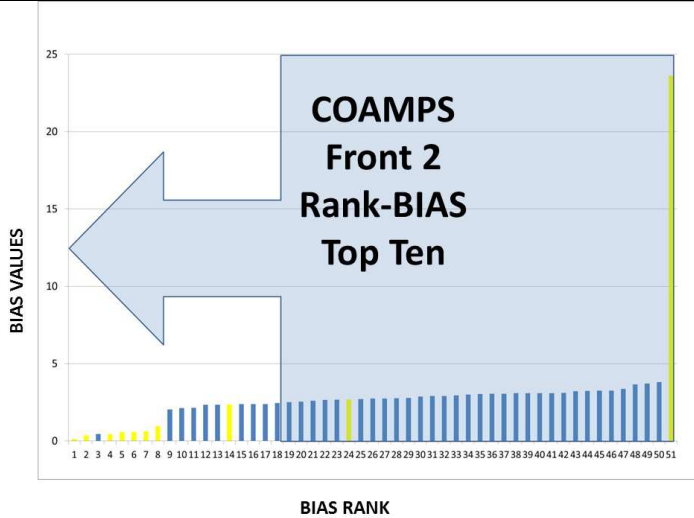
Figure 24: Ensemble Total-Model Top Ten rank data for Front 2 highlighted in yellow used for selections of associated BIAS rank data. COAMPS displayed an evenly distributed error- trend. BIAS error-trends for the MM5 and WRF models indicated a probability of decreased ensemble error associated with front 2.
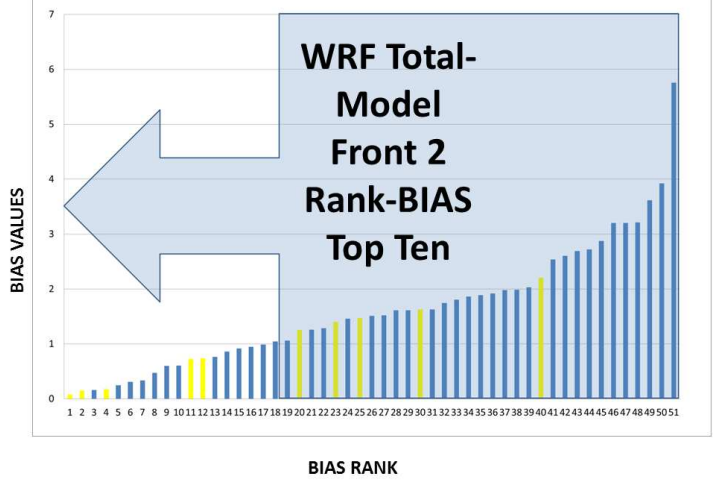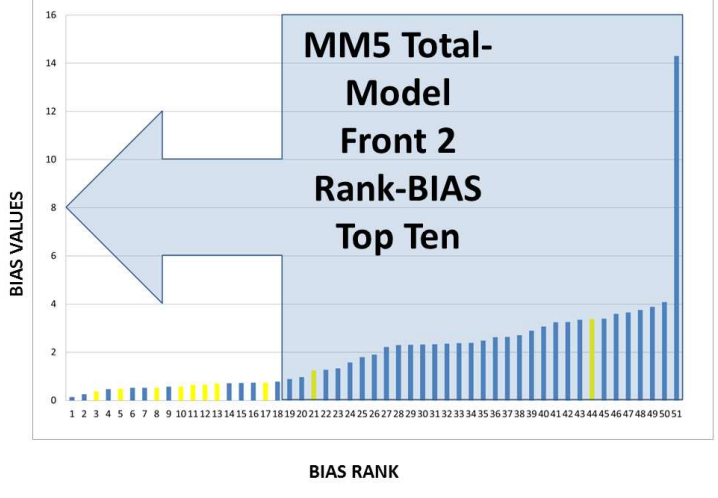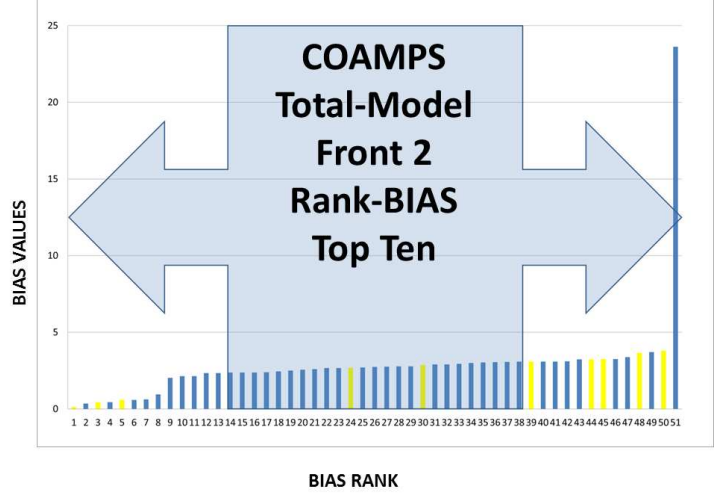
Figure 25: Ensemble Front 2 Top Ten rank data highlighted in yellow used for selections of associated RMSE rank data. COAMPS and WRF displayed an evenly distributed error-trend. RMSE error-trends for the MM5 model indicated a probability of decreased ensemble error associated with front 2.
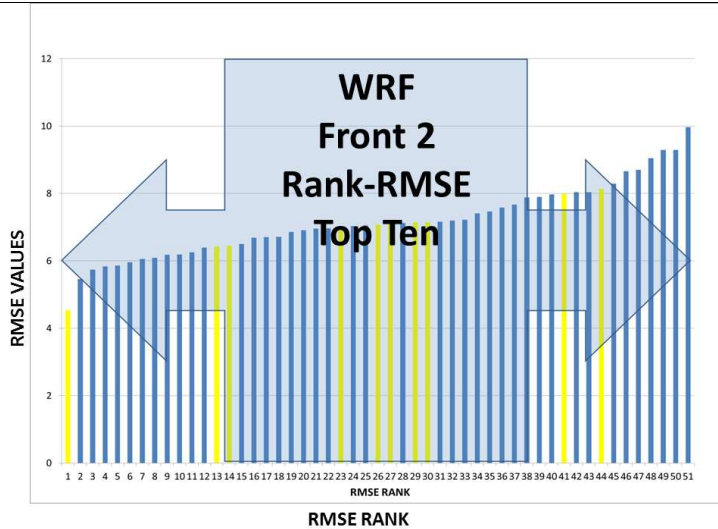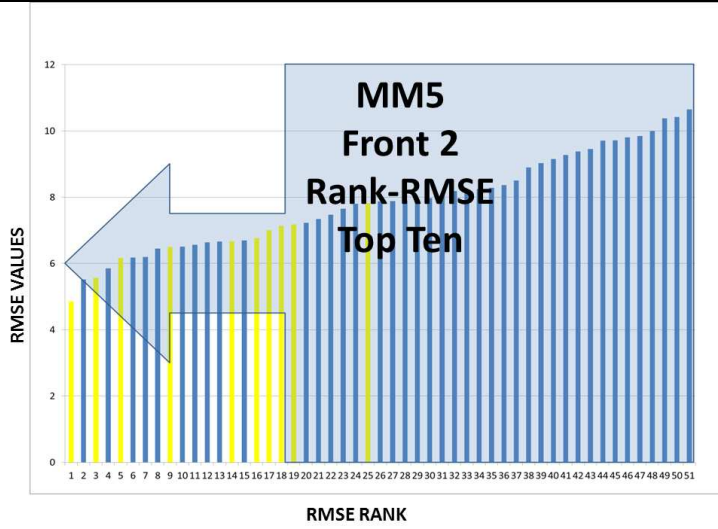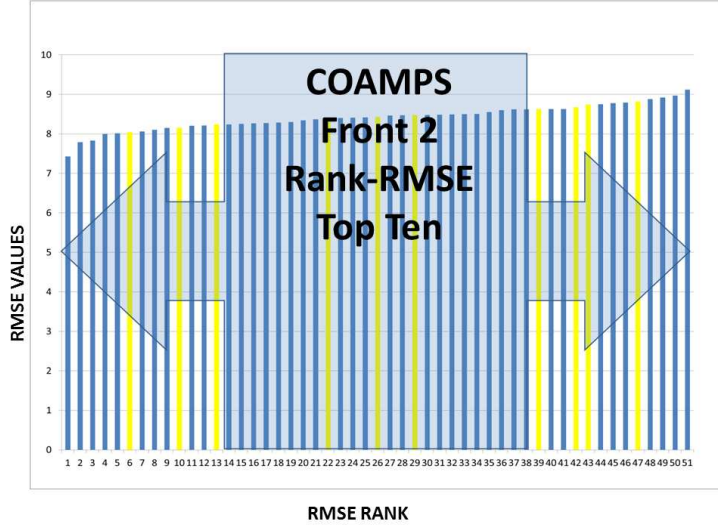
Figure 26: Ensemble Total-Model Top Ten rank data for Front 2 highlighted in yellow used for selections of associated RMSE rank data. COAMPS displayed an evenly distributed error- trend. RMSE error-trends for the MM5 and WRF models indicated a probability of decreased ensemble error associated with front 2.
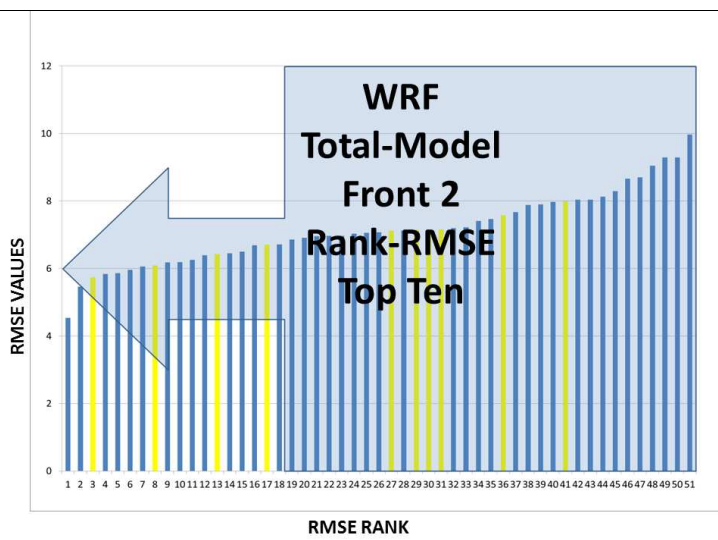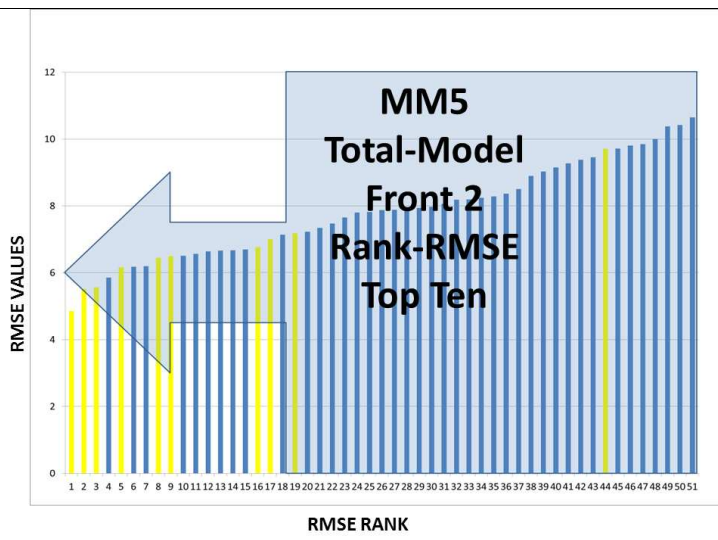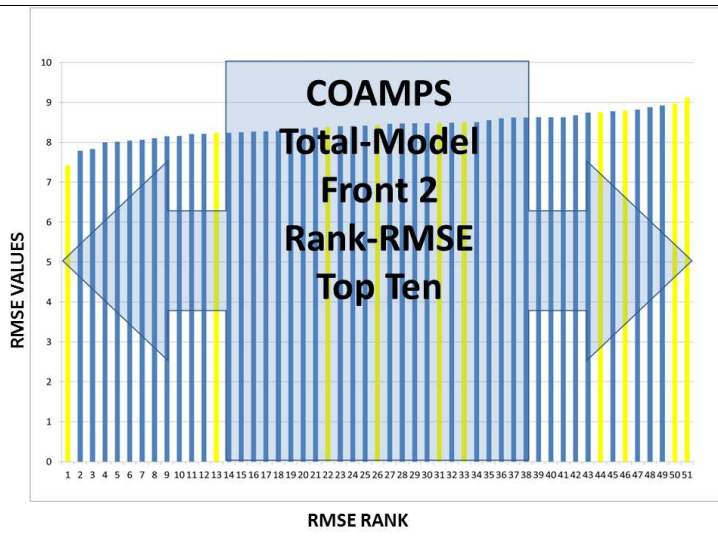
Figure 27: Ensemble Front 2 Top Ten rank data highlighted in yellow used for selections of associated BIAS+RMSE rank data. COAMPS and WRF indicated a probability of decreased ensemble error associated with front 2 when considering BIAS+RMSE rank data. Error-trends for the MM5 model displayed an evenly distributed error-trend for BIAS+RMSE rank data associated with front 2.
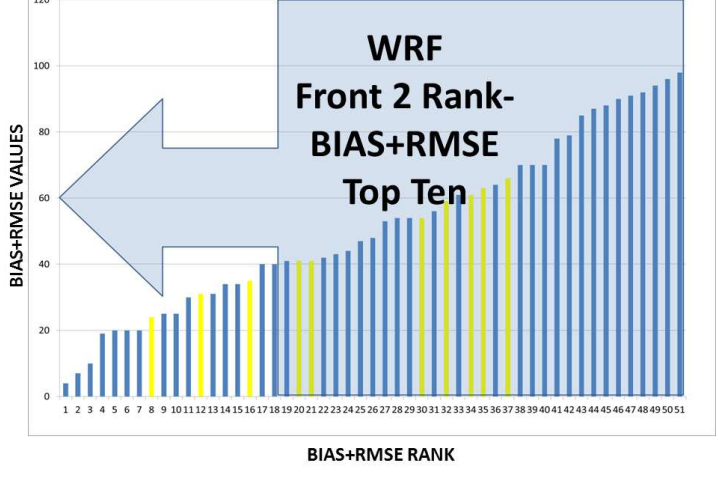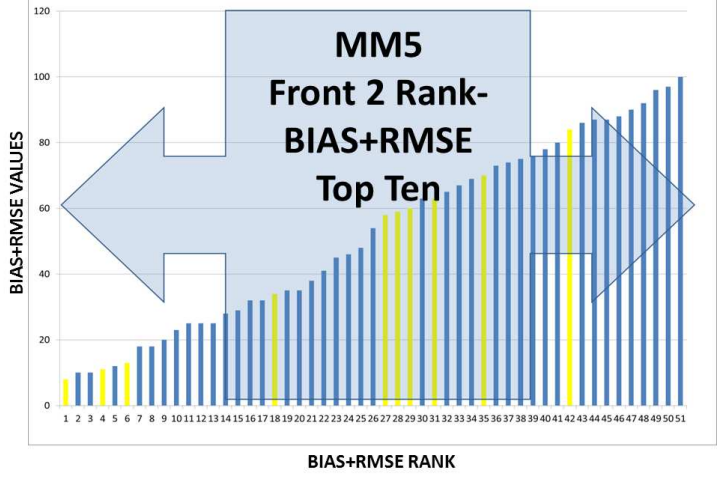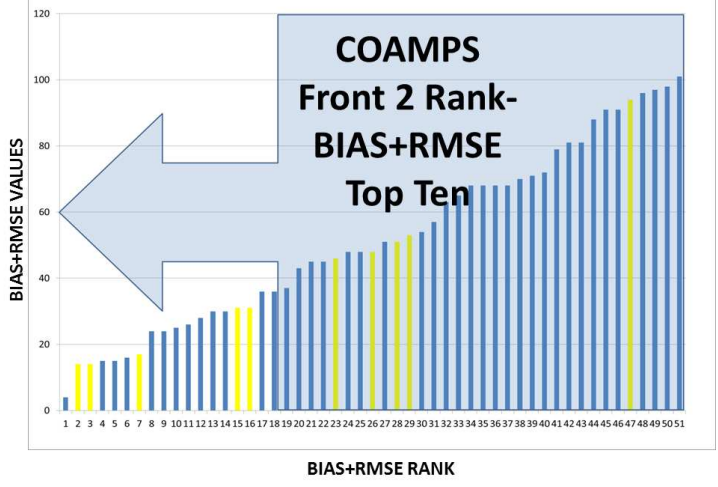
Figure 28: Ensemble Total-Model Top Ten rank data for Front 2 highlighted in yellow used for selections of associated BIAS+ RMSE rank data. RMSE error-trends for the MM5 and WRF models indicated a probability of de-creased ensemble error associated with front 2. COAMPS displayed an evenly distributed error-trend comparison with BIAS+RMSE rank data.
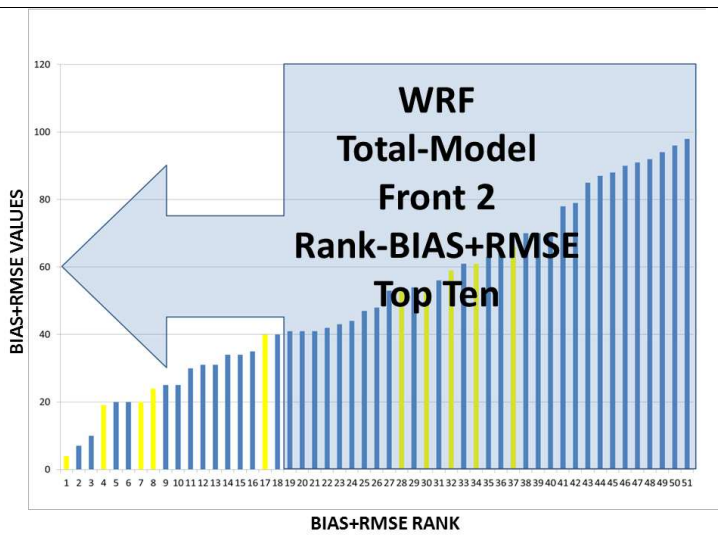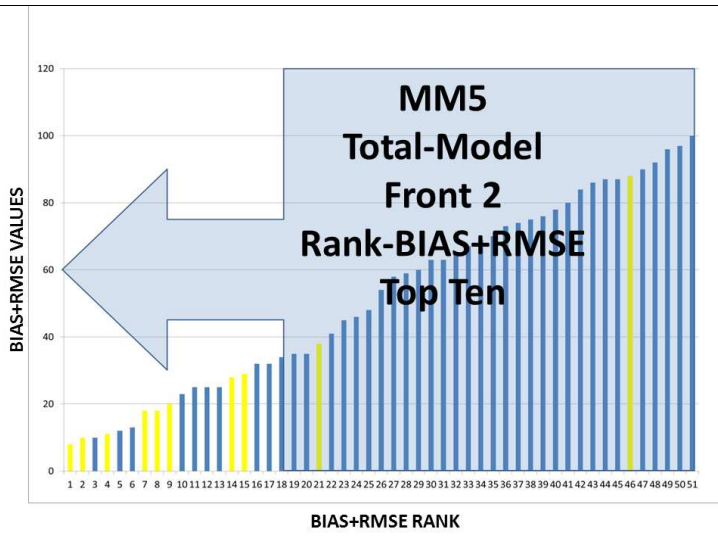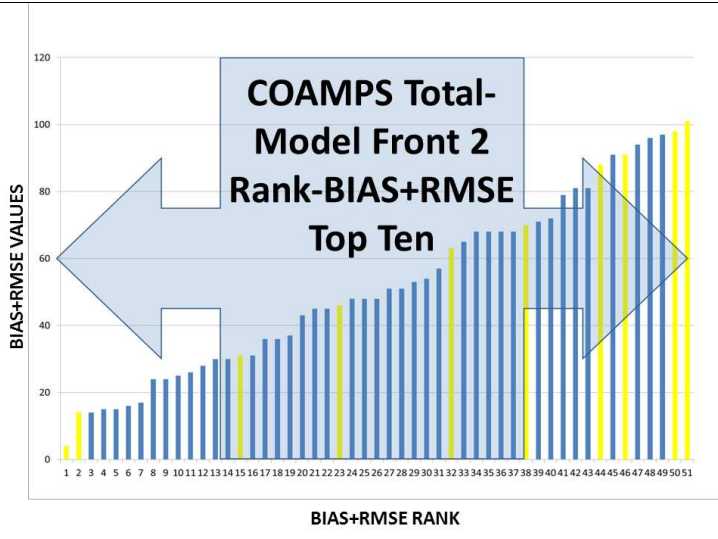
Figure 29: Ensemble Front 3 Top Ten rank data highlighted in yellow used for selections of associated BIAS rank data. All ensemble members displayed BIAS error-trend results indicating a probability of in-creased ensemble error relative to BIAS rank data for front 3.
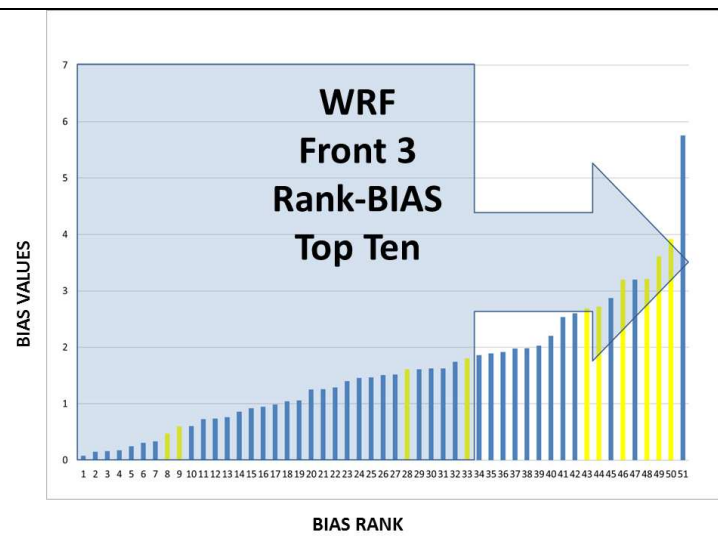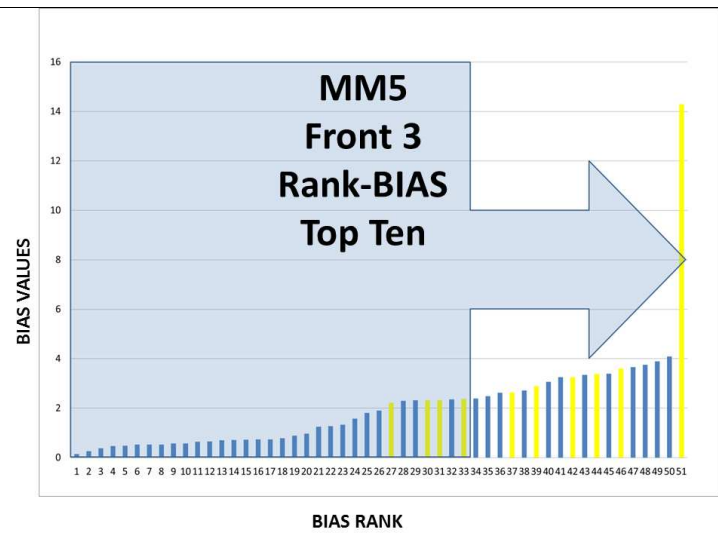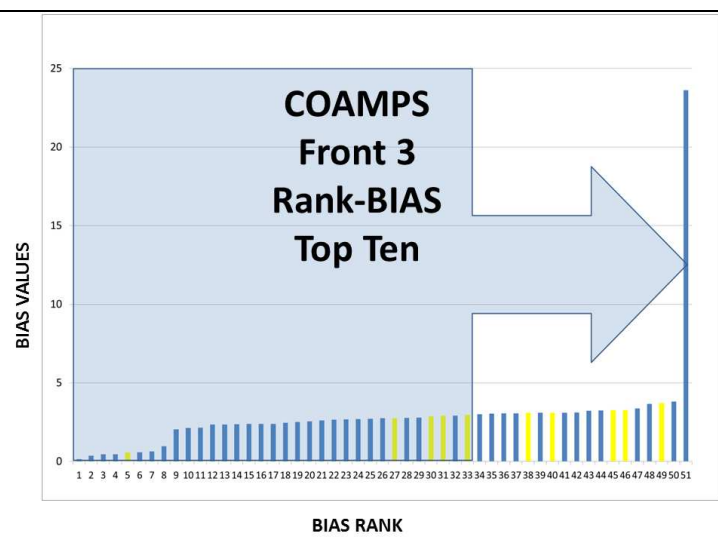
Figure 30: Ensemble Total-Model Top Ten rank data for Front 3 highlighted in yellow used for selections of associated BIAS rank data. WRF displayed an evenly distributed error-trend when compared to BIAS error rank data. But BIAS error-trends for the COAMPS and MM5 models indicated a probability of increased ensemble error associated with front 3.
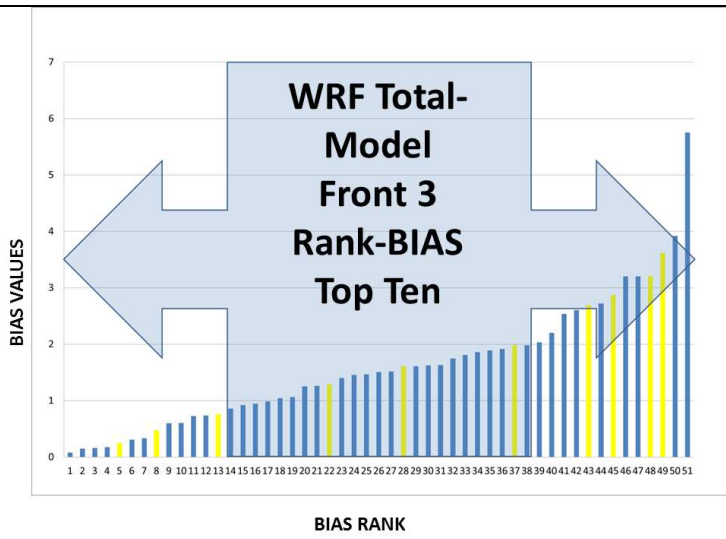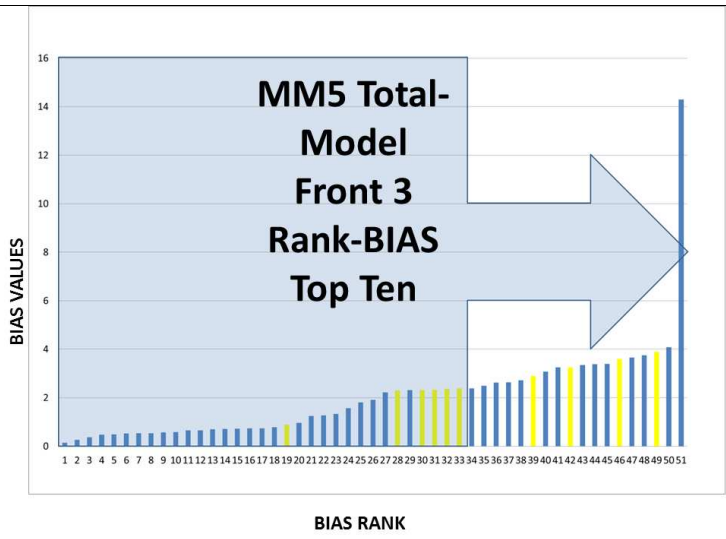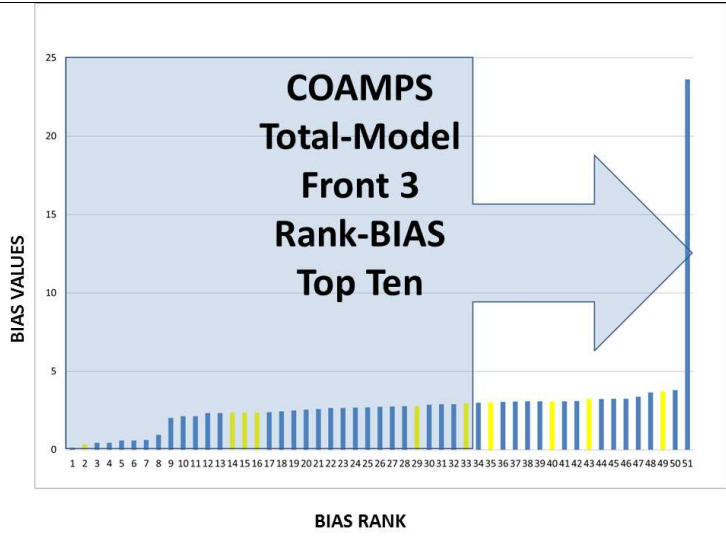
Figure 31: Ensemble Front 3 Top Ten rank data highlighted in yellow used for selections of associated RMSE rank data. All ensemble members displayed RMSE error-trend results indicating a probability of increased ensemble error relative to RMSE rank data for front 3.
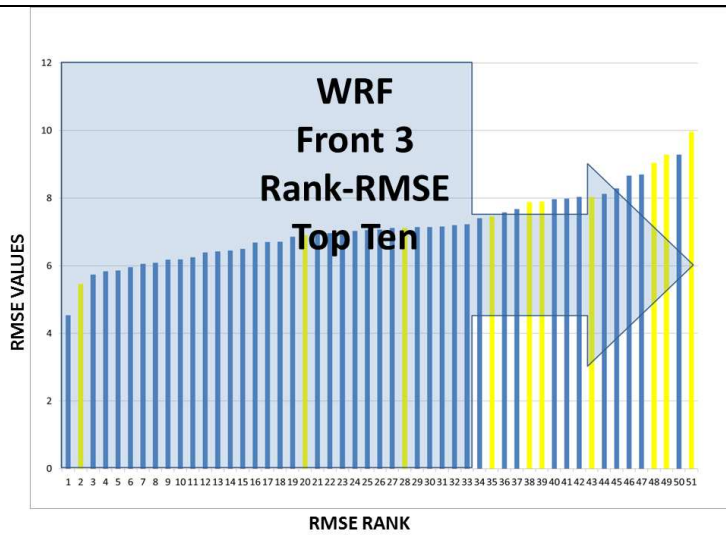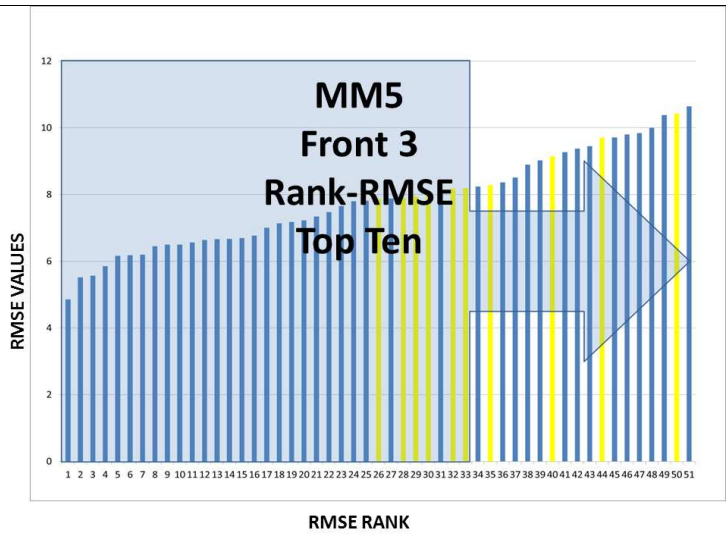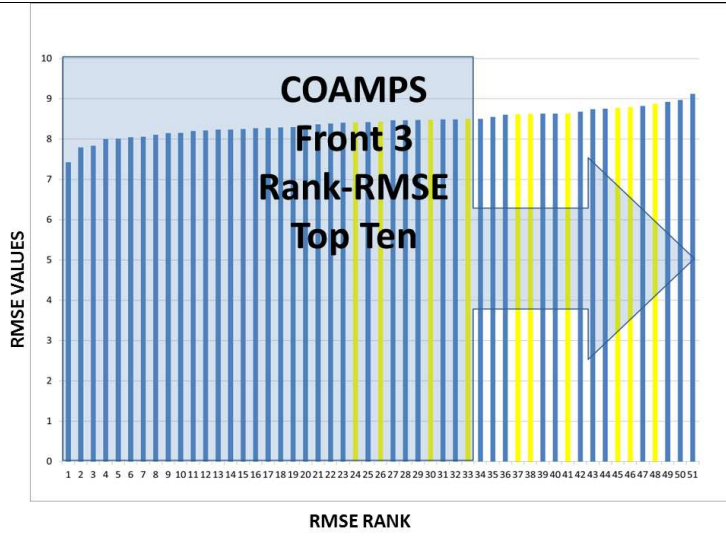
Figure 32: Ensemble Total-Model Top Ten rank data for Front 3 highlighted in yellow used for selections of associated RMSE rank data. WRF displayed an evenly distributed error-trend when compared to RMSE error rank data. But RMSE error-trends for the COAMPS and MM5 models indicated a probability of increased ensemble error associated with front 3.
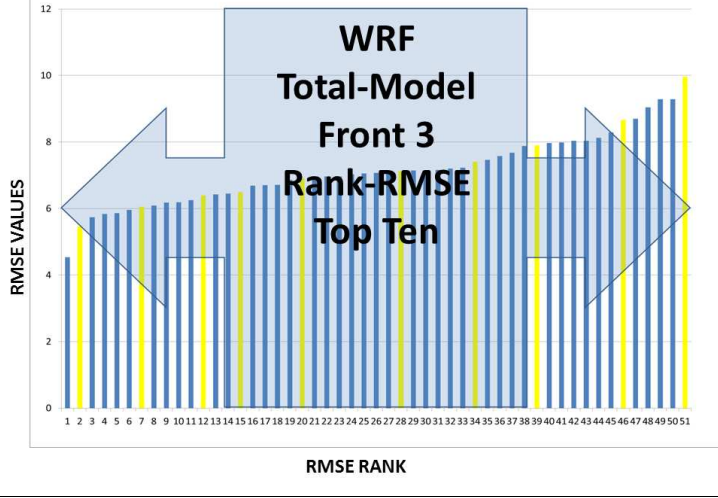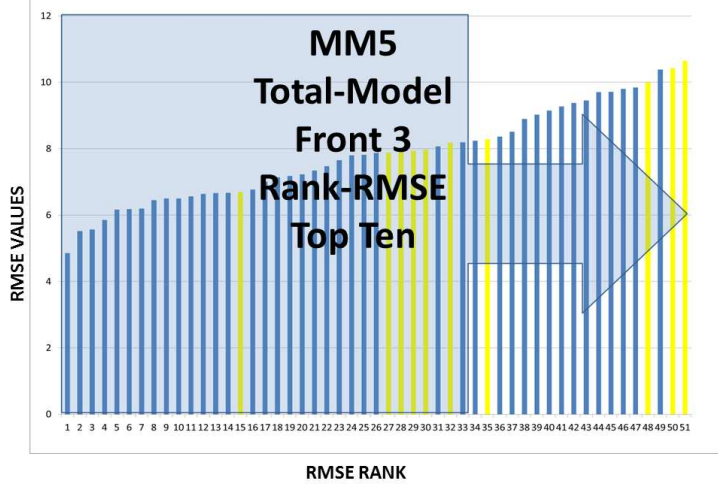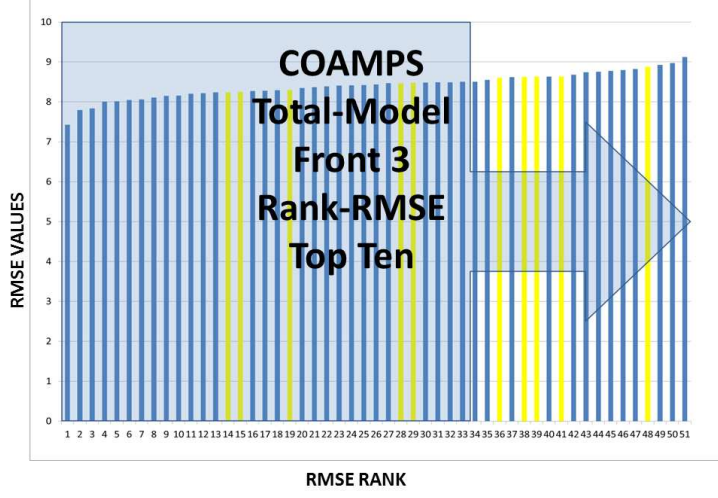
Figure 33: Ensemble Front 3 Top Ten rank data highlighted in yellow used for selections of associated BIAS+RMSE rank data. All ensemble members displayed BIAS+RMSE error-trend results indicating a probability of increased ensemble error relative to BIAS+RMSE rank data for front 3.
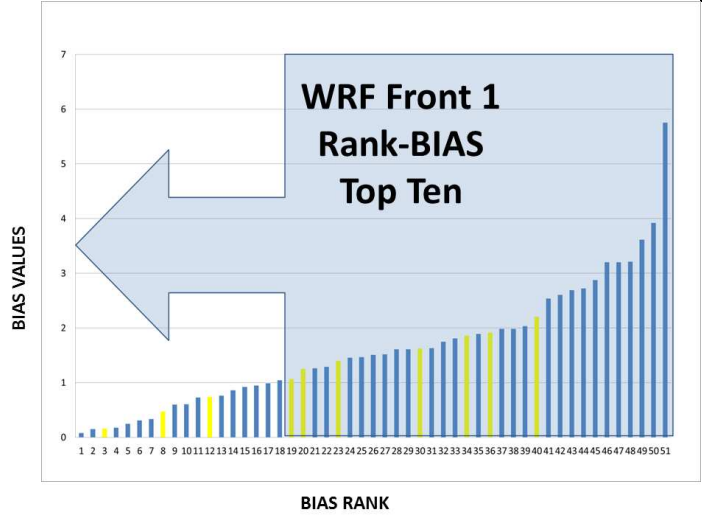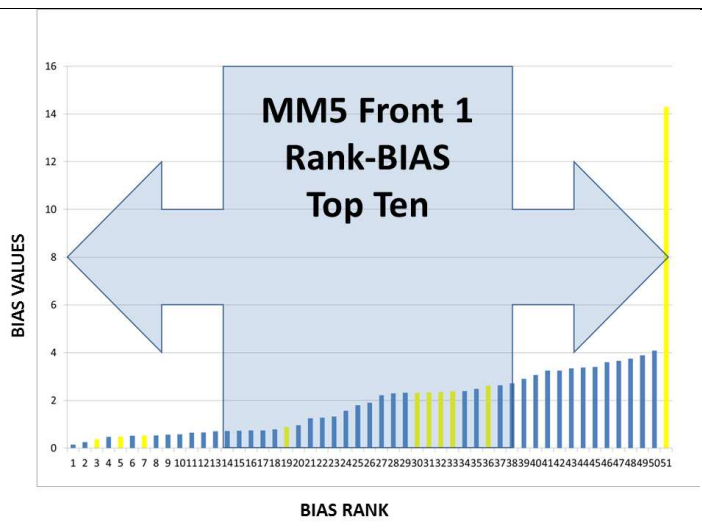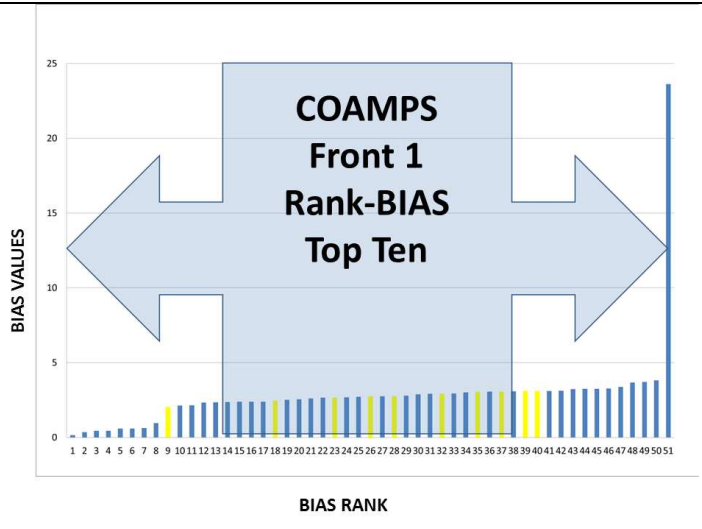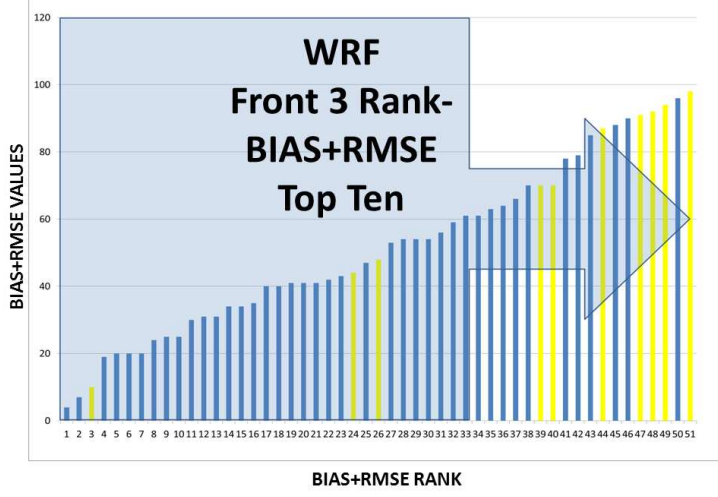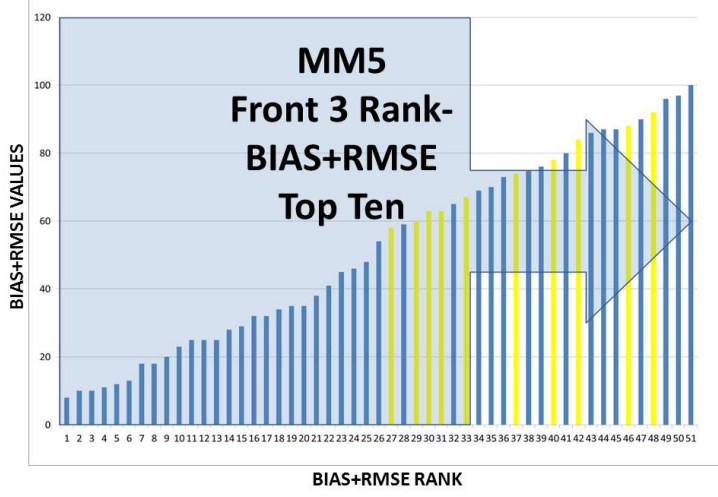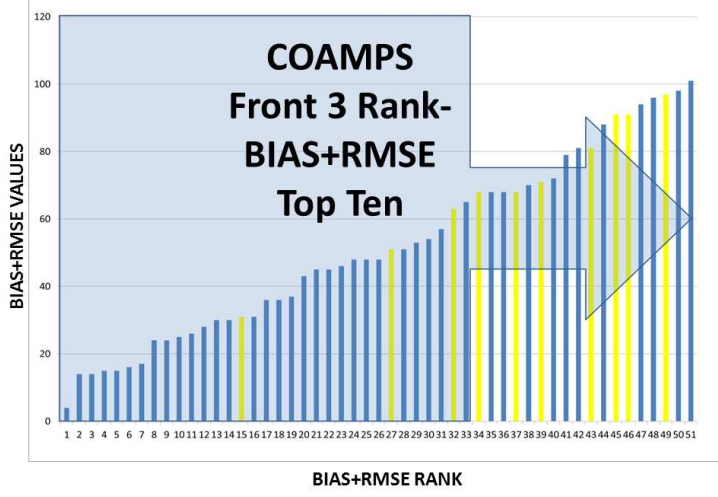
Figure 34: Ensemble Total-Model Top Ten rank data for Front 3 highlighted in yellow used for selections of associated BIAS+ RMSE rank data. All ensemble members displayed BIAS+RMSE error-trend results indicating a probability of increased ensemble error relative to BIAS+ RMSE rank data for front 3.
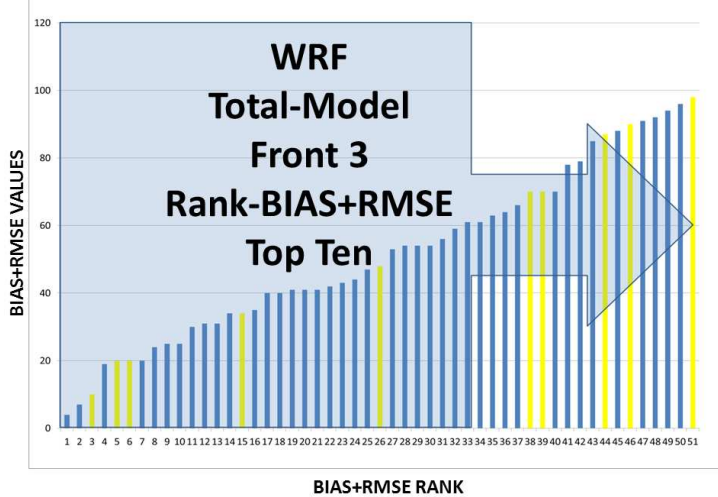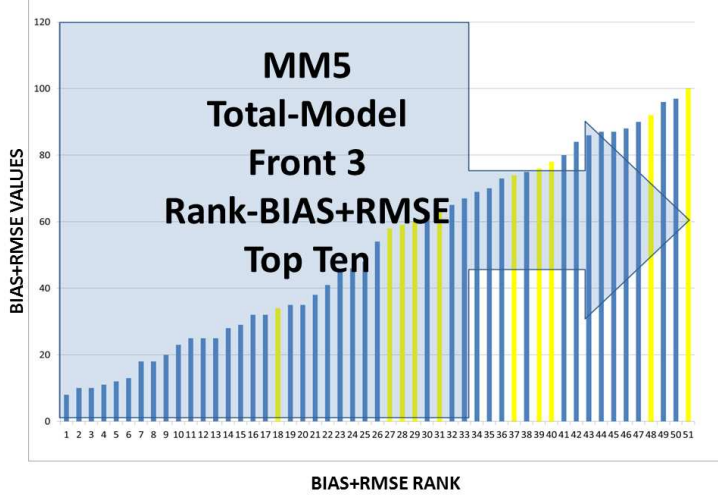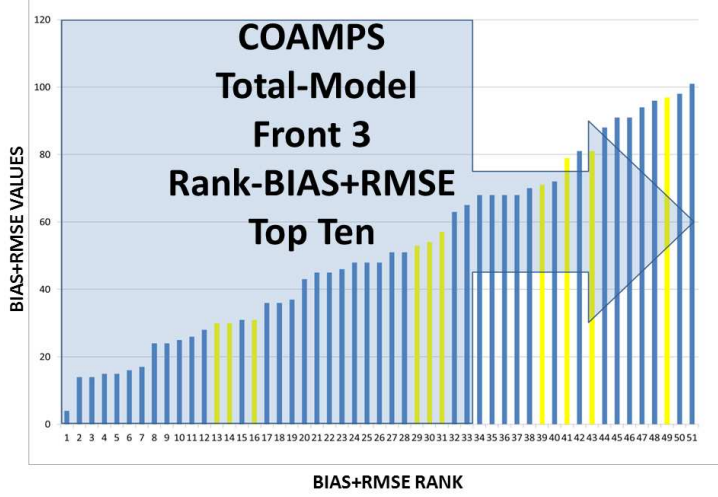
Analysis of trend performance, figures 29, 31, and 33 for the cold front 3 showed an error trend in an opposing direction as compared to the analysis of the previous two cold fronts. Consequently, selection from statistical measures from the frontal top ten rank analyses for the cold front 3 generally exhibited an error trend toward increased ensemble model error. When considering error trend plots for the Front 3 alone, 100% of the error trend plots indicate increased model error with trend values directed toward increase error. On visual examination of day 15 spaghetti plots, Figure 11, associated with cold front 3, little symmetry remained both spatially and temporally late in the forecast simulation during the 36 hour period from 0000Z, 25 December through 1200Z, 26 December 2008. This trend, furthermore, correlates well with maximum ensemble spread as illustrated in Figure 11. This trend analysis illustrated strong nonlinear processes beginning to play an active role in the ensemble probabilistic forecast process.

Looking at the final error trend analysis for Front 3 as shown in Figures 30, 32, and 34, the Total-Model Top-Ten plots showed error analysis distributed generally in a direction towards increased statistical error. The COAMPS and MM5 Total-Model error trend analysis is directed towards higher statistical error with Total-Model Top Ten plots lighted in the region of increased error for all three statistical measures. This error trend again correlates with the associated 15days - 27 December spaghetti plot diagrams, Figure 11, where ensemble spread is at its maximum extent. Error trend analysis applied to Bias, RMSE, and BIAS+RMSE statistical error ranking showed a top-ten total model rank data distribution towards higher error with the exception of the WRF model. The WRF Total-Model error trend analysis showed no definite top-ten total model run rank distribution across the range of statistical BIAS and RMSE ranks.

This is in contrast to the other ensemble members with trend results exhibiting ambiguous results where comparison data approximately spread evenly across the range of rank data for BIAS and RMSE.. Again, this error trend correlates to the increased ensemble spreading evident at the 15 days-27 December spaghetti plot diagram displayed in figure 11.

In the preceding eighteen figures, an error trend analysis technique was used to evaluate the ensemble model error as it relates to the frontal ranking for each of the three fronts observed during the period of the ensemble simulation. The error trends applied to the total model data ranking for each front displayed an associated with ensemble model error. For the first two fronts observed during the 12 – 27 December 2008 simulation, trends point towards less error rates and reduced ensemble spread as shown on the 2 days-14 December spaghetti plot, Figure 10. For front 3 (Figure 29 through Figure 34), however, the trend analysis generally favored increasing error spread for the 10 days-22 December and 15 days-27 December spaghetti plots as seen in Figures 10 and Figure 11.

Can it be said implicitly that, with a direct subjective comparison of basic statistical measures; BIAS, RMSE, and BIAS+RMSE, with mesoscale frontal ranking data over the range of finite ensemble simulation statistically emulate the varied distribution that would be expected for a PDF distribution using standard statistical analysis tools?

5.0   **Summary and conclusion:**

For all datasets used in this study, a total of 153 ensemble members using COAMPS, MM5, and WRF were produced at the inner domain set at a horizontal resolution of 36 km. All models exhibited statistically reasonable expectations in the use for the multi-model EPS and standard statistics (RMSE and BIAS). Previous research, Koračin et al. (2014), using this stochastic predictive approach confirmed that this multi-model ensemble combination clearly improved the accuracy of the forecast compared to each model when evaluated separately for all considered parameters. In addition, this research determined that all models showed error growth significantly of greater magnitude and occurring sooner than the standard error growth formula. According to Koračin el al. (2014), during the later stage of the forecast period (lead time of ten days and more), all models showed enhanced spread as evident in the corresponding time-series and spaghetti plot diagrams. Also in Koračin el al. (2014), the spaghetti diagram for COAMPS showed considerable ensemble error spreading prior to the MM5 and WRF ensemble members during the same forecast period. Following precursor analysis of ensemble simulation results, non-linear and chaotic behavior increased during the final five-day period when compared to the first five days of the ensemble forecast period. This non-linear dynamical evolution towards the completion of the model simulation further highlighted the need to incorporate those statistical tools necessary to gain insight into the evaluation and assignment of error growth correlations during the development of these deterministic processes.

In Grimit eo al.(2006), it has been shown in prior research that by measuring the ensemble spread -- error relationship with a probabilistic approach, the stochastic ensemble spread-error distribution was characterized by increasing scatter as the ensemble spread grew

larger. Also, Grimit et al. (2006) emphasized the the relationship between ensemble spread and deterministic forecast accuracy has been used as a measure of the success of using ensemble prediction systems as a means to enhance numerical prediction over medium and long-range forecast periods. Ensemble prediction will continue to be the next logical step in the development of a numerical process to consolidate the stochastic and probabilistic approaches toward more accurate numerical weather prediction. The calculation of the magnitude of ensemble model error through the use of a statistical distribution of all possible outcomes, i.e., trend analysis, can incorporation improved variety of physical parameterizations embedded in the regional and /or global EPS, the resultant mean "best guess" , which is then analyzed and further developed from the subsequent measurement of the numerical ensemble spread will lead to enhancements in the ensemble forecast prediction process. Ensemble model predictions rely heavily upon an accurate variety of physical parameterizations embedded in regional and global EPS to accomplish the computation of a precise ensemble mean. Ensemble error trend analysis can be an effective means to analyze the process efficiency of the physical parameterizations included in a particular multi-model ensemble prediction system. Once the efficiency of the physical parameterizations has been established, the focus can be directed towards determining how well the process achieves the predictability of certain mesoscale meteorological feature, in this case three cold fronts within the context of the Meso-(alpha) range occurring over the period of the simulations.

Although the basis of this research is simple in execution, can techniques commonly applied within the context of statistical analysis add validity in assessing probabilistic prediction outcomes? Using predictive -- observation measurements and then employing simple statistical

tools like BIAS and RMSE, as well as variations of both, can be used as a means to further evaluate and mitigate ensemble model error. This approach has shown that it can be another analysis instrument to evaluate both synoptic and mesoscale probabilistic tendencies. It remains, however, dependent upon the fidelity of the model forecast and observation temperature and height datasets available. The sensitivity to calculate with precision the error trends based solely on statistical ranking displayed the greatest correlation when the third front appeared at the end of the forecast run. At this point, ensemble model spread advanced to its largest extent by day 15 of the model run.   With reference to ensemble forecast prediction verification, the use of basic statistical measures presented beforehand may be able to specify the specific physical parameterizations that have the greatest influence upon multi-model for error covariance and predictability. This, in turn, will enable the use of model rank output as a means to balance forecast predictability. In research to come, these model physical processes can be retooled to make possible the assignment of a predictability factor to certain mesoscale frontal features; such as, temperature flux, surface and upper level dynamics, and precipitable water.

6.0   References:

Anthes, R. A., and T. T. Warner, 1978: Development of hydrodynamic models suitable for air pollution and other mesometeorological studies. Mon. Wea., Rev., 106, 1045-1078.

Anthes, R. A., Kuo, Y. H., Hsie, E. Y., Low-Nam, S., and Bettge, T. W. 1989. Estimation of skill and uncertainty in regional numerical models. Q. J. R. Meteorol. Soc., 115, 763-806.

Bengtsson, L., and Hodges, K. I., 2007a: The predictability of extratropical storm tracks and the sensitivity of their prediction to the observing system. Mon. Wea. Rev., 135, 315–333.

——, ——, and ——, 2007b: The prediction of extratropical storm tracks by the ECMWF and NCEP ensemble prediction systems. Mon. Wea. Rev., 135, 2545–2567.

Berner, J., S.-Y. Ha, J. P. Hacker, A. Fournier, C. Snyder, 2011: *Model Uncertainty in a Mesoscale Ensemble Prediction System: Stochastic versus Multiphysics Representations*. *Mon. Wea. Rev.*, **139**, 1972–1995. doi: http://dx.doi.org/10.1175/2010MWR3595.1

Black, T. L., 1994: The new NMC mesoscale Eta Model: Description and forecast examples. Weather Forecasting, 9, 265-278

Buizza, Roberto, P. L. Houtekamer, Gerald Pellerin, Zoltan Toth, Yuejian Zhu, Mozheng Wei, 2005*: A Comparison of the ECMWF, MSC, and NCEP Global Ensemble Prediction Systems*. Mon. Wea. Rev., 133, 1076–1097. doi: http://dx.doi.org/10.1175/MWR2905.1

Buizza, R.,, and Palmer, T. 1995. *The singular vector structure of the atmospheric global circulation*. J. Atmos. Sci., 52, 1434–1456

Dudhia, J., D. Gill, Y.-R. Guo, D. Hansen, K. Manning, and W. Wang, 1998. PSU/NCAR mesoscale modeling system tutorial class notes (MM5 modeling system version 2).[Available from the National Center for Atmospheric Research, P.O. Box 3000, Boulder,CO 80307.]

Eady, E.. 1949. *Long waves and cyclone waves*. Tellus, 1, 33-52.

Epstein, E. 1969. *Stochastic dynamic prediction*. Tellus, 21, 739-759.

Froude, L. S. R., 2009: *Regional differences in the prediction of extratropical cyclones by the ECMWF Ensemble Prediction System*. Mon. Wea. Rev., 137, 893–911.

Hodur, Richard M., 1982: Description and Evaluation of NORAPS: The Navy Operational Regional Atmospheric Prediction System. Mon. Wea. Rev., 110, 1591 – 1602.
doi: http://dx.doi.org/10.1175/1520-0493(1982)110<1591:DAEONT>2.0.CO;2

Hodur, R.M., 1997: The Naval Research Laboratory's Coupled Ocean/Atmosphere Mesoscale Prediction System (COAMPS). Mon. Wea. Rev., 135, 1414-1430.
Hodur, R.M., J. Pullen, J. Cummings, X. Hong, J.D. Doyle, P. Martin, and M.A. Rennick. 2002. The Coupled Ocean/Atmosphere Mesoscale Prediction System (COAMPS). Oceanography

15(1):88–98, http://dx.doi.org/10.5670/oceanog.2002.39.

Houtekamer, P., L. Lefaivre, J. Derome, H. Richie, and H. Mitchell, 1996. A system simulation approach to ensemble prediction. Mon. Wea. Rev., 124, 1225–1242.

Hsie, E. Y. and Kuo. Y. H., 1987: Description of the Penn State/NCAR mesoscale model version 4 (MM4). NCAR Tech. Note, NCAR/TN-282+STR, Boulder,Colorado

Huang, X.-Y., Xiao, Q., Barker, D.M., Zhang, Xin, Michalakes, J., Huang, W.,Henderson, T., Bray, J., Chen, Y., Ma, Z., Dudhia, J., Guo, Y.-R., Zhang, Xiaoyan, Won, D.-J., Lin, H.-C., Kuo, Y.-H. 2009. Four-Dimensional Variational Data Assimilation for WRF: Formulation and Preliminary Results. Mon. Wea. Rev., 137, 299-314. doi:10.1175/2008MWR2577.1.

Janjic, Z. I., 1994: The step-mountain eta coordinate model: Further developments of the convection, viscous sublayer, and turbulence closure schemes. Mon. Wea. Rev., 122, 927-945.

Jiang, J., D. Koracin, R. Vellore, M. Xiao, and J. Lewis, 2010: Using initial and boundary condition perturbations in medium-range regional ensemble forecasting with two nested domains. AGU 2010 Fall Meeting, 13-17 December 2010, San Francisco, CA.

Jiang J., D. Koracin, R. Vellore, K. Horvath, R. Belu, and T. McCord: Ensemble forecasting and uncertainty in wind and wind power prediction. EGU 2011. 03-08 April 2011, Vienna, Austria. (poster)

Jiang, J., D. Koracin, R. Vellore, K. Horvath, and R. Belu, 2011: Ensemble forecasting and uncertainty in wind and wind power prediction. EGU General Assembly, 3-8 April, 2011, Vienna, Austria, Vol. 13, EGU2011-12753-3.

Jiang, J., D. Koracin, and R. Vellore, 2012: Ensemble prediction with perturbed initial and lateral boundary conditions over complex terrain. 2012 Weather Impacts Decision Aids Workshop. Reno, NV. 13-15 March 2012.

Kalnay, E., 2008: Bred vectors: theory and applications in operational forecasting. Mediterrenean School on Mesoscale Meteorology 2008, Alghero, IT, 26-30 May 2008

Kalnay, E., *Atmospheric Modeling, Data Assimilation and Predictability* New York: Cambridge University Press 2003 pp. 364, ISBN: 9780521791793

Koračin, D., R. Vellore, J. Lewis, M. Kaplan, 2009: Predictability of coastal weather and its implications to ensemble forecasting. Presented at the Eighth Conference on Coastal Atmospheric and Oceanic Prediction and Processes, American Meteorological Society, 10-15 January 2009, Phoenix, AZ. Paper 4.3.

Koračin, D. and R. Vellore, 2009: Predictions of the west coast climate using dynamical downscaling. 34th Annual Climate Diagnostics and Prediction Workshop, Monterey, CA, 26-30 October 2009.

Koračin, D., R. Vellore, T. McCord, M. Xiao, and M. Young, 2010: Use of a WRF, MM5 and COAMPS multi-model ensemble to improve coastal weather predictions. AMS Ninth Conference on Coastal Atmospheric and Oceanic Prediction and Processes, Annapolis, MD, 26-29 September 2010. Paper J3.5.

Koračin, D, John M. Lewis, A. Young, and R. Vellore, 2014: Medium range, multi-model regional ensemble forecasting over the western U.S. AIAA Aviation 2014 Conference, Session: Numerical Weather Modeling, A SE-12, Atlanta, GA, 16-20 June 2014.

Koračin, D., Ramesh Vellore,V., Young, A., Lewis, J., Xiao, M., McCord, T., Jiang, J., Rabin, R., Horvath, K., 2014: A Case Study of 15-day Multi-model Regional Ensemble Forecasting over the Western U.S. SUmmitted to Wea. Forecasting

Lewis, J. M. 2005. Roots of ensemble forecasting. Mon. Wea. Rev., 133, 1865–1885.

Lin. Y.-L., R.D. Farley., and H.D. Orville, 1983: Bulk parameterization of the snow field in a cloud model. J.Climate Appl. Meteor., 22, 1065-1092.

Lorenz, E. 1963a. Deterministic nonperiodic flow. J. Atmos. Sci., 20, 130–141.

Lorenz, E. N. 1963b. The predictability of hydrodynamic flow. Trans. NY Acad. Sci. Series II, 25, 409-432

Lorenz, E. N., 1987: Deterministic and stochastic aspects of atmospheric dynamics. Irreversible Phenomena and Dynamical Systems Analysis in Geosciences. D. Reidel Publishing Co., 159-179.

Mellor, G. L., and T. Yamada (1982), Development of a turbulence closure model for geophysical fluid problems, Rev. Geophys., 20(4), 851−875, doi:10.1029/RG020i004p00851.

Mesinger, F., 2005: Eta Model at NCEP: Challenges overcome and lessons learned. Lecture notes, Workshop on "Design and Use of Regional Weather Prediction Models", The Abdus Salam International Centre for Theoretical Physics, Miramare, Trieste, Italy, 11-19 April 2005, 42 pp. Available online at http://agenda.ictp.trieste.it/agenda/current/askArchive.php?base=agenda&categ=a04186&id=a04186s262t1/lecture_notes

Stensrud, D. J., Bao, J.-W., and Warner, T. T. 2000. Using initial condition and model physics perturbations in short-range ensemble simulations of mesoscale convective systems. Mon. Wea. Rev., 128, 2077-2107.

Stensrud, D. J. 2001. Using short-range ensemble forecasts for predicting severe weather events. Atmos. Res., 56, 3-17.

Stensrud, D. J. and Weiss, S. J. 2002. Mesoscale model forecasts of the 3 May 1999 tornado outbreak. Wea. Forecasting, 17, 526-543.

Stensrud, D. J. 2007. Parameterization Schemes: Keys to Understanding Numerical Weather Prediction Models. Cambridge University Press, 459 pp.

Tracton, M. S., and E. Kalnay, 1993: Operational ensemble prediction at the National Meteorological Center: Practical aspects. Wea. Forecasting, 8, 379-398.

Toth, Z., and Kalnay, E. 1993. Ensemble forecasting at NMC: The generation of perturbations. Bull. Amer. Meteor. Soc., 74, 2317–2330.

Toth, Z., and Kalnay, E. 1997. Ensemble forecasting at NCEP and the breeding method. Mon. Wea. Rev., 125, 3297-3319.

Wang, Wei, Nelson L. Seaman, 1997: A Comparison Study of Convective Parameterization Schemes in a Mesoscale Model. Mon. Wea. Rev., 125, 252–278.
doi: http://dx.doi.org/10.1175/1520-0493(1997)125<0252:ACSOCP>2.0.CO;2

Appendix A

Ensemble Physical Parameterizations

Table 1A. Ensemble simulation set of physical parameterizations for MM5.

Experiment	MM5 (PBL)	MM5 (microphysics)	MM5 (Cumulus)	MM5 (Radiation)
Control	Eta M-Y	Reisner 2	Kain-Fritsch	RRTM (FRAD=4)
1	Eta M-Y	Reisner 2	Grell	CCM2 (FRAD=2)
2	Eta M-Y	Simple ice (Dudhia)	Grell	Dudhia (FRAD=2)
3	Eta M-Y	Goddard (GFSC)	Grell	Dudhia (FRAD=2)
4	Eta M-Y	Reisner 2	Betts-Miller	CCM2 (FRAD=2)
5	Eta M-Y	Reisner 2	Grell	Dudhia (FRAD=2)
6	Eta M-Y	Schultz	Betts-Miller	Dudhia (FRAD=2)
7	Eta M-Y	Simple ice (Dudhia)	Grell	CCM2 (FRAD=2)
8	Eta M-Y	Goddard (GFSC)	Betts-Miller	Dudhia (FRAD=2)
9	Eta M-Y	Reisner (no graupel)	Kain-Fritsch	Simple cloud (FRA
10	Eta M-Y	Reisner 2	Betts-Miller	RRTM (FRAD=4)
11	Eta M-Y	Simple ice (Dudhia)	Betts-Miller	Dudhia (FRAD=2)
12	Eta M-Y	Simple ice (Dudhia)	Betts-Miller	CCM2 (FRAD=2)
13	Gayno-Seaman	Schultz	Betts-Miller	CCM2 (FRAD=2)
14	Gayno-Seaman	Goddard (GFSC)	Betts-Miller	CCM2 (FRAD=2)
15	Gayno-Seaman	Reisner 2	Grell	Dudhia (FRAD=2)
16	Blackadar	Schultz	Kain-Fritsch	RRTM (FRAD=4)
17	Gayno-Seaman	Reisner 2	Betts-Miller	CCM2 (FRAD=2)
18	Blackadar	Simple ice (Dudhia)	Grell	Dudhia (FRAD=2)
19	Gayno-Seaman	Goddard (GFSC)	Grell	Simple cloud (FRA
20	Gayno-Seaman	Schultz	Kain-Fritsch	Dudhia (FRAD=2)
21	Gayno-Seaman	Simple ice (Dudhia)	Grell	CCM2 (FRAD=2)
22	Gayno-Seaman	Goddard (GFSC)	Kain-Fritsch	Simple cloud (FRA
23	Gayno-Seaman	Simple ice (Dudhia)	Kain-Fritsch	RRTM (FRAD=4)
24	Gayno-Seaman	Goddard (GFSC)	Grell	Dudhia (FRAD=2)
25	Gayno-Seaman	Goddard (GFSC)	Kain-Fritsch	CCM2 (FRAD=2)
26	Gayno-Seaman	Goddard (GFSC)	Betts-Miller	RRTM (FRAD=4)
27	Gayno-Seaman	Simple ice (Dudhia)	Kain-Fritsch	Simple cloud (FRA
28	Blackadar	Schultz	Kain-Fritsch	CCM2 (FRAD=2)
29	Gayno-Seaman	Reisner 2	Kain-Fritsch	Simple cloud (FRA
30	Burk-Thompson	Reisner 2	Betts-Miller	Simple cloud (FRA
31	Burk-Thompson	Simple ice (Dudhia)	Betts-Miller	Simple cloud (FRA
32	Burk-Thompson	Reisner 2	Kain-Fritsch	Dudhia (FRAD=2)
33	Burk-Thompson	Reisner 2	Betts-Miller	RRTM (FRAD=4)
34	Burk-Thompson	Simple ice (Dudhia)	Betts-Miller	RRTM (FRAD=4)
35	Burk-Thompson	Reisner 2	Betts-Miller	Dudhia (FRAD=2)
36	Burk-Thompson	Goddard (GFSC)	Grell	CCM2 (FRAD=2)
37	Burk-Thompson	Simple ice (Dudhia)	Betts-Miller	CCM2 (FRAD=2)
38	Burk-Thompson	Schultz	Betts-Miller	Dudhia (FRAD=2)
39	Burk-Thompson	Reisner 2	Kain-Fritsch	Simple cloud (FRA
40	Burk-Thompson	Goddard (GFSC)	Kain-Fritsch	Simple cloud (FRA
41	MRF	Reisner 2	Kain-Fritsch	Dudhia (FRAD=2)
42	MRF	Simple ice (Dudhia)	Betts-Miller	Dudhia (FRAD=2)
43	MRF	Reisner 2	Grell	CCM2 (FRAD=2)
44	MRF	Reisner 2	Kain-Fritsch	RRTM (FRAD=4)
45	MRF	Schultz	Grell	CCM2 (FRAD=2)
46	MRF	Schultz	Betts-Miller	RRTM (FRAD=4)
47	MRF	Simple ice (Dudhia)	Kain-Fritsch	RRTM (FRAD=4)
48	MRF	Goddard (GFSC)	Betts-Miller	RRTM (FRAD=4)
49	MRF	Simple ice (Dudhia)	Grell	CCM2 (FRAD=2)
50	MRF	Simple ice (Dudhia)	Grell	Dudhia (FRAD=2)

Table 2A. Ensemble simulation set of physical parameterizations for WRF.

Experiment	WRF (PBL)	WRF (Microphysics)	WRF (Cumulus)	WRF (Radiation)
Control	Mellor-Yamada-Jan	Thompson	Kain-Fritsch	Dudhia/RRTM
1	Mellor-Yamada-Jan	Goddard microphysics	Betts-Miller	GFDL/GFDL
2	Mellor-Yamada-Jan	Goddard microphysics	Kain-Fritsch	GFDL/GFDL
3	Mellor-Yamada-Jan	Lin	Kain-Fritsch	Goddard/RRTM
4	Mellor-Yamada-Jan	ETA microphysics	Kain-Fritsch	GFDL/GFDL
5	Mellor-Yamada-Jan	ETA microphysics	Betts-Miller	CAM/CAM
6	Mellor-Yamada-Jan	ETA microphysics	Kain-Fritsch	CAM/CAM
7	Mellor-Yamada-Jan	Thompson	Betts-Miller	Dudhia/RRTM
8	Mellor-Yamada-Jan	Goddard microphysics	Grell-Devenyi	GFDL/GFDL
9	Mellor-Yamada-Jan	Goddard microphysics	Betts-Miller	CAM/CAM
10	Mellor-Yamada-Jan	Thompson	Betts-Miller	CAM/CAM
11	Mellor-Yamada-Jan	Thompson	Betts-Miller	Goddard/RRTM
12	Mellor-Yamada-Jan	Lin	Grell-Devenyi	Goddard/RRTM
13	Mellor-Yamada-Jan	Lin	Betts-Miller	GFDL/GFDL
14	Mellor-Yamada-Jan	Goddard microphysics	Betts-Miller	GFDL/RRTM
15	Mellor-Yamada-Jan	Lin et al.	Kain-Fritsch	Dudhia/GFDL
16	Mellor-Yamada-Jan	ETA microphysics	Kain-Fritsch	Dudhia/CAM
17	Mellor-Yamada-Jan	WRF-single mom (6)	Betts-Miller	Goddard/RRTM
18	Mellor-Yamada-Jan	WRF-single mom (3)	Kain-Fritsch	Dudhia/RRTM
19	Mellor-Yamada-Jan	Morrison	Kain-Fritsch	Goddard/RRTM
20	Mellor-Yamada-Jan	Morrison	Betts-Miller	Goddard/RRTM
21	Mellor-Yamada-Jan	Morrison	Grell-Devenyi	Goddard/RRTM
22	YSU (new MRF)	ETA microphysics	Kain-Fritsch	GFDL/GFDL
23	YSU (new MRF)	Lin	Betts-Miller	GFDL/GFDL
24	YSU (new MRF)	Goddard microphysics	Betts-Miller	Goddard/RRTM
25	YSU (new MRF)	Lin	Kain-Fritsch	CAM/CAM
26	YSU (new MRF)	Lin	Betts-Miller	CAM/CAM
27	YSU (new MRF)	Goddard microphysics	Betts-Miller	Dudhia/RRTM
28	YSU (new MRF)	Thompson	Grell-Devenyi	GFDL/GFDL
29	YSU (new MRF)	ETA microphysics	Betts-Miller	Goddard/RRTM
30	YSU (new MRF)	ETA microphysics	Kain-Fritsch	CAM/CAM
31	YSU (new MRF)	Morrison	Kain-Fritsch	Goddard/RRTM
32	YSU (new MRF)	WRF-single mom (6)	Kain-Fritsch	Goddard/RRTM
33	YSU (new MRF)	WRF-single mom (3)	Betts-Miller	Dudhia/RRTM
34	YSU (new MRF)	WRF-single mom (6)	Betts-Miller	CAM/CAM
35	Pleim-Xiu	ETA microphysics	Betts-Miller	Goddard/RRTM
36	Pleim-Xiu	Lin	Betts-Miller	Goddard/RRTM
37	Pleim-Xiu	ETA microphysics	Grell-Devenyi	GFDL/GFDL
38	Pleim-Xiu	Goddard microphysics	Grell-Devenyi	Dudhia/RRTM
39	Pleim-Xiu	Lin	Kain-Fritsch	GFDL/GFDL
40	Pleim-Xiu	Thompson	Kain-Fritsch	GFDL/GFDL
41	Pleim-Xiu	Goddard microphysics	Grell-Devenyi	CAM/CAM
42	Pleim-Xiu	Goddard microphysics	Kain-Fritsch	CAM/CAM
43	Pleim-Xiu	WRF-single mom (6)	Kain-Fritsch	Goddard/RRTM
44	Pleim-Xiu	Morrison	Kain-Fritsch	Goddard/RRTM
45	Pleim-Xiu	Lin et al.	Kain-Fritsch	CAM/CAM
46	Pleim-Xiu	Goddard microphysics	Betts-Miller	Dudhia/RRTM
47	Pleim-Xiu	Lin	Betts-Miller	Dudhia/RRTM
48	Pleim-Xiu	Lin	Grell-Devenyi	Dudhia/RRTM
49	Pleim-Xiu	Goddard microphysics	Grell-Devenyi	Dudhia/RRTM
50	Pleim-Xiu	Lin	Kain-Fritsch	GFDL/GFDL

Table 3A. Ensemble simulation set of physical parameterizations for COAMPS.

No.	PBL	dxmeso*	Ice nucleation	Autoconversion factor
1	Mellor-Yamada (MY)	50000	Cooper and Haines (1986)	0.0004
2	Mellor-Yamada	10000	Cooper and Haines (1986)	0.0004
3	Mellor-Yamada	150000	Cooper and Haines (1986)	0.0004
4	Mellor-Yamada	150000	Cooper and Haines (1986)	0.0004
5	Mellor-Yamada	50000	Cooper and Haines (1986)	0.0004
6	Mellor-Yamada	10000	Cooper and Haines (1986)	0.0004
7	Mellor-Yamada	150000	Fletcher (1962)	0.0004
8	Mellor-Yamada	50000	Fletcher (1962)	0.0004
9	Mellor-Yamada	10000	Fletcher (1962)	0.0004
10	Mellor-Yamada	10000	Fletcher (1962)	0.001 default
11	Mellor-Yamada	50000	Fletcher (1962)	0.001 default
12	Mellor-Yamada	150000	Fletcher (1962)	0.001 default
13	Mellor-Yamada	50000	Cooper and Haines (1986)	0.001 default
14	Mellor-Yamada	10000	Cooper and Haines (1986)	0.001 default
15	Mellor-Yamada	150000	Cooper and Haines (1986)	0.001 default
16	Mellor-Yamada	150000	Cooper and Haines (1986)	0.001 default
17	Mellor-Yamada	50000	Cooper and Haines (1986)	0.001 default
18	Mellor-Yamada	10000	Cooper and Haines (1986)	0.001 default
19	Mellor-Yamada	10000	Cooper and Haines (1986)	0.002
20	Mellor-Yamada	50000	Cooper and Haines (1986)	0.002
21	Mellor-Yamada	150000	Cooper and Haines (1986)	0.002
22	Mellor-Yamada	150000	Cooper and Haines (1986)	0.002
23	Mellor-Yamada	50000	Cooper and Haines (1986)	0.002
24	Mellor-Yamada	10000	Cooper and Haines (1986)	0.002
25	Mellor-Yamada	10000	Fletcher (1962)	0.002
26	Mellor-Yamada	50000	Fletcher (1962)	0.002
27	Mellor-Yamada	150000	Fletcher (1962)	0.002
28	Modified MY version	10000	Cooper and Haines (1986)	0.0004
29	Modified MY version	50000	Cooper and Haines (1986)	0.0004
30	Modified MY version	150000	Cooper and Haines (1986)	0.0004
31	Modified MY version	150000	Cooper and Haines (1986)	0.0004
32	Modified MY version	50000	Cooper and Haines (1986)	0.0004
33	Modified MY version	10000	Cooper and Haines (1986)	0.0004
34	Modified MY version	10000	Fletcher (1962)	0.0004
35	Modified MY version	50000	Fletcher (1962)	0.0004
36	Modified MY version	150000	Fletcher (1962)	0.0004
37	Modified MY version	150000	Fletcher (1962)	0.001 default
38	Modified MY version	50000	Fletcher (1962)	0.001 default
39	Modified MY version	10000	Fletcher (1962)	0.001 default
40	Modified MY version	10000	Cooper and Haines (1986)	0.001 default
41	Modified MY version	50000	Cooper and Haines (1986)	0.001 default
42	Modified MY version	150000	Cooper and Haines (1986)	0.001 default
43	Modified MY version	150000	Cooper and Haines (1986)	0.001 default
44	Modified MY version	50000	Cooper and Haines (1986)	0.001 default
45	Modified MY version	10000	Cooper and Haines (1986)	0.001 default
46	Modified MY version	10000	Cooper and Haines (1986)	0.002
47	Modified MY version	50000	Cooper and Haines (1986)	0.002
48	Modified MY version	150000	Cooper and Haines (1986)	0.002
49	Modified MY version	150000	Cooper and Haines (1986)	0.002
51	Modified MY version	50000	Cooper and Haines (1986)	0.002
51	Modified MY version	10000	Cooper and Haines (1986)	0.002

Cumulus scheme = Kain-Fritsch parameterization (Kain and Fritsch 1993)
dxmeso=horizontal grid resolution (in m) below which cumulus scheme is turned off.*
Microphysics = Rutledge and Hobbs (1994) and Schmidt (2001)
Autoconversion factor used in the conversion of cloud water to drizzle/rain processes.
Radiation scheme follows Harshavardhan et al. (1987).
PBL scheme = Mellor-Yamada level 2.5 model (used in COAMPS 3) and modified version in COAMPS 4.

Appendix B

Ensemble Frontal Rankings

Table 1B. Front 1: Ensemble ranking with respect to physical parameterizations for COAMPS.

counter	Run	TOTAL rank	PBL	dxmeso*	Ice nucleation	Autoconversion factor
	COAMPS Front 1					
1	run1	35	Mellor-Yamada(MY)	50000	Cooper and Haines (1986)	0.0004
2	run2	52	Mellor-Yamada	10000	Cooper and Haines (1986)	0.0004
3	run3	54	Mellor-Yamada	150000	Cooper and Haines (1986)	0.0004
4	run4	15	Mellor-Yamada	150000	Cooper and Haines (1986)	0.0004
5	run5	11	Mellor-Yamada	50000	Cooper and Haines (1986)	0.0004
6	run6	27	Mellor-Yamada	10000	Cooper and Haines (1986)	0.0004
7	run7	8	Mellor-Yamada	150000	Fletcher (1962)	0.0004
8	run8	28	Mellor-Yamada	50000	Fletcher (1962)	0.0004
9	run9	50	Mellor-Yamada	10000	Fletcher (1962)	0.0004
10	run10	49	Mellor-Yamada	10000	Fletcher (1962)	0.001 default
11	run11	29	Mellor-Yamada	50000	Fletcher (1962)	0.001 default
12	run12	9	Mellor-Yamada	150000	Fletcher (1962)	0.001 default
13	run13	10	Mellor-Yamada	50000	Cooper and Haines (1986)	0.001 default
14	run14	24	Mellor-Yamada	10000	Cooper and Haines (1986)	0.001 default
15	run15	14	Mellor-Yamada	150000	Cooper and Haines (1986)	0.001 default
16	run16	33	Mellor-Yamada	150000	Cooper and Haines (1986)	0.001 default
17	run17	36	Mellor-Yamada	50000	Cooper and Haines (1986)	0.001 default
18	run18	53	Mellor-Yamada	10000	Cooper and Haines (1986)	0.001 default
19	run19	54	Mellor-Yamada	10000	Cooper and Haines (1986)	0.002
20	run20	43	Mellor-Yamada	50000	Cooper and Haines (1986)	0.002
21	run21	30	Mellor-Yamada	150000	Cooper and Haines (1986)	0.002
22	run22	13	Mellor-Yamada	150000	Cooper and Haines (1986)	0.002
23	run23	12	Mellor-Yamada	50000	Cooper and Haines (1986)	0.002
24	run24	25	Mellor-Yamada	10000	Cooper and Haines (1986)	0.002
25	run25	52	Mellor-Yamada	10000	Fletcher (1962)	0.002
26	run26	34	Mellor-Yamada	50000	Fletcher (1962)	0.002
27	run27	7	Mellor-Yamada	150000	Fletcher (1962)	0.002
28	run28	54	Modified MY version	10000	Cooper and Haines (1986)	0.0004
29	run29	46	Modified MY version	50000	Cooper and Haines (1986)	0.0004
30	run30	19	Modified MY version	150000	Cooper and Haines (1986)	0.0004
31	run31	23	Modified MY version	150000	Cooper and Haines (1986)	0.0004
32	run32	16	Modified MY version	50000	Cooper and Haines (1986)	0.0004
33	run33	40	Modified MY version	10000	Cooper and Haines (1986)	0.0004
34	run34	47	Modified MY version	10000	Fletcher (1962)	0.0004
35	run35	37	Modified MY version	50000	Fletcher (1962)	0.0004
36	run36	33	Modified MY version	150000	Fletcher (1962)	0.0004
37	run37	32	Modified MY version	150000	Fletcher (1962)	0.001 default
38	run38	41	Modified MY version	50000	Fletcher (1962)	0.001 default
39	run39	44	Modified MY version	10000	Fletcher (1962)	0.001 default
40	run40	38	Modified MY version	10000	Cooper and Haines (1986)	0.001 default
41	run41	18	Modified MY version	50000	Cooper and Haines (1986)	0.001 default
42	run42	21	Modified MY version	150000	Cooper and Haines (1986)	0.001 default
43	run43	23	Modified MY version	150000	Cooper and Haines (1986)	0.001 default
44	run44	45	Modified MY version	50000	Cooper and Haines (1986)	0.001 default
45	run45	51	Modified MY version	10000	Cooper and Haines (1986)	0.001 default
46	run46	48	Modified MY version	10000	Cooper and Haines (1986)	0.002
47	run47	42	Modified MY version	50000	Cooper and Haines (1986)	0.002
48	run48	27	Modified MY version	150000	Cooper and Haines (1986)	0.002
49	run49	20	Modified MY version	150000	Cooper and Haines (1986)	0.002
50	run50	17	Modified MY version	50000	Cooper and Haines (1986)	0.002
51	run51	39	Modified MY version	10000	Cooper and Haines (1986)	0.002

Table 2B. Front 1: Ensemble ranking with respect to physical parameterizations for MM5.

counter	Run	TOTAL rank	MM5 (PBL)	MM5 (Microphysics)	MM5 (Cumulus)	MM5 (Radiation)
		MM5 Front 1				
1	run1	26	Eta M-Y (IBLTYP=4)	Reisner 2 (IMPHYS=7)	Kain-Fritsch (ICUPA=8,ISHALLO=0)	RRTM (FRAD=4)
2	run2	25	Eta M-Y (IBLTYP=4)	Reisner 2 (IMPHYS=7)	Grell (ICUPA=3,ISHALLO=1)	CCM2 (FRAD=3)
3	run3	33	Eta M-Y (IBLTYP=4)	Simple ice (Dudhia) (IMPHYS=4)	Grell (ICUPA=3,ISHALLO=1)	Dudhia (FRAD=2)
4	run4	8	Eta M-Y (IBLTYP=4)	Goddard (GFSC) (IMPHYS=6)	Grell (ICUPA=3,ISHALLO=1)	Dudhia (FRAD=2)
5	run5	11	Eta M-Y (IBLTYP=4)	Reisner 2 (IMPHYS=7)	Betts-Miller (ICUPA=7,ISHALLO=0)	CCM2 (FRAD=3)
6	run6	27	Eta M-Y (IBLTYP=4)	Reisner 2 (IMPHYS=7)	Grell (ICUPA=3,ISHALLO=1)	Dudhia (FRAD=2)
7	run7	11	Eta M-Y (IBLTYP=4)	Schultz (IMPHYS=8)	Betts-Miller (ICUPA=7,ISHALLO=0)	Dudhia (FRAD=2)
8	run8	23	Eta M-Y (IBLTYP=4)	Simple ice (Dudhia) (IMPHYS=4)	Grell (ICUPA=3,ISHALLO=1)	CCM2 (FRAD=3)
9	run9	16	Eta M-Y (IBLTYP=4)	Goddard (GFSC) (IMPHYS=6)	Betts-Miller (ICUPA=7,ISHALLO=0)	Dudhia (FRAD=2)
10	run10	15	Eta M-Y (IBLTYP=4)	Reisner (no graupel)	Kain-Fritsch (ICUPA=8,ISHALLO=0)	Simple cloud (FRAD=1)
11	run11	16	Eta M-Y (IBLTYP=4)	Reisner 2 (IMPHYS = 7)	Betts-Miller (ICUPA=7,ISHALLO=0)	RRTM (FRAD=4)
12	run12	17	Eta M-Y (IBLTYP=4)	Simple ice (Dudhia) (IMPHYS=4)	Betts-Miller (ICUPA=7,ISHALLO=0)	Dudhia (FRAD=2)
13	run13	22	Eta M-Y (IBLTYP=4)	Simple ice (Dudhia) (IMPHYS=4)	Betts-Miller (ICUPA=7,ISHALLO=0)	CCM2 (FRAD=3)
14	run14	14	Gayno-Seaman (IBLTYP=6)	Schultz (IMPHYS=8)	Betts-Miller (ICUPA=7,ISHALLO=0)	CCM2 (FRAD=3)
15	run15	11	Gayno-Seaman (IBLTYP=6)	Goddard (GFSC) (IMPHYS=6)	Betts-Miller (ICUPA=7,ISHALLO=0)	CCM2 (FRAD=3)
16	run16	19	Gayno-Seaman (IBLTYP=6)	Reisner 2 (IMPHYS=7)	Grell (ICUPA=3,ISHALLO=1)	Dudhia (FRAD=2)
17	run17	7	Blackadar	Schultz (IMPHYS=8)	Kain-Fritsch (ICUPA=8,ISHALLO=0)	RRTM (FRAD=4)
18	run18	23	Gayno-Seaman (IBLTYP=6)	Reisner 2 (IMPHYS=7)	Betts-Miller (ICUPA=7,ISHALLO=0)	CCM2 (FRAD=3)
19	run19	5	Blackadar	Simple ice (Dudhia) (IMPHYS=4)	Grell (ICUPA=3,ISHALLO=1)	Dudhia (FRAD=2)
20	run20	11	Gayno-Seaman (IBLTYP=6)	Goddard (GFSC) (IMPHYS=6)	Grell (ICUPA=3,ISHALLO=1)	Simple cloud (FRAD=1)
21	run21	6	Gayno-Seaman (IBLTYP=6)	Schultz (IMPHYS=8)	Kain-Fritsch (ICUPA=8,ISHALLO=0)	Dudhia (FRAD=2)
22	run22	10	Gayno-Seaman (IBLTYP=6)	Simple ice (Dudhia) (IMPHYS=4)	Grell (ICUPA=3,ISHALLO=1)	CCM2 (FRAD=3)
23	run23	21	Gayno-Seaman (IBLTYP=6)	Goddard (GFSC) (IMPHYS=6)	Kain-Fritsch (ICUPA=8,ISHALLO=0)	Simple cloud (FRAD=1)
24	run24	5	Gayno-Seaman (IBLTYP=6)	Simple ice (Dudhia) (IMPHYS=4)	Kain-Fritsch (ICUPA=8,ISHALLO=0)	RRTM (FRAD=4)
25	run25	23	Gayno-Seaman (IBLTYP=6)	Goddard (GFSC) (IMPHYS=6)	Grell (ICUPA=3,ISHALLO=1)	Dudhia (FRAD=2)
26	run26	16	Gayno-Seaman (IBLTYP=6)	Goddard (GFSC) (IMPHYS=6)	Kain-Fritsch (ICUPA=8,ISHALLO=0)	CCM2 (FRAD=3)
27	run27	10	Gayno-Seaman (IBLTYP=6)	Goddard (GFSC) (IMPHYS=6)	Betts-Miller (ICUPA=7,ISHALLO=0)	RRTM (FRAD=4)
28	run28	19	Gayno-Seaman (IBLTYP=6)	Simple ice (Dudhia) (IMPHYS=4)	Kain-Fritsch (ICUPA=8,ISHALLO=0)	Simple cloud (FRAD=1)
29	run29	17	Blackadar	Schultz (IMPHYS=8)	Kain-Fritsch (ICUPA=8,ISHALLO=0)	CCM2 (FRAD=3)
30	run30	15	Gayno-Seaman (IBLTYP=6)	Reisner 2 (IMPHYS=7)	Kain-Fritsch (ICUPA=8,ISHALLO=0)	Simple cloud (FRAD=1)
31	run31	8	k-Thompson (IBLTYP=3,ISOI	Reisner 2 (IMPHYS=7)	Betts-Miller (ICUPA=7,ISHALLO=0)	Simple cloud (FRAD=1)
32	run32	10	k-Thompson (IBLTYP=3,ISOI	Simple ice (Dudhia) (IMPHYS=4)	Betts-Miller (ICUPA=7,ISHALLO=0)	Simple cloud (FRAD=1)
33	run33	23	k-Thompson (IBLTYP=3,ISOI	Reisner 2 (IMPHYS=7)	Kain-Fritsch (ICUPA=8,ISHALLO=0)	Dudhia (FRAD=2)
34	run34	10	k-Thompson (IBLTYP=3,ISOI	Reisner 2 (IMPHYS=7)	Betts-Miller (ICUPA=7,ISHALLO=0)	RRTM (FRAD=4)
35	run35	15	k-Thompson (IBLTYP=3,ISOI	Simple ice (Dudhia) (IMPHYS=4)	Betts-Miller (ICUPA=7,ISHALLO=0)	RRTM (FRAD=4)
36	run36	14	k-Thompson (IBLTYP=3,ISOI	Reisner 2 (IMPHYS=7)	Betts-Miller (ICUPA=7,ISHALLO=0)	Dudhia (FRAD=2)
37	run37	18	k-Thompson (IBLTYP=3,ISOI	Goddard (GFSC) (IMPHYS=6)	Grell (ICUPA=3,ISHALLO=1)	CCM2 (FRAD=3)
38	run38	23	k-Thompson (IBLTYP=3,ISOI	Simple ice (Dudhia) (IMPHYS=4)	Betts-Miller (ICUPA=7,ISHALLO=0)	CCM2 (FRAD=3)
39	run39	11	k-Thompson (IBLTYP=3,ISOI	Schultz (IMPHYS=8)	Betts-Miller (ICUPA=7,ISHALLO=0)	Dudhia (FRAD=2)
40	run40	12	k-Thompson (IBLTYP=3,ISOI	Reisner 2 (IMPHYS=7)	Kain-Fritsch (ICUPA=8,ISHALLO=0)	Simple cloud (FRAD=1)
41	run41	26	k-Thompson (IBLTYP=3,ISOI	Goddard (GFSC) (IMPHYS=6)	Kain-Fritsch (ICUPA=8,ISHALLO=0)	Simple cloud (FRAD=1)
42	run42	35	MRF (IBLTYP=5)	Reisner 2 (IMPHYS=7)	Kain-Fritsch (ICUPA=8,ISHALLO=0)	Dudhia (FRAD=2)
43	run43	9	MRF (IBLTYP=5)	Simple ice (Dudhia) (IMPHYS=4)	Betts-Miller (ICUPA=7,ISHALLO=0)	Dudhia (FRAD=2)
44	run44	28	MRF (IBLTYP=5)	Reisner 2 (IMPHYS=7)	Grell (ICUPA=3,ISHALLO=1)	CCM2 (FRAD=3)
45	run45	34	MRF (IBLTYP=5)	Reisner 2 (IMPHYS=7)	Kain-Fritsch (ICUPA=8,ISHALLO=0)	RRTM (FRAD=4)
46	run46	31	MRF (IBLTYP=5)	Schultz (IMPHYS=8)	Grell (ICUPA=3,ISHALLO=1)	CCM2 (FRAD=3)
47	run47	24	MRF (IBLTYP=5)	Schultz (IMPHYS=8)	Betts-Miller (ICUPA=7,ISHALLO=0)	RRTM (FRAD=4)
48	run48	23	MRF (IBLTYP=5)	Simple ice (Dudhia) (IMPHYS=4)	Kain-Fritsch (ICUPA=8,ISHALLO=0)	RRTM (FRAD=4)
49	run49	31	MRF (IBLTYP=5)	Goddard (GFSC) (IMPHYS=6)	Betts-Miller (ICUPA=7,ISHALLO=0)	RRTM (FRAD=4)
50	run50	28	MRF (IBLTYP=5)	Simple ice (Dudhia) (IMPHYS=4)	Grell (ICUPA=3,ISHALLO=1)	CCM2 (FRAD=3)
51	run51	13	MRF (IBLTYP=5)	Simple ice (Dudhia) (IMPHYS=4)	Grell (ICUPA=3,ISHALLO=1)	Dudhia (FRAD=2)

Table 3B. Front 1: Ensemble ranking with respect to physical parameterizations for WRF.

counter	Run	TOTAL rank	WRF (PBL)	WRF (Microphysics)	WRF (Cumulus)	WRF (Radiation)
	WRF Front 1					
1	run1	7	Mellor-Yamada-Jan	Thompson (MM5 : Reisner 2)	Kain-Fritsch (MM5: Kain-Fritsch)	Dudhia/RRTM
2	run2	12	Mellor-Yamada-Jan	Goddard microphysics (MM5: GSFC)	Betts-Miller (MM5: Betts-Miller)	GFDL/GFDL (Not in MM5)
3	run3	23	Mellor-Yamada-Jan	Goddard microphysics (MM5: GSFC)	Kain-Fritsch (MM5: Kain-Fritsch)	GFDL/GFDL
4	run4	10	Mellor-Yamada-Jan	Lin et al. (MM5: GSFC)	Kain-Fritsch (MM5: Kain-Fritsch)	Goddard/RRTM
5	run5	6	Mellor-Yamada-Jan	Eta microphysics (Not in MM5)	Kain-Fritsch (MM5: Kain-Fritsch)	GFDL/GFDL
6	run6	13	Mellor-Yamada-Jan	Eta microphysics (Not in MM5)	Betts-Miller (MM5: Betts-Miller)	CAM/CAM
7	run7	16	Mellor-Yamada-Jan	Eta microphysics (Not in MM5)	Kain-Fritsch (MM5: Kain-Fritsch)	CAM/CAM
8	run8	7	Mellor-Yamada-Jan	Thompson (MM5 : Reisner 2)	Betts-Miller (MM5: Betts-Miller)	Dudhia/RRTM
9	run9	12	Mellor-Yamada-Jan	Goddard microphysics (MM5: GSFC)	Grell-Devenyi (MM5: Grell scheme)	GFDL/GFDL
10	run10	8	Mellor-Yamada-Jan	Goddard microphysics (MM5: GSFC)	Betts-Miller (MM5: Betts-Miller)	CAM/CAM
11	run11	10	Mellor-Yamada-Jan	Thompson (MM5 : Reisner 2)	Betts-Miller (MM5: Betts-Miller)	CAM/CAM
12	run12	17	Mellor-Yamada-Jan	Thompson (MM5 : Reisner 2)	Betts-Miller (MM5: Betts-Miller)	Goodard/RRTM
13	run13	17	Mellor-Yamada-Jan	Lin et al. (MM5: GSFC)	Grell-Devenyi (MM5: Grell scheme)	Goddard/RRTM
14	run14	13	Mellor-Yamada-Jan	Lin et al. (MM5: GSFC)	Betts-Miller (MM5: Betts-Miller)	GFDL/GFDL
15	run15	11	Mellor-Yamada-Jan	Goddard microphysics (MM5: GSFC)	Betts-Miller (MM5: Betts-Miller)	GFDL/RRTM
16	run16	6	Mellor-Yamada-Jan	Lin et al. (MM5: GSFC)	Kain-Fritsch (MM5: Kain-Fritsch)	Dudhia/GFDL
17	run17	13	Mellor-Yamada-Jan	Eta microphysics (Not in MM5)	Kain-Fritsch (MM5: Kain-Fritsch)	Dudhia/CAM
18	run18	13	Mellor-Yamada-Jan	WRF-single mom (6) (MM5: Reisner 1)	Betts-Miller (MM5: Betts-Miller)	Goddard/RRTM
19	run19	8	Mellor-Yamada-Jan	WRF-single mom (3) (MM5: simple ice)	Kain-Fritsch (MM5: Kain-Fritsch)	Dudhia/RRTM
20	run20	18	Mellor-Yamada-Jan	Morrison (Not in MM5)	Kain-Fritsch (MM5: Kain-Fritsch)	Goddard/RRTM
21	run21	8	Mellor-Yamada-Jan	Morrison (Not in MM5)	Betts-Miller (MM5: Betts-Miller)	Goddard/RRTM
22	run22	16	Mellor-Yamada-Jan	Morrison (Not in MM5)	Grell-Devenyi (MM5: Grell scheme)	Goddard/RRTM
23	run23	15	YSU (new MRF)	Eta microphysics (Not in MM5)	Kain-Fritsch (MM5: Kain-Fritsch)	GFDL/GFDL
24	run24	4	YSU (new MRF)	Lin et al. (MM5: GSFC)	Betts-Miller (MM5: Betts-Miller)	GFDL/GFDL
25	run25	9	YSU (new MRF)	Goddard microphysics (MM5: GSFC)	Betts-Miller (MM5: Betts-Miller)	Goddard/RRTM
26	run26	6	YSU (new MRF)	Lin et al. (MM5: GSFC)	Kain-Fritsch (MM5: Kain-Fritsch)	CAM/CAM
27	run27	16	YSU (new MRF)	Lin et al. (MM5: GSFC)	Betts-Miller (MM5: Betts-Miller)	CAM/CAM
28	run28	18	YSU (new MRF)	Goddard microphysics (MM5: GSFC)	Betts-Miller (MM5: Betts-Miller)	Dudhia/RRTM
29	run29	11	YSU (new MRF)	Thompson (MM5 : Reisner 2)	Grell-Devenyi (MM5: Grell scheme)	GFDL/GFDL
30	run30	6	YSU (new MRF)	Eta microphysics (Not in MM5)	Betts-Miller (MM5: Betts-Miller)	Goddard/RRTM
31	run31	7	YSU (new MRF)	Eta microphysics (Not in MM5)	Kain-Fritsch (MM5: Kain-Fritsch)	CAM/CAM
32	run32	11	YSU (new MRF)	Morrison (Not in MM5)	Kain-Fritsch (MM5: Kain-Fritsch)	Goddard/RRTM
33	run33	15	YSU (new MRF)	WRF-single mom(6) (MM5: Reisner 1)	Kain-Fritsch (MM5: Kain-Fritsch)	Goddard/RRTM
34	run34	7	YSU (new MRF)	WRF-single mom(3) (MM5: Simple ice)	Betts-Miller (MM5: Betts-Miller)	Dudhia/RRTM
35	run35	9	YSU (new MRF)	WRF-single mom(6) (MM5: Reisner 1)	Betts-Miller (MM5: Betts-Miller)	CAM/CAM
36	run36	8	Pleim-Xiu	Eta microphysics (Not in MM5)	Betts-Miller (MM5: Betts-Miller)	Goddard/RRTM
37	run37	15	Pleim-Xiu	Lin et al. (MM5: GSFC)	Betts-Miller (MM5: Betts-Miller)	Goddard/RRTM
38	run38	20	Pleim-Xiu	Eta microphysics (Not in MM5)	Grell-Devenyi (MM5: Grell scheme)	GFDL/GFDL
39	run39	22	Pleim-Xiu	Goddard microphysics (MM5: GSFC)	Grell-Devenyi (MM5: Grell scheme)	Dudhia/RRTM
40	run40	6	Pleim-Xiu	Lin et al. (MM5: GSFC)	Kain-Fritsch (MM5: Kain-Fritsch)	GFDL/GFDL
41	run41	19	Pleim-Xiu	Thompson (MM5 : Reisner 2)	Kain-Fritsch (MM5: Kain-Fritsch)	GFDL/GFDL
42	run42	16	Pleim-Xiu	Goddard microphysics (MM5: GSFC)	Grell-Devenyi (MM5: Grell scheme)	CAM/CAM
43	run43	9	Pleim-Xiu	Goddard microphysics (MM5: GSFC)	Kain-Fritsch (MM5: Kain-Fritsch)	CAM/CAM
44	run44	11	Pleim-Xiu	WRF-single mom(6) (MM5: Reisner 1)	Kain-Fritsch (MM5: Kain-Fritsch)	Goddard/RRTM
45	run45	10	Pleim-Xiu	Morrison (Not in MM5)	Kain-Fritsch (MM5: Kain-Fritsch)	Goddard/RRTM
46	run46	18	Pleim-Xiu	Lin et al. (MM5: GSFC)	Kain-Fritsch (MM5: Kain-Fritsch)	CAM/CAM
47	run47	16	Pleim-Xiu	Goddard microphysics (MM5: GSFC)	Betts-Miller (MM5: Betts-Miller)	Dudhia/RRTM
48	run48	20	Pleim-Xiu	Lin et al. (MM5: GSFC)	Betts-Miller (MM5: Betts-Miller)	Dudhia/RRTM
49	run49	12	Pleim-Xiu	Lin et al. (MM5: GSFC)	Grell-Devenyi (MM5: Grell scheme)	Dudhia/RRTM
50	run50	7	Pleim-Xiu	Goddard microphysics (MM5: GSFC)	Grell-Devenyi (MM5: Grell scheme)	Dudhia/RRTM
51	run51	21	Pleim-Xiu	Lin et al. (MM5: GSFC)	Kain-Fritsch (MM5: Kain-Fritsch)	GFDL/GFDL

Table 4B. Front 2: Ensemble ranking with respect to physical parameterizations for COAMPS.

counter	Run	TOTAL rank	PBL	dxmeso*	Ice nucleation	Autoconversion factor
	COAMPS Front 2					
1	run1	47	Mellor-Yamada(MY)	50000	Cooper and Haines (1986)	0.0004
2	run2	51	Mellor-Yamada	10000	Cooper and Haines (1986)	0.0004
3	run3	14	Mellor-Yamada	150000	Cooper and Haines (1986)	0.0004
4	run4	49	Mellor-Yamada	150000	Cooper and Haines (1986)	0.0004
5	run5	31	Mellor-Yamada	50000	Cooper and Haines (1986)	0.0004
6	run6	41	Mellor-Yamada	10000	Cooper and Haines (1986)	0.0004
7	run7	47	Mellor-Yamada	150000	Fletcher (1962)	0.0004
8	run8	17	Mellor-Yamada	50000	Fletcher (1962)	0.0004
9	run9	15	Mellor-Yamada	10000	Fletcher (1962)	0.0004
10	run10	47	Mellor-Yamada	10000	Fletcher (1962)	0.001 default
11	run11	50	Mellor-Yamada	50000	Fletcher (1962)	0.001 default
12	run12	38	Mellor-Yamada	150000	Fletcher (1962)	0.001 default
13	run13	33	Mellor-Yamada	50000	Cooper and Haines (1986)	0.001 default
14	run14	36	Mellor-Yamada	10000	Cooper and Haines (1986)	0.001 default
15	run15	39	Mellor-Yamada	150000	Cooper and Haines (1986)	0.001 default
16	run16	13	Mellor-Yamada	150000	Cooper and Haines (1986)	0.001 default
17	run17	22	Mellor-Yamada	50000	Cooper and Haines (1986)	0.001 default
18	run18	29	Mellor-Yamada	10000	Cooper and Haines (1986)	0.001 default
19	run19	43	Mellor-Yamada	10000	Cooper and Haines (1986)	0.002
20	run20	41	Mellor-Yamada	50000	Cooper and Haines (1986)	0.002
21	run21	10	Mellor-Yamada	150000	Cooper and Haines (1986)	0.002
22	run22	55	Mellor-Yamada	150000	Cooper and Haines (1986)	0.002
23	run23	52	Mellor-Yamada	50000	Cooper and Haines (1986)	0.002
24	run24	53	Mellor-Yamada	10000	Cooper and Haines (1986)	0.002
25	run25	19	Mellor-Yamada	10000	Fletcher (1962)	0.002
26	run26	18	Mellor-Yamada	50000	Fletcher (1962)	0.002
27	run27	53	Mellor-Yamada	150000	Fletcher (1962)	0.002
28	run28	34	Modified MY version	10000	Cooper and Haines (1986)	0.0004
29	run29	31	Modified MY version	50000	Cooper and Haines (1986)	0.0004
30	run30	5	Modified MY version	150000	Cooper and Haines (1986)	0.0004
31	run31	43	Modified MY version	150000	Cooper and Haines (1986)	0.0004
32	run32	26	Modified MY version	50000	Cooper and Haines (1986)	0.0004
33	run33	38	Modified MY version	10000	Cooper and Haines (1986)	0.0004
34	run34	29	Modified MY version	10000	Fletcher (1962)	0.0004
35	run35	23	Modified MY version	50000	Fletcher (1962)	0.0004
36	run36	6	Modified MY version	150000	Fletcher (1962)	0.0004
37	run37	7	Modified MY version	150000	Fletcher (1962)	0.001 default
38	run38	27	Modified MY version	50000	Fletcher (1962)	0.001 default
39	run39	43	Modified MY version	10000	Fletcher (1962)	0.001 default
40	run40	37	Modified MY version	10000	Cooper and Haines (1986)	0.001 default
41	run41	30	Modified MY version	50000	Cooper and Haines (1986)	0.001 default
42	run42	12	Modified MY version	150000	Cooper and Haines (1986)	0.001 default
43	run43	8	Modified MY version	150000	Cooper and Haines (1986)	0.001 default
44	run44	35	Modified MY version	50000	Cooper and Haines (1986)	0.001 default
45	run45	28	Modified MY version	10000	Cooper and Haines (1986)	0.001 default
46	run46	38	Modified MY version	10000	Cooper and Haines (1986)	0.002
47	run47	40	Modified MY version	50000	Cooper and Haines (1986)	0.002
48	run48	9	Modified MY version	150000	Cooper and Haines (1986)	0.002
49	run49	13	Modified MY version	150000	Cooper and Haines (1986)	0.002
50	run50	22	Modified MY version	50000	Cooper and Haines (1986)	0.002
51	run51	23	Modified MY version	10000	Cooper and Haines (1986)	0.002

Table 5B. Front 2: Ensemble ranking with respect to physical parameterizations for MM5.

counter	Run	TOTAL rank	MM5 (PBL)	MM5 (Microphysics)	MM5 (Cumulus)	MM5 (Radiation)
	MM5 Front 2					
1	run1	34	Eta M-Y (IBLTYP=4)	Reisner 2 (IMPHYS=7)	Kain-Fritsch (ICUPA=8,ISHALLO=0)	RRTM (FRAD=4)
2	run2	27	Eta M-Y (IBLTYP=4)	Reisner 2 (IMPHYS=7)	Grell (ICUPA=3,ISHALLO=1)	CCM2 (FRAD=3)
3	run3	13	Eta M-Y (IBLTYP=4)	Simple ice (Dudhia) (IMPHYS=4)	Grell (ICUPA=3,ISHALLO=1)	Dudhia (FRAD=2)
4	run4	14	Eta M-Y (IBLTYP=4)	Goddard (GFSC) (IMPHYS=6)	Grell (ICUPA=3,ISHALLO=1)	Dudhia (FRAD=2)
5	run5	19	Eta M-Y (IBLTYP=4)	Reisner 2 (IMPHYS=7)	Betts-Miller (ICUPA=7,ISHALLO=0)	CCM2 (FRAD=3)
6	run6	19	Eta M-Y (IBLTYP=4)	Reisner 2 (IMPHYS=7)	Grell (ICUPA=3,ISHALLO=1)	Dudhia (FRAD=2)
7	run7	33	Eta M-Y (IBLTYP=4)	Schultz (IMPHYS=8)	Betts-Miller (ICUPA=7,ISHALLO=0)	Dudhia (FRAD=2)
8	run8	7	Eta M-Y (IBLTYP=4)	Simple ice (Dudhia) (IMPHYS=4)	Grell (ICUPA=3,ISHALLO=1)	CCM2 (FRAD=3)
9	run9	38	Eta M-Y (IBLTYP=4)	Goddard (GFSC) (IMPHYS=6)	Betts-Miller (ICUPA=7,ISHALLO=0)	Dudhia (FRAD=2)
10	run10	11	Eta M-Y (IBLTYP=4)	Reisner (no graupel)	Kain-Fritsch (ICUPA=8,ISHALLO=0)	Simple cloud (FRAD=1)
11	run11	9	Eta M-Y (IBLTYP=4)	Reisner 2 (IMPHYS = 7)	Betts-Miller (ICUPA=7,ISHALLO=0)	RRTM (FRAD=4)
12	run12	42	Eta M-Y (IBLTYP=4)	Simple ice (Dudhia) (IMPHYS=4)	Betts-Miller (ICUPA=7,ISHALLO=0)	Dudhia (FRAD=2)
13	run13	31	Eta M-Y (IBLTYP=4)	Simple ice (Dudhia) (IMPHYS=4)	Betts-Miller (ICUPA=7,ISHALLO=0)	CCM2 (FRAD=3)
14	run14	8	Gayno-Seaman (IBLTYP=6)	Schultz (IMPHYS=8)	Betts-Miller (ICUPA=7,ISHALLO=0)	CCM2 (FRAD=3)
15	run15	35	Gayno-Seaman (IBLTYP=6)	Goddard (GFSC) (IMPHYS=6)	Betts-Miller (ICUPA=7,ISHALLO=0)	CCM2 (FRAD=3)
16	run16	33	Gayno-Seaman (IBLTYP=6)	Reisner 2 (IMPHYS=7)	Grell (ICUPA=3,ISHALLO=1)	Dudhia (FRAD=2)
17	run17	14	Blackadar	Schultz (IMPHYS=8)	Kain-Fritsch (ICUPA=8,ISHALLO=0)	RRTM (FRAD=4)
18	run18	44	Gayno-Seaman (IBLTYP=6)	Reisner 2 (IMPHYS=7)	Betts-Miller (ICUPA=7,ISHALLO=0)	CCM2 (FRAD=3)
19	run19	47	Blackadar	Simple ice (Dudhia) (IMPHYS=4)	Grell (ICUPA=3,ISHALLO=1)	Dudhia (FRAD=2)
20	run20	42	Gayno-Seaman (IBLTYP=6)	Goddard (GFSC) (IMPHYS=6)	Grell (ICUPA=3,ISHALLO=1)	Simple cloud (FRAD=1)
21	run21	40	Gayno-Seaman (IBLTYP=6)	Schultz (IMPHYS=8)	Kain-Fritsch (ICUPA=8,ISHALLO=0)	Dudhia (FRAD=2)
22	run22	37	Gayno-Seaman (IBLTYP=6)	Simple ice (Dudhia) (IMPHYS=4)	Grell (ICUPA=3,ISHALLO=1)	CCM2 (FRAD=3)
23	run23	32	Gayno-Seaman (IBLTYP=6)	Goddard (GFSC) (IMPHYS=6)	Kain-Fritsch (ICUPA=8,ISHALLO=0)	Simple cloud (FRAD=1)
24	run24	36	Gayno-Seaman (IBLTYP=6)	Simple ice (Dudhia) (IMPHYS=4)	Kain-Fritsch (ICUPA=8,ISHALLO=0)	RRTM (FRAD=4)
25	run25	39	Gayno-Seaman (IBLTYP=6)	Goddard (GFSC) (IMPHYS=6)	Grell (ICUPA=3,ISHALLO=1)	Dudhia (FRAD=2)
26	run26	4	Gayno-Seaman (IBLTYP=6)	Goddard (GFSC) (IMPHYS=6)	Kain-Fritsch (ICUPA=8,ISHALLO=0)	CCM2 (FRAD=3)
27	run27	37	Gayno-Seaman (IBLTYP=6)	Goddard (GFSC) (IMPHYS=6)	Betts-Miller (ICUPA=7,ISHALLO=0)	RRTM (FRAD=4)
28	run28	34	Gayno-Seaman (IBLTYP=6)	Simple ice (Dudhia) (IMPHYS=4)	Kain-Fritsch (ICUPA=8,ISHALLO=0)	Simple cloud (FRAD=1)
29	run29	24	Blackadar	Schultz (IMPHYS=8)	Kain-Fritsch (ICUPA=8,ISHALLO=0)	CCM2 (FRAD=3)
30	run30	19	Gayno-Seaman (IBLTYP=6)	Reisner 2 (IMPHYS=7)	Kain-Fritsch (ICUPA=8,ISHALLO=0)	Simple cloud (FRAD=1)
31	run31	24	k-Thompson (IBLTYP=3,ISOI	Reisner 2 (IMPHYS=7)	Betts-Miller (ICUPA=7,ISHALLO=0)	Simple cloud (FRAD=1)
32	run32	46	k-Thompson (IBLTYP=3,ISOI	Simple ice (Dudhia) (IMPHYS=4)	Betts-Miller (ICUPA=7,ISHALLO=0)	Simple cloud (FRAD=1)
33	run33	11	k-Thompson (IBLTYP=3,ISOI	Reisner 2 (IMPHYS=7)	Kain-Fritsch (ICUPA=8,ISHALLO=0)	Dudhia (FRAD=2)
34	run34	27	k-Thompson (IBLTYP=3,ISOI	Reisner 2 (IMPHYS=7)	Betts-Miller (ICUPA=7,ISHALLO=0)	RRTM (FRAD=4)
35	run35	9	k-Thompson (IBLTYP=3,ISOI	Simple ice (Dudhia) (IMPHYS=4)	Betts-Miller (ICUPA=7,ISHALLO=0)	RRTM (FRAD=4)
36	run36	6	k-Thompson (IBLTYP=3,ISOI	Reisner 2 (IMPHYS=7)	Betts-Miller (ICUPA=7,ISHALLO=0)	Dudhia (FRAD=2)
37	run37	28	k-Thompson (IBLTYP=3,ISOI	Goddard (GFSC) (IMPHYS=6)	Grell (ICUPA=3,ISHALLO=1)	CCM2 (FRAD=3)
38	run38	21	k-Thompson (IBLTYP=3,ISOI	Simple ice (Dudhia) (IMPHYS=4)	Betts-Miller (ICUPA=7,ISHALLO=0)	CCM2 (FRAD=3)
39	run39	34	k-Thompson (IBLTYP=3,ISOI	Schultz (IMPHYS=8)	Betts-Miller (ICUPA=7,ISHALLO=0)	Dudhia (FRAD=2)
40	run40	18	k-Thompson (IBLTYP=3,ISOI	Reisner 2 (IMPHYS=7)	Kain-Fritsch (ICUPA=8,ISHALLO=0)	Simple cloud (FRAD=1)
41	run41	44	k-Thompson (IBLTYP=3,ISOI	Goddard (GFSC) (IMPHYS=6)	Kain-Fritsch (ICUPA=8,ISHALLO=0)	Simple cloud (FRAD=1)
42	run42	42	MRF (IBLTYP=5)	Reisner 2 (IMPHYS=7)	Kain-Fritsch (ICUPA=8,ISHALLO=0)	Dudhia (FRAD=2)
43	run43	20	MRF (IBLTYP=5)	Simple ice (Dudhia) (IMPHYS=4)	Betts-Miller (ICUPA=7,ISHALLO=0)	Dudhia (FRAD=2)
44	run44	18	MRF (IBLTYP=5)	Reisner 2 (IMPHYS=7)	Grell (ICUPA=3,ISHALLO=1)	CCM2 (FRAD=3)
45	run45	23	MRF (IBLTYP=5)	Reisner 2 (IMPHYS=7)	Kain-Fritsch (ICUPA=8,ISHALLO=0)	RRTM (FRAD=4)
46	run46	35	MRF (IBLTYP=5)	Schultz (IMPHYS=8)	Grell (ICUPA=3,ISHALLO=1)	CCM2 (FRAD=3)
47	run47	29	MRF (IBLTYP=5)	Schultz (IMPHYS=8)	Betts-Miller (ICUPA=7,ISHALLO=0)	RRTM (FRAD=4)
48	run48	40	MRF (IBLTYP=5)	Simple ice (Dudhia) (IMPHYS=4)	Kain-Fritsch (ICUPA=8,ISHALLO=0)	RRTM (FRAD=4)
49	run49	42	MRF (IBLTYP=5)	Goddard (GFSC) (IMPHYS=6)	Betts-Miller (ICUPA=7,ISHALLO=0)	RRTM (FRAD=4)
50	run50	43	MRF (IBLTYP=5)	Simple ice (Dudhia) (IMPHYS=4)	Grell (ICUPA=3,ISHALLO=1)	CCM2 (FRAD=3)
51	run51	47	MRF (IBLTYP=5)	Simple ice (Dudhia) (IMPHYS=4)	Grell (ICUPA=3,ISHALLO=1)	Dudhia (FRAD=2)

Table 6B. Front 2: Ensemble ranking with respect to physical parameterizations for WRF.

counter	Run	TOTAL rank	WRF (PBL)	WRF (Microphysics)	WRF (Cumulus)	WRF (Radiation)
	WRF Front 2					
1	run1	22	Mellor-Yamada-Jan	Thompson (MM5 : Reisner 2)	Kain-Fritsch (MM5: Kain-Fritsch)	Dudhia/RRTM
2	run2	7	Mellor-Yamada-Jan	Goddard microphysics (MM5: GSFC)	Betts-Miller (MM5: Betts-Miller)	GFDL/GFDL (Not in MM5)
3	run3	42	Mellor-Yamada-Jan	Goddard microphysics (MM5: GSFC)	Kain-Fritsch (MM5: Kain-Fritsch)	GFDL/GFDL
4	run4	8	Mellor-Yamada-Jan	Lin et al. (MM5: GSFC)	Kain-Fritsch (MM5: Kain-Fritsch)	Goddard/RRTM
5	run5	4	Mellor-Yamada-Jan	Eta microphysics (Not in MM5)	Kain-Fritsch (MM5: Kain-Fritsch)	GFDL/GFDL
6	run6	13	Mellor-Yamada-Jan	Eta microphysics (Not in MM5)	Betts-Miller (MM5: Betts-Miller)	CAM/CAM
7	run7	14	Mellor-Yamada-Jan	Eta microphysics (Not in MM5)	Kain-Fritsch (MM5: Kain-Fritsch)	CAM/CAM
8	run8	30	Mellor-Yamada-Jan	Thompson (MM5 : Reisner 2)	Betts-Miller (MM5: Betts-Miller)	Dudhia/RRTM
9	run9	5	Mellor-Yamada-Jan	Goddard microphysics (MM5: GSFC)	Grell-Devenyi (MM5: Grell scheme)	GFDL/GFDL
10	run10	21	Mellor-Yamada-Jan	Goddard microphysics (MM5: GSFC)	Betts-Miller (MM5: Betts-Miller)	CAM/CAM
11	run11	38	Mellor-Yamada-Jan	Thompson (MM5 : Reisner 2)	Betts-Miller (MM5: Betts-Miller)	CAM/CAM
12	run12	19	Mellor-Yamada-Jan	Thompson (MM5 : Reisner 2)	Betts-Miller (MM5: Betts-Miller)	Goodard/RRTM
13	run13	24	Mellor-Yamada-Jan	Lin et al. (MM5: GSFC)	Grell-Devenyi (MM5: Grell scheme)	Goddard/RRTM
14	run14	5	Mellor-Yamada-Jan	Lin et al. (MM5: GSFC)	Betts-Miller (MM5: Betts-Miller)	GFDL/GFDL
15	run15	22	Mellor-Yamada-Jan	Goddard microphysics (MM5: GSFC)	Betts-Miller (MM5: Betts-Miller)	GFDL/RRTM
16	run16	23	Mellor-Yamada-Jan	Lin et al. (MM5: GSFC)	Kain-Fritsch (MM5: Kain-Fritsch)	Dudhia/GFDL
17	run17	8	Mellor-Yamada-Jan	Eta microphysics (Not in MM5)	Kain-Fritsch (MM5: Kain-Fritsch)	Dudhia/CAM
18	run18	16	Mellor-Yamada-Jan	WRF-single mom (6) (MM5: Reisner 1)	Betts-Miller (MM5: Betts-Miller)	Goddard/RRTM
19	run19	31	Mellor-Yamada-Jan	WRF-single mom (3) (MM5: simple ice)	Kain-Fritsch (MM5: Kain-Fritsch)	Dudhia/RRTM
20	run20	52	Mellor-Yamada-Jan	Morrison (Not in MM5)	Kain-Fritsch (MM5: Kain-Fritsch)	Goddard/RRTM
21	run21	27	Mellor-Yamada-Jan	Morrison (Not in MM5)	Betts-Miller (MM5: Betts-Miller)	Goddard/RRTM
22	run22	47	Mellor-Yamada-Jan	Morrison (Not in MM5)	Grell-Devenyi (MM5: Grell scheme)	Goddard/RRTM
23	run23	39	YSU (new MRF)	Eta microphysics (Not in MM5)	Kain-Fritsch (MM5: Kain-Fritsch)	GFDL/GFDL
24	run24	26	YSU (new MRF)	Lin et al. (MM5: GSFC)	Betts-Miller (MM5: Betts-Miller)	GFDL/GFDL
25	run25	43	YSU (new MRF)	Goddard microphysics (MM5: GSFC)	Betts-Miller (MM5: Betts-Miller)	Goddard/RRTM
26	run26	22	YSU (new MRF)	Lin et al. (MM5: GSFC)	Kain-Fritsch (MM5: Kain-Fritsch)	CAM/CAM
27	run27	34	YSU (new MRF)	Lin et al. (MM5: GSFC)	Betts-Miller (MM5: Betts-Miller)	CAM/CAM
28	run28	38	YSU (new MRF)	Goddard microphysics (MM5: GSFC)	Betts-Miller (MM5: Betts-Miller)	Dudhia/RRTM
29	run29	39	YSU (new MRF)	Thompson (MM5 : Reisner 2)	Grell-Devenyi (MM5: Grell scheme)	GFDL/GFDL
30	run30	23	YSU (new MRF)	Eta microphysics (Not in MM5)	Betts-Miller (MM5: Betts-Miller)	Goddard/RRTM
31	run31	10	YSU (new MRF)	Eta microphysics (Not in MM5)	Kain-Fritsch (MM5: Kain-Fritsch)	CAM/CAM
32	run32	28	YSU (new MRF)	Morrison (Not in MM5)	Kain-Fritsch (MM5: Kain-Fritsch)	Goddard/RRTM
33	run33	31	YSU (new MRF)	WRF-single mom(6) (MM5: Reisner 1)	Kain-Fritsch (MM5: Kain-Fritsch)	Goddard/RRTM
34	run34	15	YSU (new MRF)	WRF-single mom(3) (MM5: Simple ice)	Betts-Miller (MM5: Betts-Miller)	Dudhia/RRTM
35	run35	30	YSU (new MRF)	WRF-single mom(6) (MM5: Reisner 1)	Betts-Miller (MM5: Betts-Miller)	CAM/CAM
36	run36	13	Pleim-Xiu	Eta microphysics (Not in MM5)	Betts-Miller (MM5: Betts-Miller)	Goddard/RRTM
37	run37	31	Pleim-Xiu	Lin et al. (MM5: GSFC)	Betts-Miller (MM5: Betts-Miller)	Goddard/RRTM
38	run38	40	Pleim-Xiu	Eta microphysics (Not in MM5)	Grell-Devenyi (MM5: Grell scheme)	GFDL/GFDL
39	run39	47	Pleim-Xiu	Goddard microphysics (MM5: GSFC)	Grell-Devenyi (MM5: Grell scheme)	Dudhia/RRTM
40	run40	33	Pleim-Xiu	Lin et al. (MM5: GSFC)	Kain-Fritsch (MM5: Kain-Fritsch)	GFDL/GFDL
41	run41	44	Pleim-Xiu	Thompson (MM5 : Reisner 2)	Kain-Fritsch (MM5: Kain-Fritsch)	GFDL/GFDL
42	run42	48	Pleim-Xiu	Goddard microphysics (MM5: GSFC)	Grell-Devenyi (MM5: Grell scheme)	CAM/CAM
43	run43	51	Pleim-Xiu	Goddard microphysics (MM5: GSFC)	Kain-Fritsch (MM5: Kain-Fritsch)	CAM/CAM
44	run44	48	Pleim-Xiu	WRF-single mom(6) (MM5: Reisner 1)	Kain-Fritsch (MM5: Kain-Fritsch)	Goddard/RRTM
45	run45	50	Pleim-Xiu	Morrison (Not in MM5)	Kain-Fritsch (MM5: Kain-Fritsch)	Goddard/RRTM
46	run46	38	Pleim-Xiu	Lin et al. (MM5: GSFC)	Kain-Fritsch (MM5: Kain-Fritsch)	CAM/CAM
47	run47	14	Pleim-Xiu	Goddard microphysics (MM5: GSFC)	Betts-Miller (MM5: Betts-Miller)	Dudhia/RRTM
48	run48	49	Pleim-Xiu	Lin et al. (MM5: GSFC)	Betts-Miller (MM5: Betts-Miller)	Dudhia/RRTM
49	run49	43	Pleim-Xiu	Lin et al. (MM5: GSFC)	Grell-Devenyi (MM5: Grell scheme)	Dudhia/RRTM
50	run50	37	Pleim-Xiu	Goddard microphysics (MM5: GSFC)	Grell-Devenyi (MM5: Grell scheme)	Dudhia/RRTM
51	run51	9	Pleim-Xiu	Lin et al. (MM5: GSFC)	Kain-Fritsch (MM5: Kain-Fritsch)	GFDL/GFDL

Table 7B. Front 3: Ensemble ranking with respect to physical parameterizations for COAMPS.

counter	Run	TOTAL rank	PBL	dxmeso*	Ice nucleation	Autoconversion factor
	COAMPS Front 3					
1	run26	8	Mellor-Yamada	50000	Fletcher (1962)	0.002
2	run36	9	Modified MY version	150000	Fletcher (1962)	0.0004
3	run9	10	Mellor-Yamada	10000	Fletcher (1962)	0.0004
4	run18	10	Mellor-Yamada	10000	Cooper and Haines (1986)	0.001 default
5	run10	11	Mellor-Yamada	10000	Fletcher (1962)	0.001 default
6	run11	13	Mellor-Yamada	50000	Fletcher (1962)	0.001 default
7	run2	14	Mellor-Yamada	10000	Cooper and Haines (1986)	0.0004
8	run25	15	Mellor-Yamada	10000	Fletcher (1962)	0.002
9	run39	16	Modified MY version	10000	Fletcher (1962)	0.001 default
10	run8	17	Mellor-Yamada	50000	Fletcher (1962)	0.0004
11	run17	18	Mellor-Yamada	50000	Cooper and Haines (1986)	0.001 default
12	run14	19	Mellor-Yamada	10000	Cooper and Haines (1986)	0.001 default
13	run23	19	Mellor-Yamada	50000	Cooper and Haines (1986)	0.002
14	run13	21	Mellor-Yamada	50000	Cooper and Haines (1986)	0.001 default
15	run19	21	Mellor-Yamada	10000	Cooper and Haines (1986)	0.002
16	run20	21	Mellor-Yamada	50000	Cooper and Haines (1986)	0.002
17	run6	24	Mellor-Yamada	10000	Cooper and Haines (1986)	0.0004
18	run1	25	Mellor-Yamada(MY)	50000	Cooper and Haines (1986)	0.0004
19	run24	25	Mellor-Yamada	10000	Cooper and Haines (1986)	0.002
20	run16	26	Mellor-Yamada	150000	Cooper and Haines (1986)	0.001 default
21	run45	27	Modified MY version	10000	Cooper and Haines (1986)	0.001 default
22	run47	27	Modified MY version	50000	Cooper and Haines (1986)	0.002
23	run22	28	Mellor-Yamada	150000	Cooper and Haines (1986)	0.002
24	run21	29	Mellor-Yamada	150000	Cooper and Haines (1986)	0.002
25	run37	31	Modified MY version	150000	Fletcher (1962)	0.001 default
26	run38	33	Modified MY version	50000	Fletcher (1962)	0.001 default
27	run43	33	Modified MY version	150000	Cooper and Haines (1986)	0.001 default
28	run46	33	Modified MY version	10000	Cooper and Haines (1986)	0.002
29	run3	35	Mellor-Yamada	150000	Cooper and Haines (1986)	0.0004
30	run5	36	Mellor-Yamada	50000	Cooper and Haines (1986)	0.0004
31	run27	37	Mellor-Yamada	150000	Fletcher (1962)	0.002
32	run40	38	Modified MY version	10000	Cooper and Haines (1986)	0.001 default
33	run28	39	Modified MY version	10000	Cooper and Haines (1986)	0.0004
34	run34	42	Modified MY version	10000	Fletcher (1962)	0.0004
35	run33	43	Modified MY version	10000	Cooper and Haines (1986)	0.0004
36	run41	43	Modified MY version	50000	Cooper and Haines (1986)	0.001 default
37	run44	46	Modified MY version	50000	Cooper and Haines (1986)	0.001 default
38	run51	46	Modified MY version	10000	Cooper and Haines (1986)	0.002
39	run29	47	Modified MY version	50000	Cooper and Haines (1986)	0.0004
40	run35	47	Modified MY version	50000	Fletcher (1962)	0.0004
41	run15	48	Mellor-Yamada	150000	Cooper and Haines (1986)	0.001 default
42	run4	50	Mellor-Yamada	150000	Cooper and Haines (1986)	0.0004
43	run30	50	Modified MY version	150000	Cooper and Haines (1986)	0.0004
44	run32	50	Modified MY version	50000	Cooper and Haines (1986)	0.0004
45	run50	51	Modified MY version	50000	Cooper and Haines (1986)	0.002
46	run42	52	Modified MY version	150000	Cooper and Haines (1986)	0.001 default
47	run48	52	Modified MY version	150000	Cooper and Haines (1986)	0.002
48	run31	53	Modified MY version	150000	Cooper and Haines (1986)	0.0004
49	run49	55	Modified MY version	150000	Cooper and Haines (1986)	0.002
50	run12	57	Mellor-Yamada	150000	Fletcher (1962)	0.001 default
51	run7	58	Mellor-Yamada	150000	Fletcher (1962)	0.0004

Table 8B. Front 3: Ensemble ranking with respect to physical parameterizations for MM5.

	Run	TOTAL rank	MM5 (PBL)	MM5 (Microphysics)	MM5 (Cumulus)	MM5 (Radiation)
			MM5 Front 3			
1	run39	7	k-Thompson (IBLTYP=3,ISOI	Schultz (IMPHYS=8)	Betts-Miller (ICUPA=7,ISHALLO=0)	Dudhia (FRAD=2)
2	run31	9	k-Thompson (IBLTYP=3,ISOI	Reisner 2 (IMPHYS=7)	Betts-Miller (ICUPA=7,ISHALLO=0)	Simple cloud (FRAD=1)
3	run19	10	Blackadar	Simple ice (Dudhia) (IMPHYS=4)	Grell (ICUPA=3,ISHALLO=1)	Dudhia (FRAD=2)
4	run22	10	Gayno-Seaman (IBLTYP=6)	Simple ice (Dudhia) (IMPHYS=4)	Grell (ICUPA=3,ISHALLO=1)	CCM2 (FRAD=3)
5	run27	10	Gayno-Seaman (IBLTYP=6)	Goddard (GFSC) (IMPHYS=6)	Betts-Miller (ICUPA=7,ISHALLO=0)	RRTM (FRAD=4)
6	run45	10	MRF (IBLTYP=5)	Reisner 2 (IMPHYS=7)	Kain-Fritsch (ICUPA=8,ISHALLO=0)	RRTM (FRAD=4)
7	run16	11	Gayno-Seaman (IBLTYP=6)	Reisner 2 (IMPHYS=7)	Grell (ICUPA=3,ISHALLO=1)	Dudhia (FRAD=2)
8	run18	12	Gayno-Seaman (IBLTYP=6)	Reisner 2 (IMPHYS=7)	Betts-Miller (ICUPA=7,ISHALLO=0)	CCM2 (FRAD=3)
9	run21	13	Gayno-Seaman (IBLTYP=6)	Schultz (IMPHYS=8)	Kain-Fritsch (ICUPA=8,ISHALLO=0)	Dudhia (FRAD=2)
10	run5	14	Eta M-Y (IBLTYP=4)	Reisner 2 (IMPHYS=7)	Betts-Miller (ICUPA=7,ISHALLO=0)	CCM2 (FRAD=3)
11	run9	14	Eta M-Y (IBLTYP=4)	Goddard (GFSC) (IMPHYS=6)	Betts-Miller (ICUPA=7,ISHALLO=0)	Dudhia (FRAD=2)
12	run37	14	k-Thompson (IBLTYP=3,ISOI	Goddard (GFSC) (IMPHYS=6)	Grell (ICUPA=3,ISHALLO=1)	CCM2 (FRAD=3)
13	run43	15	MRF (IBLTYP=5)	Simple ice (Dudhia) (IMPHYS=4)	Betts-Miller (ICUPA=7,ISHALLO=0)	Dudhia (FRAD=2)
14	run1	16	Eta M-Y (IBLTYP=4)	Reisner 2 (IMPHYS=7)	Kain-Fritsch (ICUPA=8,ISHALLO=0)	RRTM (FRAD=4)
15	run3	16	Eta M-Y (IBLTYP=4)	Simple ice (Dudhia) (IMPHYS=4)	Grell (ICUPA=3,ISHALLO=1)	Dudhia (FRAD=2)
16	run34	16	k-Thompson (IBLTYP=3,ISOI	Reisner 2 (IMPHYS=7)	Betts-Miller (ICUPA=7,ISHALLO=0)	RRTM (FRAD=4)
17	run25	17	Gayno-Seaman (IBLTYP=6)	Goddard (GFSC) (IMPHYS=6)	Grell (ICUPA=3,ISHALLO=1)	Dudhia (FRAD=2)
18	run44	17	MRF (IBLTYP=5)	Reisner 2 (IMPHYS=7)	Grell (ICUPA=3,ISHALLO=1)	CCM2 (FRAD=3)
19	run41	19	k-Thompson (IBLTYP=3,ISOI	Goddard (GFSC) (IMPHYS=6)	Kain-Fritsch (ICUPA=8,ISHALLO=0)	Simple cloud (FRAD=1)
20	run28	20	Gayno-Seaman (IBLTYP=6)	Simple ice (Dudhia) (IMPHYS=4)	Kain-Fritsch (ICUPA=8,ISHALLO=0)	Simple cloud (FRAD=1)
21	run49	21	MRF (IBLTYP=5)	Goddard (GFSC) (IMPHYS=6)	Betts-Miller (ICUPA=7,ISHALLO=0)	RRTM (FRAD=4)
22	run12	22	Eta M-Y (IBLTYP=4)	Simple ice (Dudhia) (IMPHYS=4)	Betts-Miller (ICUPA=7,ISHALLO=0)	Dudhia (FRAD=2)
23	run24	22	Gayno-Seaman (IBLTYP=6)	Simple ice (Dudhia) (IMPHYS=4)	Kain-Fritsch (ICUPA=8,ISHALLO=0)	RRTM (FRAD=4)
24	run20	23	Gayno-Seaman (IBLTYP=6)	Goddard (GFSC) (IMPHYS=6)	Grell (ICUPA=3,ISHALLO=1)	Simple cloud (FRAD=1)
25	run48	23	MRF (IBLTYP=5)	Simple ice (Dudhia) (IMPHYS=4)	Kain-Fritsch (ICUPA=8,ISHALLO=0)	RRTM (FRAD=4)
26	run51	23	MRF (IBLTYP=5)	Simple ice (Dudhia) (IMPHYS=4)	Grell (ICUPA=3,ISHALLO=1)	Dudhia (FRAD=2)
27	run2	24	Eta M-Y (IBLTYP=4)	Reisner 2 (IMPHYS=7)	Grell (ICUPA=3,ISHALLO=1)	CCM2 (FRAD=3)
28	run15	24	Gayno-Seaman (IBLTYP=6)	Goddard (GFSC) (IMPHYS=6)	Betts-Miller (ICUPA=7,ISHALLO=0)	CCM2 (FRAD=3)
29	run47	24	MRF (IBLTYP=5)	Schultz (IMPHYS=8)	Betts-Miller (ICUPA=7,ISHALLO=0)	RRTM (FRAD=4)
30	run17	26	Blackadar	Schultz (IMPHYS=8)	Kain-Fritsch (ICUPA=8,ISHALLO=0)	RRTM (FRAD=4)
31	run23	27	Gayno-Seaman (IBLTYP=6)	Goddard (GFSC) (IMPHYS=6)	Kain-Fritsch (ICUPA=8,ISHALLO=0)	Simple cloud (FRAD=1)
32	run30	27	Gayno-Seaman (IBLTYP=6)	Reisner 2 (IMPHYS=7)	Kain-Fritsch (ICUPA=8,ISHALLO=0)	Simple cloud (FRAD=1)
33	run38	27	k-Thompson (IBLTYP=3,ISOI	Simple ice (Dudhia) (IMPHYS=4)	Betts-Miller (ICUPA=7,ISHALLO=0)	CCM2 (FRAD=3)
34	run46	28	MRF (IBLTYP=5)	Schultz (IMPHYS=8)	Grell (ICUPA=3,ISHALLO=1)	CCM2 (FRAD=3)
35	run13	29	Eta M-Y (IBLTYP=4)	Simple ice (Dudhia) (IMPHYS=4)	Betts-Miller (ICUPA=7,ISHALLO=0)	CCM2 (FRAD=3)
36	run14	29	Gayno-Seaman (IBLTYP=6)	Schultz (IMPHYS=8)	Betts-Miller (ICUPA=7,ISHALLO=0)	CCM2 (FRAD=3)
37	run29	29	Blackadar	Schultz (IMPHYS=8)	Kain-Fritsch (ICUPA=8,ISHALLO=0)	CCM2 (FRAD=3)
38	run32	30	k-Thompson (IBLTYP=3,ISOI	Simple ice (Dudhia) (IMPHYS=4)	Betts-Miller (ICUPA=7,ISHALLO=0)	Simple cloud (FRAD=1)
39	run50	30	MRF (IBLTYP=5)	Simple ice (Dudhia) (IMPHYS=4)	Grell (ICUPA=3,ISHALLO=1)	CCM2 (FRAD=3)
40	run42	31	MRF (IBLTYP=5)	Reisner 2 (IMPHYS=7)	Kain-Fritsch (ICUPA=8,ISHALLO=0)	Dudhia (FRAD=2)
41	run4	32	Eta M-Y (IBLTYP=4)	Goddard (GFSC) (IMPHYS=6)	Grell (ICUPA=3,ISHALLO=1)	Dudhia (FRAD=2)
42	run8	32	Eta M-Y (IBLTYP=4)	Simple ice (Dudhia) (IMPHYS=4)	Grell (ICUPA=3,ISHALLO=1)	CCM2 (FRAD=3)
43	run36	32	k-Thompson (IBLTYP=3,ISOI	Reisner 2 (IMPHYS=7)	Betts-Miller (ICUPA=7,ISHALLO=0)	Dudhia (FRAD=2)
44	run10	34	Eta M-Y (IBLTYP=4)	Reisner (no graupel)	Kain-Fritsch (ICUPA=8,ISHALLO=0)	Simple cloud (FRAD=1)
45	run26	35	Gayno-Seaman (IBLTYP=6)	Goddard (GFSC) (IMPHYS=6)	Kain-Fritsch (ICUPA=8,ISHALLO=0)	CCM2 (FRAD=3)
46	run40	35	k-Thompson (IBLTYP=3,ISOI	Reisner 2 (IMPHYS=7)	Kain-Fritsch (ICUPA=8,ISHALLO=0)	Simple cloud (FRAD=1)
47	run11	37	Eta M-Y (IBLTYP=4)	Reisner 2 (IMPHYS = 7)	Betts-Miller (ICUPA=7,ISHALLO=0)	RRTM (FRAD=4)
48	run33	37	k-Thompson (IBLTYP=3,ISOI	Reisner 2 (IMPHYS=7)	Kain-Fritsch (ICUPA=8,ISHALLO=0)	Dudhia (FRAD=2)
49	run35	37	k-Thompson (IBLTYP=3,ISOI	Simple ice (Dudhia) (IMPHYS=4)	Betts-Miller (ICUPA=7,ISHALLO=0)	RRTM (FRAD=4)
50	run6	38	Eta M-Y (IBLTYP=4)	Reisner 2 (IMPHYS=7)	Grell (ICUPA=3,ISHALLO=1)	Dudhia (FRAD=2)
51	run7	40	Eta M-Y (IBLTYP=4)	Schultz (IMPHYS=8)	Betts-Miller (ICUPA=7,ISHALLO=0)	Dudhia (FRAD=2)

Table 9B. Front 3: Ensemble ranking with respect to physical parameterizations for WRF.

counter	Run	TOTAL rank	WRF (PBL)	WRF (Microphysics)	WRF (Cumulus)	WRF (Radiation)
	WRF Front 3					
1	run20	7	Mellor-Yamada-Jan	Morrison (Not in MM5)	Kain-Fritsch (MM5: Kain-Fritsch)	Goddard/RRTM
2	run38	7	Pleim-Xiu	Eta microphysics (Not in MM5)	Grell-Devenyi (MM5: Grell scheme)	GFDL/GFDL
3	run42	8	Pleim-Xiu	Goddard microphysics (MM5: GSFC)	Grell-Devenyi (MM5: Grell scheme)	CAM/CAM
4	run13	9	Mellor-Yamada-Jan	Lin et al. (MM5: GSFC)	Grell-Devenyi (MM5: Grell scheme)	Goddard/RRTM
5	run39	10	Pleim-Xiu	Goddard microphysics (MM5: GSFC)	Grell-Devenyi (MM5: Grell scheme)	Dudhia/RRTM
6	run45	10	Pleim-Xiu	Morrison (Not in MM5)	Kain-Fritsch (MM5: Kain-Fritsch)	Goddard/RRTM
7	run28	11	YSU (new MRF)	Goddard microphysics (MM5: GSFC)	Betts-Miller (MM5: Betts-Miller)	Dudhia/RRTM
8	run29	12	YSU (new MRF)	Thompson (MM5 : Reisner 2)	Grell-Devenyi (MM5: Grell scheme)	GFDL/GFDL
9	run22	14	Mellor-Yamada-Jan	Morrison (Not in MM5)	Grell-Devenyi (MM5: Grell scheme)	Goddard/RRTM
10	run27	14	YSU (new MRF)	Lin et al. (MM5: GSFC)	Betts-Miller (MM5: Betts-Miller)	CAM/CAM
11	run50	14	Pleim-Xiu	Goddard microphysics (MM5: GSFC)	Grell-Devenyi (MM5: Grell scheme)	Dudhia/RRTM
12	run37	16	Pleim-Xiu	Lin et al. (MM5: GSFC)	Betts-Miller (MM5: Betts-Miller)	Goddard/RRTM
13	run26	17	YSU (new MRF)	Lin et al. (MM5: GSFC)	Kain-Fritsch (MM5: Kain-Fritsch)	CAM/CAM
14	run40	17	Pleim-Xiu	Lin et al. (MM5: GSFC)	Kain-Fritsch (MM5: Kain-Fritsch)	GFDL/GFDL
15	run41	17	Pleim-Xiu	Thompson (MM5 : Reisner 2)	Kain-Fritsch (MM5: Kain-Fritsch)	GFDL/GFDL
16	run32	18	YSU (new MRF)	Morrison (Not in MM5)	Kain-Fritsch (MM5: Kain-Fritsch)	Goddard/RRTM
17	run16	19	Mellor-Yamada-Jan	Lin et al. (MM5: GSFC)	Kain-Fritsch (MM5: Kain-Fritsch)	Dudhia/RRTM
18	run25	20	YSU (new MRF)	Goddard microphysics (MM5: GSFC)	Betts-Miller (MM5: Betts-Miller)	Goddard/RRTM
19	run30	20	YSU (new MRF)	Eta microphysics (Not in MM5)	Betts-Miller (MM5: Betts-Miller)	Goddard/RRTM
20	run49	20	Pleim-Xiu	Lin et al. (MM5: GSFC)	Grell-Devenyi (MM5: Grell scheme)	Dudhia/RRTM
21	run17	21	Mellor-Yamada-Jan	Eta microphysics (Not in MM5)	Kain-Fritsch (MM5: Kain-Fritsch)	Dudhia/CAM
22	run21	21	Mellor-Yamada-Jan	Morrison (Not in MM5)	Betts-Miller (MM5: Betts-Miller)	Goddard/RRTM
23	run35	21	YSU (new MRF)	WRF-single mom(6) (MM5: Reisner 1)	Betts-Miller (MM5: Betts-Miller)	CAM/CAM
24	run19	23	Mellor-Yamada-Jan	WRF-single mom (3) (MM5: simple ice)	Kain-Fritsch (MM5: Kain-Fritsch)	Dudhia/RRTM
25	run23	23	YSU (new MRF)	Eta microphysics (Not in MM5)	Kain-Fritsch (MM5: Kain-Fritsch)	GFDL/GFDL
26	run18	24	Mellor-Yamada-Jan	WRF-single mom (6) (MM5: Reisner 1)	Betts-Miller (MM5: Betts-Miller)	Goddard/RRTM
27	run24	24	YSU (new MRF)	Lin et al. (MM5: GSFC)	Betts-Miller (MM5: Betts-Miller)	GFDL/GFDL
28	run44	24	Pleim-Xiu	WRF-single mom(6) (MM5: Reisner 1)	Kain-Fritsch (MM5: Kain-Fritsch)	Goddard/RRTM
29	run48	25	Pleim-Xiu	Lin et al. (MM5: GSFC)	Betts-Miller (MM5: Betts-Miller)	Dudhia/RRTM
30	run14	27	Mellor-Yamada-Jan	Lin et al. (MM5: GSFC)	Betts-Miller (MM5: Betts-Miller)	GFDL/GFDL
31	run33	27	YSU (new MRF)	WRF-single mom(6) (MM5: Reisner 1)	Kain-Fritsch (MM5: Kain-Fritsch)	Goddard/RRTM
32	run36	27	Pleim-Xiu	Eta microphysics (Not in MM5)	Betts-Miller (MM5: Betts-Miller)	Goddard/RRTM
33	run47	27	Pleim-Xiu	Goddard microphysics (MM5: GSFC)	Betts-Miller (MM5: Betts-Miller)	Dudhia/RRTM
34	run31	29	YSU (new MRF)	Eta microphysics (Not in MM5)	Kain-Fritsch (MM5: Kain-Fritsch)	CAM/CAM
35	run3	30	Mellor-Yamada-Jan	Goddard microphysics (MM5: GSFC)	Kain-Fritsch (MM5: Kain-Fritsch)	GFDL/GFDL
36	run9	30	Mellor-Yamada-Jan	Goddard microphysics (MM5: GSFC)	Grell-Devenyi (MM5: Grell scheme)	GFDL/GFDL
37	run10	30	Mellor-Yamada-Jan	Goddard microphysics (MM5: GSFC)	Betts-Miller (MM5: Betts-Miller)	CAM/CAM
38	run4	31	Mellor-Yamada-Jan	Lin et al. (MM5: GSFC)	Kain-Fritsch (MM5: Kain-Fritsch)	Goddard/RRTM
39	run5	31	Mellor-Yamada-Jan	Eta microphysics (Not in MM5)	Kain-Fritsch (MM5: Kain-Fritsch)	GFDL/GFDL
40	run6	31	Mellor-Yamada-Jan	Eta microphysics (Not in MM5)	Betts-Miller (MM5: Betts-Miller)	CAM/CAM
41	run7	31	Mellor-Yamada-Jan	Eta microphysics (Not in MM5)	Kain-Fritsch (MM5: Kain-Fritsch)	CAM/CAM
42	run8	31	Mellor-Yamada-Jan	Thompson (MM5 : Reisner 2)	Betts-Miller (MM5: Betts-Miller)	Dudhia/RRTM
43	run11	31	Mellor-Yamada-Jan	Thompson (MM5 : Reisner 2)	Betts-Miller (MM5: Betts-Miller)	CAM/CAM
44	run12	31	Mellor-Yamada-Jan	Thompson (MM5 : Reisner 2)	Betts-Miller (MM5: Betts-Miller)	Goodard/RRTM
45	run15	31	Mellor-Yamada-Jan	Goddard microphysics (MM5: GSFC)	Betts-Miller (MM5: Betts-Miller)	GFDL/RRTM
46	run34	31	YSU (new MRF)	WRF-single mom(3) (MM5: Simple ice)	Betts-Miller (MM5: Betts-Miller)	Dudhia/RRTM
47	run43	31	Pleim-Xiu	Goddard microphysics (MM5: GSFC)	Kain-Fritsch (MM5: Kain-Fritsch)	CAM/CAM
48	run46	31	Pleim-Xiu	Lin et al. (MM5: GSFC)	Kain-Fritsch (MM5: Kain-Fritsch)	CAM/CAM
49	run51	31	Pleim-Xiu	Lin et al. (MM5: GSFC)	Kain-Fritsch (MM5: Kain-Fritsch)	GFDL/GFDL
50	run1	32	Mellor-Yamada-Jan	Thompson (MM5 : Reisner 2)	Kain-Fritsch (MM5: Kain-Fritsch)	Dudhia/RRTM
51	run2	32	Mellor-Yamada-Jan	Goddard microphysics (MM5: GSFC)	Betts-Miller (MM5: Betts-Miller)	GFDL/GFDL (Not in MM5)

Appendix C

Ensemble Model Physics Option Lists

C.1 COAMPS Model Physics Options

- Resolvable-scale microphysics schemes:

    o autoconversion parameter (Rutledge and Hobbs 1983, Lin et al. 1983, Kessler, 1969)

    Note: No conversion unless cloud water mixing ratio .> auto-conv
    ice nucleation processes (Fletcher 1962; Cooper and Haines 1996).

- Cumulus parameterization schemes:

    o Kain-Fritsch cumulus scheme (Kain and Fritsch 1993; Kain 2004)

- Planetary boundary layer process parameterization

    o Mellor-Yamada (MY) level 2.5 and 3 models (Mellor and Yamada, 1974, 1982; Burk and Thompson 1989; Janjić 2001) with a prognostic equation for turbulence kinetic energy
    o MY modified to allow the PBL to operate in saturated conditions (Ballard et al., 1991; Shafran et al. 2000)

- Atmospheric radiation schemes ()

    o longwave and shortwave (Harshvardhan 1987, Fu-Liou 1992,1993)

Table 1C. COAMPS Model Glossary of Symbols and Units

Symbol	Description	Value	SI Units
A'	Thermodynamic term in PREVP		$m\ s\ kg^{-1}$
$\overline{a}$	Thermodynamic term in PDEPI		$m\ s\ kg^{-1}$
a	Constant in fallspeed relation for graupel	19.3	$m^{(1-b)}\ s^{-1}$
a	Constant in M-Z relation	0.008	$g\ m^{3(b'-1)}\ mm^{-6b'}$
a'	Constant in linear fallspeed relation for rain	3×10^3	s^{-1}
a''	Constant in fallspeed relation for snow	1.139	$m^{(1-b)}\ s^{-1}$
a_0	Coefficient in polynomial fallspeed relation for rain	-0.267	$m\ s^{-1}$
a_1	Coefficient in polynomial fallspeed relation for rain	5.15×10^3	s^{-1}
a_2	Coefficient in polynomial fallspeed relation for rain	-1.0225×10^6	$m^{-1}\ s^{-1}$
a_3	Coefficient in polynomial fallspeed relation for rain	7.55×10^7	$m^{-2}\ s^{-1}$
B'	Thermodynamic term		$m\ s\ kg^{-1}$
B''	Thermodynamic term		$m\ s\ kg^{-1}$
$\overline{b}$	Fallspeed exponent of graupel	0.37	
b	Fallspeed exponent for snow	0.11	
b'	Constant in M-Z relation	0.605	
C	Capacitance of ice crystal		F
c_p	Specific heat of air at constant pressure	1.005×10^3	$J\ kg^{-1}\ K^{-1}$
c_w	Specific heat of liquid water at $0°$ C	4218	$J\ kg^{-1}\ K^{-1}$
D_1	Diameter of hexagonal plate		m
D_0	Initial diameter of cloud ice crystals	12.9×10^{-6}	m
D_G	Graupel diameter		m
D_R	Raindrop diameter		m
D_S	Snowflake diameter		m
$dB(Z_R)$	$10 \log_{10}$ (radar reflectivity factor for rain)		
$dB(Z_S)$	$10 \log_{10}$ (radar reflectivity factor for snow)		
E_{GC}	Graupel/cloud water collection efficiency	1	
E_{GI}	Graupel/cloud ice collection efficiency	0.1	
E_{GR}	Graupel/ rain collection efficiency	1	
E_{GS}	Graupel/snow collection efficiency	0.1	
E_{RC}	Rain/cloud water collection efficiency	1	
E_{RI}	Rain/cloud ice collection efficiency	1	
E_{SC}	Snow/cloud water collection efficiency	1	
E_{SI}	Snow/cloud ice collection efficiency	0.1	
E_{SR}	Snow/rain collection efficiency	1	
$\overline{E_t}$	Average diameter of cloud ice crystals		m
e_{si}	Saturation vapor pressure for ice		$N\ m^{-2}$
e_{sw}	Saturation vapor pressure for water		$N\ m^{-2}$
F	Ventilation factor for rain and graupel		
F'	Ventilation factor for snow		
K_a	Thermal conductivity of air	2.43×10^{-2}	$J\ m^{-1}\ s^{-1}\ K^{-1}$
L_f	Latent heat of fusion	3.34×10^5	$J\ kg^{-1}$
L_s	Latent heat of sublimation	2.5×10^6	$J\ kg^{-1}$
L_c	Latent heat of condensation	2.25×10^6	$J\ kg^{-1}$
$\overline{M_c}$	Average mass of cloud droplet	4×10^{-12}	kg
$\overline{M_I}$	Average mass of cloud ice particle	6×10^{-12}	kg
M_i	Average mass of cloud ice crystal		kg
M_{max}	Maximum mass of cloud ice crystal	9.4×10^{-10}	kg
M_0	Initial mass of cloud ice crystal	10^{-12}	kg
M_G	Mass of graupel per unit volume of air		$kg\ m^{-3}$
M_R	Mass of rain per unit volume of air		$kg\ m^{-3}$
M_S	Mass of snow per unit volume of air		$kg\ m^{-3}$
M_w	Molecular weight of water	18.0160	
M_{melt}	Mass of melted snow		kg

Table 1C. COAMPS Model Glossary of Symbols and Units

Symbol	Description	Value	SI Units
$M(D_G)$	Mass of graupel particle of diameter D_G		kg
$M(D_R)$	Mass of raindrop of diameter D_R		kg
$M(D_S)$	Mass of snowflake of diameter D_S		kg
$N_{DG}dD_G$	Number of concentration of graupel particles with diameters between D_G and $D_G + d\,D_G$		m^{-3}
$N_{DR}dD_R$	Number of concentration of raindrops with diameters between D_R and $D_R + d\,D_R$		m^{-3}
$N_{DS}dD_S$	Number of concentration of snowflakes with diameters between D_S and $D_S + d\,D_S$		m^{-3}
N_{0G}	Intercept value in graupel size distribution	4×10^6	m^{-4}
N_{0R}	Intercept value in raindrop size distribution	8×10^6	m^{-4}
N_{0S}	Intercept value in snowflake size distribution	4×10^6	m^{-4}
n_{ci}	Number concentration of cloud ice crystals		m^{-3}
$\bar{n}_c$	Number concentration of cloud water droplets		m^{-3}
n_i	Number concentration of ice nuclei		m^{-3}
n_0	Constant in expression for ice nuclei concentration	variable	m^{-3}
p	Pressure		$N\,m^{-2}$
p_0	Constant in empirical relation	10^6	$N\,m^{-2}$
PCOND	Condensation of water vapor		$kg\,m^{-3}\,s^{-1}$
PCONV	Conversion of cloud ice to snow		$kg\,m^{-3}\,s^{-1}$
PDEPI	Depositional growth of cloud ice		$kg\,m^{-3}\,s^{-1}$
PGACI	Collection of cloud ice by graupel		$kg\,m^{-3}\,s^{-1}$
PGACR	Collection of rain by graupel		$kg\,m^{-3}\,s^{-1}$
PGACRM	Enhanced melting of graupel due to accretion of rain		$kg\,m^{-3}\,s^{-1}$
PGACS	Collection of snow by graupel		$kg\,m^{-3}\,s^{-1}$
PGACW	Collection of cloud water by graupel		$kg\,m^{-3}\,s^{-1}$
PGACWM	Enhanced melting of graupel due to accretion of cloud water		$kg\,m^{-3}\,s^{-1}$
PGDEP	Depositional growth of graupel		$kg\,m^{-3}\,s^{-1}$
PGMLT	Melting of graupel		$kg\,m^{-3}\,s^{-1}$
PGSHR	Shedding of accreted water by graupel		$kg\,m^{-3}\,s^{-1}$
PIACR	Collection of rain by cloud ice		$kg\,m^{-3}\,s^{-1}$
PMLTEV	Evaporation of melting snow		$kg\,m^{-3}\,s^{-1}$
PMLTGE	Evaporation of melting graupel		$kg\,m^{-3}\,s^{-1}$
PRACI	Collection of cloud ice by rain		$kg\,m^{-3}\,s^{-1}$
PRACS	Collection of snow by rain		$kg\,m^{-3}\,s^{-1}$
PRACW	Collection of cloud water by rainwater		$kg\,m^{-3}\,s^{-1}$
PRAUT	Autoconversion of cloud water		$kg\,m^{-3}\,s^{-1}$
PREVP	Evaporation of rainwater		$kg\,m^{-3}\,s^{-1}$
PSACI	Collection of cloud ice by snow		$kg\,m^{-3}\,s^{-1}$
PSACR	Collection of rain by snow		$kg\,m^{-3}\,s^{-1}$
PSACW	Collection of cloud water by snow		$kg\,m^{-3}\,s^{-1}$
PSDEP	Depositional growth of snow		$kg\,m^{-3}\,s^{-1}$
PSFI	Conversion of cloud ice to snow in the Bergeron process		$kg\,m^{-3}\,s^{-1}$
PSFW	Conversion of cloud water to snow in the Bergeron process		$kg\,m^{-3}\,s^{-1}$
PSMLT	Melting of snow		$kg\,m^{-3}\,s^{-1}$
PSMLTI	Melting of cloud ice		$kg\,m^{-3}\,s^{-1}$
PINT	Initiation of cloud ice		$kg\,m^{-3}\,s^{-1}$
q_c	Mixing ratio of cloud water		$kg\,kg^{-1}$
q_i	Mixing ratio of cloud ice		$kg\,kg^{-1}$
q_{imax}	Conversion of cloud ice to snow threshold		$kg\,kg^{-1}$
q_0	Mixing ratio threshold for PRAUT	7×10^{-4}	$kg\,kg^{-1}$
q_r	Mixing ratio of rainwater		$kg\,kg^{-1}$
q_s	Mixing ratio of snow		$kg\,kg^{-1}$

Table 1C. COAMPS Model Glossary of Symbols and Units

Symbol	Description	Value	SI Units
q_{s0}	Mixing ratio of snow at top of feeder zone		kg kg^{-1}
q_{si}	Saturation mixing ratio with respect to ice		kg kg^{-1}
q_{sw}	Saturation mixing ratio with respect to water		kg kg^{-1}
q_v	Mixing ratio of water vapor		kg kg^{-1}
R^*	Universal gas constant	8.314×10^3	J kmol^{-1} K^{-1}
R_e	Reynolds number		
R_w	Gas constant for water vapor	4.61×10^2	J kg^{-1} K^{-1}
S	Saturation ratio with respect to water		
S_c	Schmidt number	0.6	
S_C	Source term for cloud water		kg m^{-3} s^{-1}
S_h	Diabatic heating terms		K kg m^{-3} s^{-1}
S_I	Source term for cloud ice		kg m^{-3} s^{-1}
S_i	Saturation ratio with respect to ice		kg m^{-3} s^{-1}
S_0	Represents sources and sinks for q		kg m^{-3} s^{-1}
S_R	Source term for rain		kg m^{-3} s^{-1}
S_S	Source term for snow		kg m^{-3} s^{-1}
S_V	Source term for water vapor		kg m^{-3} s^{-1}
T	Temperature		K
T_0	Reference temperature	273.16	K
t	Time		s
u	Horizontal windspeed		m s^{-1}
V	Mass-weighted fallspeed of precipitation		m s^{-1}
V_R	Mass-weighted fallspeed for rain		m s^{-1}
$V_R(D_R)$	Fallspeed of raindrop of diameter D_R		m s^{-1}
V_S	Mass-weighted fallspeed for snow		m s^{-1}
$V_S(D_S)$	Fallspeed of snowflake for diameter D_S		m s^{-1}
w	Vertical air velocity		m s^{-1}
x	Horizontal distance		m
Z	Equivalent radar reflectivity factor		mm^6 m^{-3}
z	Vertical distance		m
α	Rate coefficient for autoconversion	0.001	s^{-1}
β	Constant in ice crystal concentration	0.6	deg^{-1}
Γ	Gamma function		
Γ_d	Dry adiabatic lapse rate	9.8×10^{-3}	K m^{-1}
ε_0	Permittivity of free space	8.854×10^{-12}	C^2 N^{-1} m^{-2}
ρ	Air density		kg m^{-3}
ρ_L	Density of water	10^3	kg m^{-3}
ρ_S	Density of snow	100 (Type 1) 200 (Type 2)	kg m^{-3} kg m^{-3}
λ_R	Slope of raindrop size distribution		m^{-1}
λ_S	Slope of snow size distribution		m^{-1}
χ	Diffusivity of water vapor in air	2.26×10^{-5}	m^2 s^{-1}
μ	Dynamic viscosity of air	1.718×10^{-5}	kg m^{-1} s^{-1}
Δ_t	Time increment	10	s
Δ_x	Horizontal spatial increment	4000	m
Δ_z	Vertical spatial increment	200	m

C.2 MM5 Model Physics Options

Precipitation physics

Cumulus parameterization schemes:
- ☐ Anthes-Kuo
- ☐ Grell
- ☐ Kain-Fritsch
- ☐ New Kain-Fritsch (including shallow convection physics)
- ☐ Betts-Miller
- ☐ Arakawa-Schubert

Resolvable-scale microphysics schemes:
- ☐ Removal of supersaturation
- ☐ Hsie's warm rain scheme
- ☐ Dudhia's simple ice scheme
- ☐ Reisner's mixed-phase scheme
- ☐ Reisner's mixed-phase scheme with graupel
- ☐ NASA/Goddard microphysics with hail/graupel
- ☐ Schultz mixed-phase scheme with graupel

Planetary boundary layer process parameterization
- o Bulk formula
- o Blackadar scheme
- o Burk-Thompson (Mellor-Yamada 1.5-order/level-2.5 scheme)
- o Eta TKE scheme (Janjic, 1990, 1994)
- o MRF scheme (Hong and Pan 1996)
- o Gayno-Seaman scheme (Gayno 1994)

Surface layer process parameterization
- o fluxes of momentum, sensible and latent heat
- o ground temperature prediction using energy balance equation
- o variable land use catagories (defaults are 13, 16 and 24)
- o 5-layer soil model
- o OSU land-surface model (V3.1 - V3.5)
- o Noah land-surface model (since V3.6)
- o Pleim-Xiu land-surface model (V3 only)

Atmospheric radiation schemes
- o Simple cooling
- o Dudhia's long- and short-wave radiation scheme
- o NCAR/CCM2 radiation scheme
- o RRTM long-wave radiation scheme (Mlawer et al., 1997) (V3 oCumulus and shallow

convection parameterization,
- o Kain-Fritsch with shallow convection,

o   Betts-Miller-Janjic,
o   Grell-Devenyi ensemble scheme,
o   New Grell 3D ensemble scheme,
o   Grell-Freitas ensemble scheme (v3.5),
o   Tiedtke,
o   New SAS (Simplied Arakawa-Schubert) from GFS,
o   Old SAS (from GFS too),
o   Zhang-McFarlane,
o   University of Washington shallow convection,
o   GRIMS shallow convection (v3.5),

Planetary boundary layer process parameterization
o   Yonsei University (S. Korea) with improved stable BL
o   Mellor-Yamada-Janjic
o   Asymmetric Convective Model (ACM2)
o   Quasi-normal scale elimination/Eddy diffusivity/ mass flux (QNSE-EDMF) (v3.4)
o   Level 2.5 and 3 Mellor-Yamada Nakanishi Niino (MYNN) PBL
o   Bougeault-Lacarrere PBL
o   University of Washington TKE PBL
o   Total energy - mass flux (TEMF) scheme
o   Grenier-Bretherton-McCaa TKE PBL (v3.5)
o   MRF

Surface layer process parameterization
o   similarity theory MM5 - may be run with a 1-D ocean mixed layer model
o   Eta or MYJ
o   PX
o   QNSE
o   MYNN
o   TEMF
o   Revised MM5 scheme (v3.4)

land-surface process parameterization
o   slab soil model (5-layer thermal diffusion)
o   Unified Noah land-surface model
o   Urban canopy model (works with Noah LSM)
o   Multi-layer building environment parameterization (BEP, works with Noah, and requires
o   BouLac and MYJ PBL)
o   Building energy model (BEM, works with Noah and requires BouLac and MYJ PBL)
o   RUC LSM
o   PX LSM
o   Noah-MP (v3.4)
o   SSiB (v3.4)
o   CLM4 (v3.5)
☐   use of fractional sea-ice
☐   WRF-Hydro (v3.5)

Atmospheric radiation schemes

longwave radiation
o   RRTM
o   CAM
o   RRTMG
o   Goddard
o   Fu-Liou-Gu

shortwave radiation
o   simple MM5 scheme, with Zaengl radiation/topography (slope and shadowing) effects
o   Goddard (old)
o   CAM
o   RRTMG
o   Goddard
o   Fu-Liou-Gu

ocean physics
o   single-column mixed layer ocean model
o   3D Price-Weller-Pinkel (PWP) ocean model

sub-grid turbulence
o   constant K diffusion
o   2-D Smagorinsky
o   predicted TKE
o   nonlinear backscatter and anisotropy (NBA) turbulence option for LES (new in V3.2)

land-use categories determine surface properties
SST, greenness fraction, seaice and albedo update during long simulations
analysis nudging, 3-D and surface (new in V3.1)
observation nudging (new in V2.2)
spectral nudging using gridded analyses (new in V3.1)